ENERGY EXCHANGE THROUGH AN ANNUAL SEA ICE COVER

by

Peter Schwerdtfeger, B.Sc., M.Sc., (Melbourne).

A thesis submitted to the Faculty of Graduate Studies and Research in partial fulfilment of the requirements for the degree of Doctor of Philosophy.

Department of Physics,
McGill University,
Montreal.

March 1962

ACKNOWLEDGEMENTS

It is a pleasure to record the efforts and assistance of many persons associated with McGill University and the Defence Research Northern Laboratory, Fort Churchill.

Firstly, I wish to express my gratitude to my Director of Research, Professor E.R.Pounder, for his introduction to a field of physical research new to me. Frequent discussions with him have been of great importance to the structure of this thesis.

Many criticisms offered by Mr.J.R.Addison, Dr.M.P.Langleben and Dr.E.Vowinckel during long conversations have been of value and interest.

A large number of personnel at the Defence Research Northern Laboratory contributed to the success of the field work, particularly Dr.J.Brandy, who made many of the laboratory's facilities available from January to May, 1961. It is not possible to note the generous assistance of all concerned at D.R.N.L., but Mr.P.Graystone in 1959-60 and Mr.N.Harrison in 1960-61 must be mentioned for providing invaluable assistance in materializing the recording station. The electrical power supply was designed and built by Mr.P.Beadle, and much of the necessary hardware was devised by Mr.S.Nelson.

At the drafting board, Mr.R.W.Schwerdtfeger kindly applied his skill in the preparation of a number of graphs whose drawing defied the use of normal templates.

Finally, I wish to record my appreciation of my wife's typing. Whilst facing a demanding family, she performed the task confronting her with poise and competence.

This work was supported by a National Research Council grant, A-820, and by the Defence Research Board through D.D.P. contracts GC-69-900109, GC-69-000105 and GC-69-100108.

INTRODUCTION

Determination of the energy fluxes resulting from incident solar radiation is fundamental to an understanding of the physical conditions prevailing at any point on the earth's surface. Comprehensive work on the balance of thermal energy in temperate regions has been performed and reported, particularly by Thornthwaite and Halstead, (TH54). However, results of similar completeness are lacking for oceanic regions, a fact illustrated by the omission of detail for these areas in Budyko's world atlas of heat balance, (Bu55). The determination of the energy budget is particularly interesting in the Arctic, where an immense latent heat is involved in the freezing and subsequent melting of the oceans. During the winter, the northern ocean is thus a vast reservoir of thermal energy, but at the onset of summer, the ice must melt before an appreciable temperature rise can take place in the atmosphere. The climate in the neighbourhood of the arctic seas is marked by less pronounced extremes than that of continental Siberia, and because of the time required for freezing and melting of the ice, shows a relative delay in seasonal temperatures. This fact is strikingly illustrated in the atlas by Goodall and Darby (GD45) whose records for coastal west Greenland and continental Siberia at about 70°N, show yearly ranges of mean monthly temperatures of 20°C and 70°C respectively, with a relative one month delay for the former's peak values.

There are two main approaches in seeking energy budget data on an ice cover. On permanent ice, information must be sought over a period of at least one year, and because of the large mass of ice, the initial and final heat energy content of the cover will be among the important observations recorded. In contrast, on an annual cover, because of the relatively rapid rate of accretion of new ice, precise observations taken over relatively short periods of time may be of considerable value. Measurement of the conducted heat flux in the ice is far more important than on a permanent cover, where investigation of the thickness and tendency of the energy content over a number of years is relevant. The duration of measurements required is determined mainly by the accuracy with which the time taken for upper surface temperature phenomena to diffuse to the lower boundary can be established, and by the time required for a useful overlap in upper and lower surface phenomena. This time increases with exponential tendencies, and for a 5 metre ice cover may involve many weeks, which fact makes the study of temperature diffusion in sea ice important.

Considerable difference of opinion exists as to the relative magnitudes of several of the important energy fluxes measured in polar regions. With respect to the evaporative flux, for example, two extreme views have been held by Iakovlev (Ia58) and Untersteiner (Un61). The former has reported both positive and negative mean values whose magnitude during several months is of the same order as the net radiation. Untersteiner on the other hand, has held evaporation and condensation to be less important. Since Iakovlev obtained his figures as residual values, Untersteiner has shown that these may be considerably reduced if the former's estimate of the heat content of the ice cover is revised. Iakovlev appears to have obtained a low value for the heat energy content of the ice through employing the specific heat figure for fresh water ice. The method of leaving the determination of the magnitude of evaporation and condensation to a process of elimination is clearly not satisfactory.

The uncertainty in the relative magnitudes of the various energy fluxes encountered on an ice cover serves to illustrate the current lack of data on the simultaneous and sensibly continuous observation of radiation, conduction below the solid surface, convection and evaporation in the lower atmosphere and the heat content of the ice. The chief components have been measured in great detail by various observers at different times and places, particularly radiation, a field in which the work of Liljequist in the Antarctic (Li56) is a valuable source of information and data.

Although there is certainly little comprehensive information on permanent ice covers, there appears to be an absence of any complete data for an annual sea ice cover. This type of surface was thus chosen for a thorough examination. The observation and correlation of the dominant energy fluxes listed above and the state of the ice cover formed the final aim of this thesis. It is important to note that the magnitude of the conducted heat flux in the ice of an annual cover may be orders of magnitude above that observed in glaciers or other solid surfaces of the earth. This makes the former a special case, results from which are not easily compared with those from other terrains. An understanding of this conducted flux from its origin at the freezing boundary layer, to its transmission with vertical variations in the cover due to capacitive storing, requires a thorough knowledge of those physical properties of sea ice associated with thermal processes.

Compared to fresh water ice, whose physical properties are well known, sea ice is a relatively complex substance whose transition to a completely solid mixture of pure ice and solid salts is completed only at extremely low temperatures rarely encountered in nature. The physical properties of sea ice are thus strongly dependent on salinity, temperature and time. Many of these properties are still not fully understood or accurately known. As has already been seen, the specific heat is an important term in the calculation of the heat energy content of an ice cover. Malmgren, however, whose calculated values of the specific heat of sea ice (Ma33) are in general use, neglected the direct contribution of the brine present in inclusions, which leads to errors at higher temperatures if his equation is used. It has been found necessary to re-examine the question of specific and latent heats of sea ice and distinguish between the freezing and melting points, which has enabled significant observations in this range. Similarly, because the thermal conductivity is a necessary parameter in the description of the thermal behaviour of ice, the sea ice model suggested by Anderson (An58) has been modified and extended in the present work to the case of saline ice containing air bubbles, enabling the completion of calculations of conductivity and density, which were confirmed to some extent in experimental observations.

The diffusion equation has been solved for the case of a general variation of surface temperature, and shown to be applicable in the thermal studies of sea ice. This theoretical work led to the formulation of an analogue circuit which it is expected will greatly simplify the study of ice temperatures and growth rates, and the heat flux through a cover.

The theoretical and laboratory studies of the properties of ice are considered fundamentally important in achieving the final aim of this thesis. For this reason they appear as earlier chapters rather than as appendices.

Two seasons of field work at Button Bay, shown on the accompanying map as an indentation in the Hudson Bay coastline near Churchill, were involved in the collection of data discussed in the later chapters. The data used was obtained during the second winter, January to May 1961. During the previous season, instrumentation, timing and automation of observations, wind generation of electricity and power supply stabilization as well as heating for the recording equipment hut underwent extensive development. Although greater accuracy might be expected from measurements at similar sites by additional observations during following winters, the order of magnitude and nature of the interdependence of the energy fluxes have been established.

Much of the completed work might contribute to the art of forecasting the state of the Arctic seas. It has long been evident that this has important practical applications, particularly because the formation of ice governs the nature and duration of surface transport. Most forecasting methods apart from the statistical but including that based on analogue computation require detailed information on the physical properties of sea ice, and all require some meteorological information, both of which this thesis has attempted to provide.

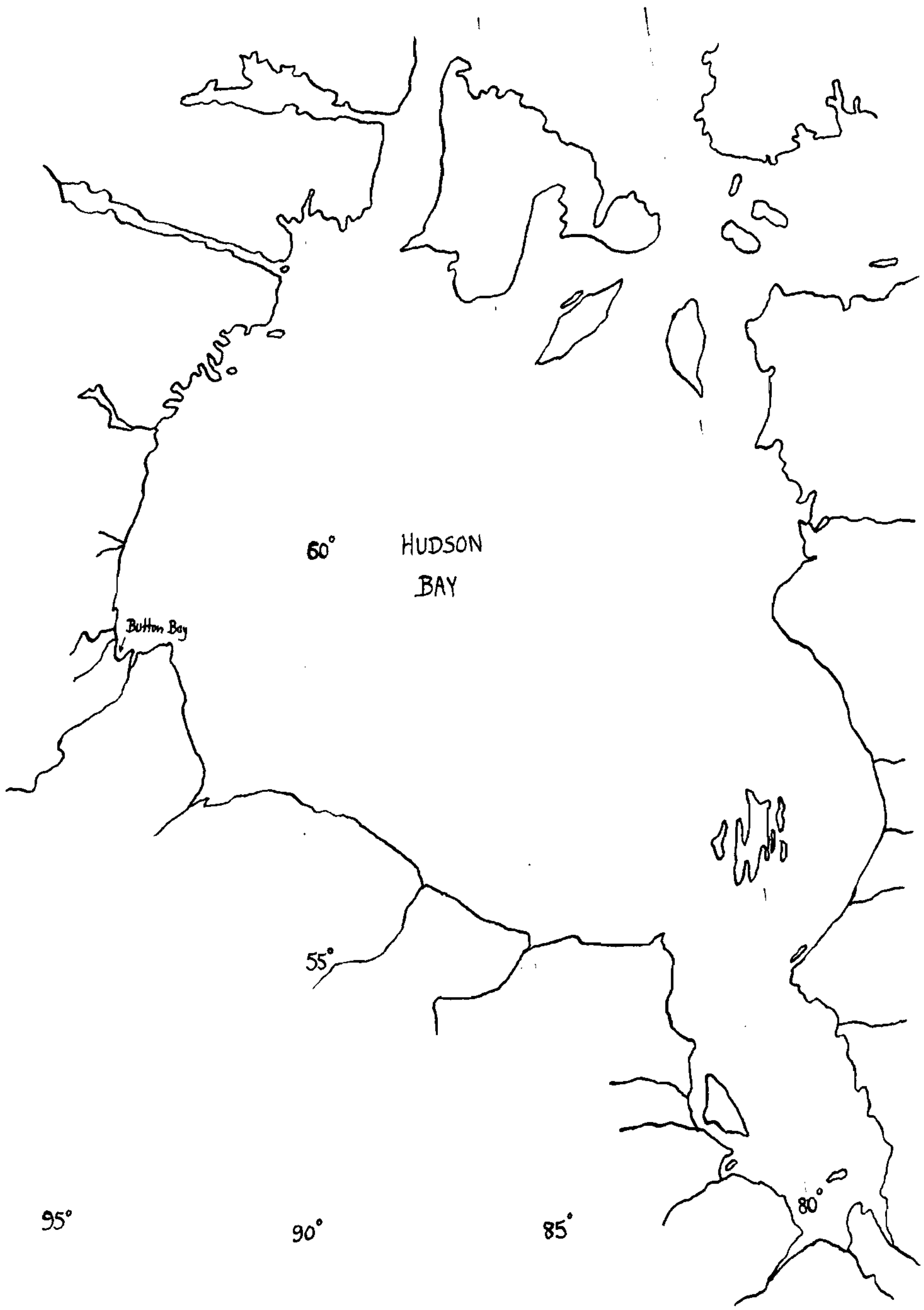
60°
HUDSON
BAY
Button Bay
55°
95°
90°
85°
80°

CHAPTER 1

THE SPECIFIC AND LATENT HEATS OF SEA ICE

CHAPTER 2

THE THERMAL CONDUCTIVITY OF SEA ICE

CHAPTER 3

THE DIFFUSION EQUATION

CHAPTER 4

THE GROWTH OF SEA ICE

CHAPTER 5

THE FLUXES OF THERMAL ENERGY AND THEIR MEASUREMENT

CHAPTER 6

THE RESULTS OF A WINTER'S RECORDS ON HUDSON BAY

ANNUAL ICE

CHAPTER 1

THE SPECIFIC AND LATENT HEATS OF SEA ICE

1.1 The Composition of Sea Ice and the Concept of Salinity.

When sea water is cooled to its freezing point, pure ice crystals form, separating from the brine which initially remains in contact with the sea. As freezing progresses, some pockets of brine are cut off so that the resulting ice as a whole is composed of pure ice, brine, solid salt crystals and air bubbles. The latter have negligible influence on the specific heat, but the continuous change in relative abundance of the other constituents with temperature leads to an abnormally large specific heat. At temperatures not far removed from the freezing point, further freezing of the interior brine is the major heat releasing process.

The total mass of dissolved solid material in grams contained in one kilogram of solution is the usual oceanographic definition of salinity. This is also applied to sea ice and the mass of salt in grams per kilogram of sea ice is usually quoted in parts per thousand (‰). The salinity of sea ice may well be considered a convenient property to which other more complex properties, including thermal, electrical and mechanical, may be referred. However, because the salts in sea ice consist of many ions, chief amongst which are: Na^+, Ca^+, K^+, Mg^+, Cl^-, SO_4^{--} and CO_3^{--}, the specification is in general insufficient to fix the relative ionic content of the ice.

As the phase diagram in figure (1.1.i), of Nelson and Thompson (NT54) shows, above a temperature of -8.2°C, all salts trapped within the body of the ice are in solution. Down to this temperature limit, the relative concentration of the ions is as in sea water and the specification of salinity

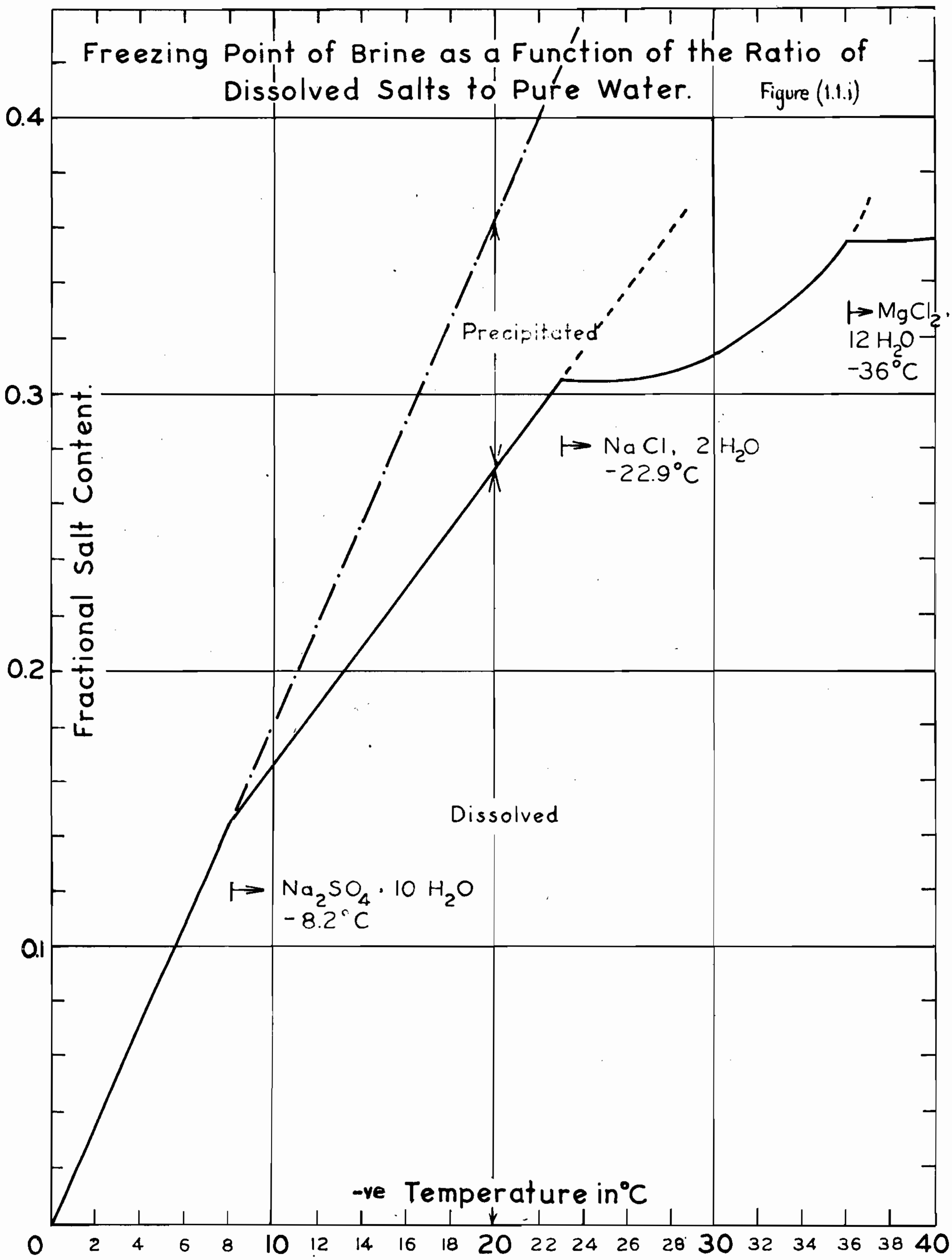
Freezing Point of Brine as a Function of the Ratio of Dissolved Salts to Pure Water.
Figure (1.1.i)
0.4
0.3
0.2
0.1
Fractional Salt Content.
Precipitated
Dissolved
$MgCl_2$ · 12 H_2O −36°C
NaCl, 2 H_2O −22.9°C
Na_2SO_4 · 10 H_2O −8.2°C
-ve Temperature in°C
0 2 4 6 8 10 12 14 16 18 20 22 24 26 28 30 32 34 36 38 40

alone is usually unambiguous. Below -8.2°C, $Na_2SO_4.10\ H_2O$ is the first salt to precipitate, so that on migration of brine in the ice, the relative local concentrations of ions in the ice will be altered. In this case, the specification of salinity alone is not always sufficient to account for all of the ice's properties. It should be noted however, that the dependence of the properties of sea ice on the salinity is greater above -8.2°C, in which region knowledge of the salinity alone is sufficient unless the ice concerned has undergone a significant temperature excursion to colder temperatures and returned. Between -8.2 and -23°C, even the complete absence of $Na_2SO_4.10\ H_2O$ crystals in a particular region of ice will affect the specific heat of 10‰ saline ice by less than 1% at -20°C and 2% at -10°C. For ice of lower salinity, this error will be even less. In geophysical investigations, this is not a serious discrepancy.

Theories based on the salinity of ice expressed in terms of ions present would be time dependent and bound to the thermal history of the ice concerned. The complexity of the resulting mathematical expressions would preclude their use in any practical application.

A result of many measurements by Malmgren in the Arctic Ocean (Ma33), was to show that the salinity calculated from chlorinity differed from that found by hydrometric determinations, by less than 5% for given ice samples. This leads to the belief that the use of the concept of salinity usually results in good approximation in describing the thermal behaviour of sea ice. It should be noted however, that the ionic analysis of the upper 10 cm. of sea ice by Addison (Ad60), has shown that significant variations in the relative ionic concentrations may occur.

It is important to note that in the results of Nelson and Thompson shown, the usual concept of salinity is not used. The composition is given by the fractional salt content, or ratio of the dissolved salts to pure water. For dilute solutions, the difference between salinity and fractional salt content may often be inappreciable, but it is most important when discussing solutions having the concentrations of the brines trapped in sea ice.

1.2 The Specific Heat of Ice between the Freezing Point and -8.2°C.

There is no substitution of the ions listed earlier in the ice lattice, so that it is reasonable to assume that at the freezing point, the brine in the interior cells has the same salt content as the sea water from which the ice was formed.

If σ is the salinity of the sea ice as a whole, and s the fractional salt content of the brine according to the usage of Nelson and Thompson, within the ice at a temperature θ, then the total mass of pure water in unit mass of sea ice at that temperature is given by:

$$w = \frac{\sigma}{s} \qquad (1.2.1)$$

and the mass of pure ice by:

$$m = 1 - \sigma - \frac{\sigma}{s} \qquad (1.2.2)$$

A change in temperature of the ice causes a change in fractional salt content of the brine because of further freezing, and the difference in mass of unfrozen water per unit mass of sea ice may be expressed as:

$$dw = \frac{\sigma}{s^2}\, ds \qquad (1.2.3)$$

Figure (1.1.i) shows that the relation between s and θ is linear over the range being considered, so that:

$$s = \alpha\theta \qquad (1.2.4)$$

This linear relationship between s and θ is the sole reason for keeping the concept of fractional salt content for the brine. If the salinity of the brine is given by σ_b , then we have:

$$s = \frac{\sigma_b}{1 - \sigma_b}$$

so that the function connecting σ_b and θ is too complex for a simple interchange of variables.

Using equation (1.2.4) to eliminate s from (1.2.3), we obtain:

$$dw = - \frac{\sigma}{\alpha\theta^2} d\theta \qquad (1.2.5)$$

Essentially the specific heat of sea ice depends on the amount of water substance changing state during temperature changes, and the specific heats of pure ice and water. Since the direct contribution to the specific heat of sea ice of 4‰ salinity by the thermal capacity of its salts is of the order of 0.0008, this is considered negligible. The effects of heats of crystallisation (or dilution) are also neglected, since for example according to data quoted by Lange (La52), the infinite dilution of 0.004 gm. of NaCl involves less than 0.008 calories. Considering the small change in dilution over a range of 1°C, the importance of this term vanishes completely, even though it may be of the order of ten times as large for an equal amount of sodium sulphate.

The heat dQ absorbed by unit mass of sea ice during a temperature increase of $d\theta$ can thus be written as:

$$dQ = dwL_i + (1 - \sigma - \frac{\sigma}{s}) \, c_i \, d\theta + \frac{\sigma}{s} c_w \, d\theta \qquad (1.2.6)$$

where c_w is the specific heat of water, c_i that of pure ice and L_i its latent heat of formation. The specific heat of sea ice then follows from equations (1.2.4,5,6):

$$c_s = -\alpha L_i \frac{\sigma}{s^2} + (1 - \sigma - \frac{\sigma}{s})\, c_i + (\frac{\sigma}{s})\, c_w$$

$$c_s = -\frac{\sigma}{\alpha\theta^2} L_i + \frac{\sigma}{\alpha\theta}(c_w - c_i) + c_i \qquad (1.2.7)$$

the term σc_i may be considered negligible for natural sea ice.

Table (1.3.i) shows the results of calculation, using c.g.s. values of $L_i = 79.69$, $c_i = 0.48$, $c_w = 1.01$ and $\alpha = -0.0182^\circ C^{-1}$, for a number of ice salinities.

1.3 The Specific Heat of Ice between -8.2 and -23°C.

The results summarized in figure (1.1.i) indicate that a continuous deposition of $Na_2SO_4.10\ H_2O$ only, takes place between -8.2 and -23°C. In this range it is convenient to consider s gm. of dissolved salt and p gm. of precipitate (not including its water of crystallization) to be associated with each gm. of water. Assuming a linear rate of deposition of $Na_2SO_4.10\ H_2O$, the quantity of precipitate at any temperature can be calculated by extrapolating the initial section of the phase graph as shown. This extrapolated graph then indicates the salinity of the brine as it would have been had no crystallization taken place, so that the difference between the actual and projected values is equal to the corresponding relative mass of precipitate. In 1 gm. of sea ice there are thus w gm. water, ws gm. dissolved salt, and wp gm. of precipitated salt with which βwp gm. of water are combined in crystals. For $Na_2SO_4.10\ H_2O$, $\beta = 1.27$. Thus in general, the mass of unfrozen pure water is given by:

$$w = \frac{\sigma}{s+p} \qquad (1.3.1)$$

and the mass of pure ice by:

$$m = 1 - \sigma - \frac{\sigma}{s+p}(1 + \beta p) \qquad (1.3.2)$$

The change in mass of unfrozen water substance per unit mass of sea ice for a change in salinity ds and associated precipitate dp is:

$$dw = -\sigma\frac{ds+dp}{(s+p)^2} \qquad (1.3.3)$$

Again, figure (1.1.i) shows that:

$$s+p = \alpha\theta \quad \text{and} \quad p = \alpha'\theta \qquad (1.3.4)$$

hence:

$$dw = -\frac{\sigma}{\alpha\theta^2}\, d\theta \qquad (1.3.5)$$

as before.

The heat dQ absorbed by unit mass of sea ice during a temperature increase of $d\theta$ is now:

$$dQ = dwL_i + \left(1-\sigma-\frac{\sigma}{s+p}(1+\beta p)\right)c_i\, d\theta + \left(\frac{\sigma}{s+p}\right)c_w\, d\theta + \left(\frac{\sigma}{s+p}\,.p(1+\beta)\right)c_h\, d\theta \qquad (1.3.6)$$

where c_h is the specific heat of the precipitated hydrate. The last term of equation (1.3.6) accounts for the direct contribution of the specific heat of sodium sulphate decahydrate crystals. Using equations (1.3.4,5,6) the specific heat of sea ice follows:

$$c_s = -\frac{\sigma}{\alpha\theta^2}L_i + \frac{\sigma}{\alpha\theta}(c_w - c_i) + c_i - \frac{\sigma\alpha'}{\alpha}\left(\beta c_i - (1+\beta)\, c_h\right)$$

Since $\frac{\alpha'}{\alpha} < 1$, and βc_i and $(1+\beta).c_h$ are of the same order of magnitude, the last term may be neglected, so that we have:

$$c_s = -\frac{\sigma}{\alpha\theta^2}L_i + \frac{\sigma}{\alpha\theta}(c_w - c_i) + c_i \qquad (1.3.7)$$

Calculations with this formula, with c_i varying monotonically from 0.48 to 0.46, and other constants as before in section 2, complete Table

(1.3.i). The information contained in this table is presented in figure (1.4.ii) in graphical form.

1.4 Latent Heat of Ice Formation.

The presence of salts in water depresses the freezing point by an amount which can be determined from the temperature-composition graph; at this temperature a definite amount of pure ice will form, enclosing brine having the salinity of the sea water. The amount of pure ice present in unit mass of sea ice at the temperature of freezing is: $(1 - \sigma - \frac{\sigma}{s})$. For ice frozen from water of salt content s, the latent heat of formation is thus:

$$L_s = (1 - \sigma - \frac{\sigma}{s}) \cdot L_i \qquad (1.4.1)$$

Table (1.4.i) shows the latent heat calculated as a function of ice salinity.

When the temperature of sea ice is increased, brine cells within the ice become more dilute by melting ice. This process continues until all the ice is molten. The resulting brine at this stage has a salinity equal to that of the original ice, so that for ice of salinity 4‰, the final melting point is about -0.2°C. The heat required in this process must be considered as specific heat, as it is associated with a continuous change in temperature. One is thus forced to conclude that a latent heat, which according to the usual concept implies a release or absorption of heat at constant temperature, does not exist during the melting of sea ice.

The apparent latent heat anomaly of sea ice is explained by the fact that on initial freezing, the ice is in contact with sea water, from which however, the ice on the surface of the cover, or ice removed for observation, is usually isolated. A true latent heat could be observed were ice to be

Table (1.3.i)

The Specific Heat of Sea Ice between -2 and -23°C.

Salinity of Ice in ‰	Temperature in °C										
	-2	-4	-6	-8	-10	-12	-14	-16	-18	-20	-22
0	0.48	0.48	0.48	0.48	0.48	0.47	0.47	0.47	0.47	0.47	0.46
1	1.61	0.77	0.60	0.55	0.52	0.51	0.50	0.49	0.48	0.48	0.47
2	2.73	1.05	0.73	0.62	0.57	0.54	0.52	0.51	0.50	0.49	0.49
4	4.97	1.62	0.98	0.77	0.66	0.61	0.57	0.55	0.53	0.52	0.51
6	7.22	2.19	1.21	0.91	0.75	0.67	0.62	0.59	0.56	0.54	0.53
8	9.46	2.75	1.47	1.05	0.85	0.74	0.67	0.62	0.59	0.57	0.55
10	11.71	3.32	1.71	1.20	0.94	0.80	0.72	0.66	0.62	0.59	0.57

melted while in contact with sea water of constant concentration. This for example occurs during the final stages of the breakup of an ice cover, when small floes are awash in the sea.

Since the bulk of the ice within a cover is usually not in contact with sea water, it is necessary to consider the specific heat of established ice between its final freezing point and the final melting point. The temperature records of Iakovlev (Ia55), kept on an arctic ice island and partially reproduced in figure (3.5.i), show that during July and August the upper ice surface is between 0 and -1°C, with all of the ice at a temperature above the initial freezing point. It is thus clear that knowledge of the specific heat of sea ice is necessary at temperatures above freezing point.

The specific heat of ice at temperatures higher than -2°C, calculated from equation (1.2.7), is also tabulated in (1.4.i). Figure (1.4.ii) shows the specific heat of ice as a function of salinity over the entire temperature range considered in sections 1.3 and 1.4.

Using equation (1.2.7), it is possible to calculate the heat Q_m, required to melt unit mass of ice at a certain initial temperature θ_o.

$$Q_m = \int_{\theta_o}^{\theta_m} \left(- \frac{\sigma}{\alpha\theta^2} L_i + \frac{\sigma}{\alpha\theta} (c_w - c_i) + c_i \right) d\theta \qquad (1.4.2)$$

where $\theta_m = \frac{\sigma}{\alpha}$ is the final melting point.

Completing the integration of (1.4.2), we have:

$$Q_m = (L_i - c_i\theta_o) (1 - \frac{\sigma}{\alpha\theta_o}) + \frac{(c_w - c_i)\sigma}{\alpha} \ln \frac{\sigma}{\alpha\theta_o} \qquad (1.4.3)$$

inserting the c.g.s. values $L_i = 79.67$, $c_i = 0.48$, $\theta \geqslant -8$, $c_w = 1.0$ and $\alpha = - 1.8 \times 10^{-2}$, enables the compilation of table (1.4.iii) below.

SPECIFIC HEAT OF SEA ICE.

Figure (1.4.ii).

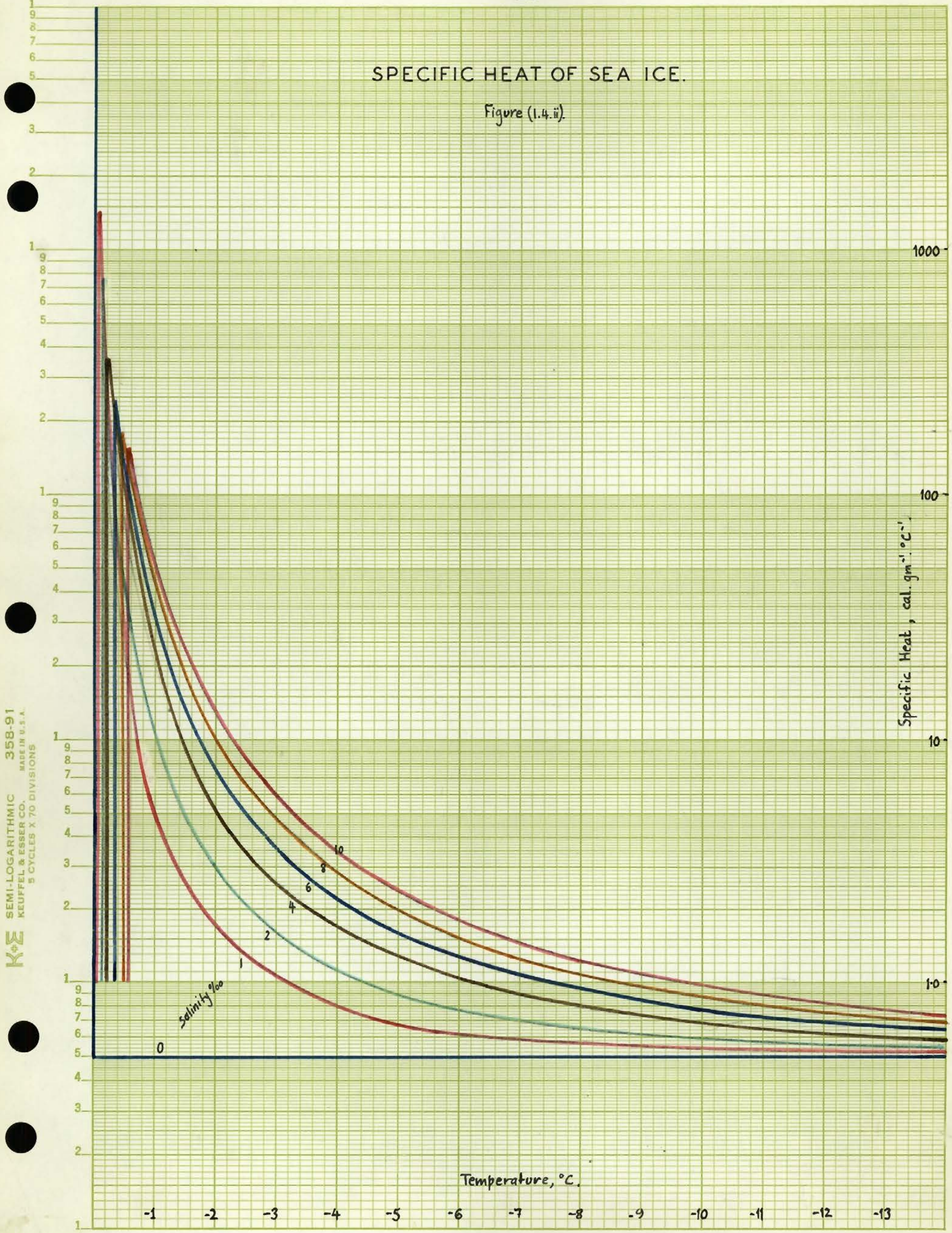

Table (1.4.i)

Latent Heat of Sea Ice.

L.H. of Formation	Final M.P.	Max. S.H.
79.69 $cal.gm^{-1}$	$0^{\circ}C$	∞ $cal.gm^{-1}{}^{\circ}C^{-1}$
77.6	-0.05_6	1435
75.1	-0.11	718
70.4	-0.22	359
65.8	-0.33	240
61.3	-0.44	180

Table (1.4.iii)

Heat Required for the Complete Melting of 1 gm. of Isolated Sea Ice.

Salinity of Ice, in ‰	Initial Temp. -0.5	-1.0	-2.0 °C
0	79.92	80.15	80.63
1	71.11	75.79	78.50
2	62.43	71.39	76.43
4	44.85	62.70	71.94
6	26.77	53.64	67.52
8	9.63	45.08	63.25

The above applies to ice frozen from sea water of 34‰ salinity, or having a fractional salt content of 0.035.

In concluding this theoretical discussion, the recent work of Anderson (An60) on this subject should be discussed. The theoretical specific heats presented by him are based on the original work of Malmgren (Ma33). Anderson's definition of the specific heat as the heat involved in a one degree temperature change is different from the conventional definition of this property, in that the former is given by the gradient of the chord joining two points and the latter by that of the tangent at a given point on the temperature curve. The finite difference definition leads to the peaks in the specific heat curve at the melting point being less pronounced. Anderson shows large discontinuities in the specific heat of sea ice at the temperatures of the commencement of precipitation of some of the salts, but notably not sodium sulphate. The tabulated results appear to attribute this effect to heats of crystallisation, or solution. Because precipitation on cooling proceeds gradually, and because we have noted earlier that 0.004 gm. of NaCl absorbs less than 0.008 calories on infinite dilution, these discontinuities are unlikely. A second set of breaks near to the precipitation point for $MgCl_2$ would actually be expected to be of opposite sign, because of the positive heat of solution. The author of this thesis was not able to observe discontinuities in the rate of melting of sea ice. In these experiments samples of ice were allowed to melt in open vacuum flasks at constant room temperature, the temperature being measured at two minute time intervals in the neighbourhood of the sodium chloride $-23^{\circ}C$ and the sodium sulphate decahydrate $-8.2^{\circ}C$ points. An examination of a number of sea ice temperature profiles also failed to show a preference of the ice to remain at these temperatures.

1.5 The Measurement of the Specific Heat of Sea Ice.

The insufficiency of published data on the specific heat of saline ice has made it desirable to develop a method of checking the validity of the theoretically calculated values. There is a particular need for measurements which extend into the temperature interval between the freezing and final melting points for an extensive range of salinities.

Because the specific heat of sea ice is a continuous non-linear function of the temperature, it would be extremely tedious and the results of questionable accuracy, to measure the specific heat directly over the small temperature intervals necessary. Near to the melting point especially, the intervals would have to be so minute, that normal laboratory thermometers capable of resolving to within $0.02^{\circ}C$ are inadequate. Both Malmgren (Ma33) and Nazintsev (Na59) preferred to work over intervals of some $2^{\circ}C$, and thus obtained mean values for the specific heat over that temperature range. An alternative procedure has been chosen in the present instance. The total heat involved per unit mass of sea ice over an arbitrary temperature interval of up to several degrees centigrade was compared with the corresponding theoretical definite integral over the same range.

Electrical heating of samples in a vacuum flask calorimeter was chosen as the most convenient simple laboratory method for the determination of specific heats. In order to ensure a uniform temperature distribution, it is necessary to immerse ice samples in a liquid which is immiscible with water and which does not dissolve the inorganic salts found in sea ice. The liquid must have no components changing phase over a temperature range extending from about -40° to $+ 30^{\circ}C$. Normal heptane is a suitable liquid, being a pure hydrocarbon freezing at $-90.6^{\circ}C$ and boiling at $98.4^{\circ}C$.

The mixture in the vacuum flask was heated electrically through a central heating coil, the energy being uniformly distributed by a stirring rod surrounding the coil. A source of power at constant voltage was arranged by having a 12 volt accumulator on continual charge from a primary power source. A second heating coil duplicating that in the calorimeter was connected across the battery when the calorimeter's heating coil was not in operation. As the charging current from the primary source was adjusted to match the discharge through one of the heating coils, there was no perceptible change in the accumulator's condition during the calorimetry. This greatly simplified the accurate assessment of the energy absorbed by the mixture in the calorimeter.

Initially it was necessary to determine the thermal water equivalent of the calorimeter and the specific heat of normal heptane. This was accomplished using distilled water and pure ice respectively as standards. The

Table (1.5.ii)

Salinity in ‰	Temperature Range in °C.	Change in Heat Content in cal. gm.$^{-1}$. Exptl. Value	Max. possible Error	Theoretical Value	Uncertainty
1.2	- 1.24 -0.48	5.80	1.1	6.35	0.12
	- 4.44 -0.74	7.84	0.55	7.75	0.16
	- 6.34 -0.62	10.0	0.77	10.6	0.21
	-10.38 -2.54	5.24	0.32	5.36	0.11
	-24.22 -2.86	11.6	0.6	12.0	0.24
2.5	- 3.24 -1.00	9.05	0.85	8.75	0.18
	- 6.02 -1.16	10.1	0.7	10.1	0.2
	- 7.22 -0.84	14.2	0.9	14.7	0.3
	- 9.30 -0.52	26.2	1.6	24.2	0.5
	-25.34 -3.02	15.5	0.9	14.1	0.3
4.4	- 0.86 -0.58	12.1	4.9	10.2	0.2
	- 2.86 -0.88	14.7	1.5	16.4	0.3
	- 8.36 -1.24	15.9	1.0	16.8	0.3
	-24.68 -3.78	15.0	0.8	14.4	0.3
	-26.20 -3.64	12.1	0.6	11.4	0.2
9.6	- 5.30 -0.64	55.8	4.0	60.6	1.3
	-10.36 -0.74	56.1	3.4	58.2	1.2
	-11.40 -1.36	34.9	2.0	32.7	0.7
	-23.72 -4.00	20.7	1.1	19.0	0.4
	-24.56 -2.88	22.6	1.2	24.2	0.5

specific heat of a sample of sea ice was then determined by using a mixture of approximately 300 gm. of small pieces of ice and 300 gm. normal heptane. After temperature equilibrium, this mixture was heated at the rate of about 50 watt for times of the order of ten minutes, the resulting change in temperature being observed.

The electrical method of calorimetry necessitates only one temperature difference being measured. An alternative method involving the method of mixtures required two temperature differences to be observed, and because the thermometry is crucial, this latter method proved less satisfactory.

The samples of sea ice used in the calorimetry were crushed into small pieces which were then thoroughly mixed in a large cold container. Part of the crushed ice was removed and its melt brought to 15°C for a salinity determination by calibrated hydrometer, the remainder being used in a number of trials in the calorimeter.

Table (1.5.ii) summarizes the results of the experimental determinations. When the amplitudes calculated for each result are taken into account, there is an overlap between experimental and theoretical values in each case. The error in the experimental determinations is due mainly to lack of accuracy in the measurement of the temperature interval, and to uncertainty in the specific heat for normal heptane and the quantity of electrical power supplied. The accuracy of the theoretical values depends mainly on the validity of the phase diagram referred to earlier.

CHAPTER 2

THE THERMAL CONDUCTIVITY OF SEA ICE

2.1 Introduction.

The components of sea ice, namely pure ice, brine, air, and below -8.2°C, solid salt crystals, have widely differing thermal conductivities. The thermal conductivity is thus strongly dependent on its composition, which may be specified by the density, salinity and temperature.

Anderson's approach of neglecting the presence of air bubbles in sea ice, has prevented his theory from demonstrating the two interesting and important assymptotic tendencies of the thermal conductivity. As will be shown, this quantity is mainly determined by the salinity at high temperatures and by the density at low temperatures. This is because the salinity determines the amount of brine, whose relative volume becomes more important near to the melting point. At the lower temperature range when the ice is largely solid, the most important factor in the density is the air bubble content.

As in the discussion of specific heat, it is simplest to consider ice in the temperature range between the freezing point and -8.2°C, below which the precipitation of $Na_2SO_4 . 10\ H_2O$ commences and complicates analysis. As the relative amount of liquid present in the ice becomes large towards the final melting point, the discussion of conductivity becomes meaningless as the increased mobility of the brine permits convective heat transfer.

2.2 The Composition and Air Bubble Content of Sea Ice above $-8.2^{o}C$.

If the salinity of the ice is σ and the fractional salt content of the enclosed brine is s, then the mass of unfrozen brine in unit mass of sea ice is given by:

$$b = \frac{\sigma}{s} + \sigma \tag{2.2.1}$$

and the mass of pure ice by:

$$m = 1 - \sigma - \frac{\sigma}{s} \tag{2.2.2}$$

the mass of air being negligible.

By volume however, unit mass of sea ice contains a volume $(\frac{\sigma}{s}+\sigma).\frac{1}{\rho_w.(1+s)}$ of brine, and $\frac{1-\sigma-\frac{\sigma}{s}}{\rho_i}$ of ice; ρ_w and ρ_i being the densities of pure water and ice respectively. Thus unit volume of sea ice contains a volume of brine given by:

$$V_b = \rho_s \, \sigma . \frac{1+s}{s} . \frac{1}{\rho_w(1+s)} = \frac{\sigma \rho_s}{s \rho_w} \tag{2.2.3}$$

and pure ice by:

$$V_i = \frac{\rho_s}{\rho_i}\left(1 - \sigma - \frac{\sigma}{s}\right) \tag{2.2.4}$$

where ρ_s is the density of sea ice.

It is now seen that the volume of air contained in unit volume of sea ice is given by:

$$\nu = 1 - \rho_s \left(\frac{\sigma}{s \rho_w} + \frac{1-\sigma-\frac{\sigma}{s}}{\rho_i} \right) \tag{2.2.5}$$

In the range being considered, $\rho_w = 0.999$, $\rho_i = 0.917$, and $s = \alpha\theta$, where θ is the temperature and $\frac{1}{\alpha} = -55$ (from the results of Nelson and Thompson).

Inserting these values:

$$\nu = 1 - \rho_s \left(\frac{1 - \sigma}{0.917} + \frac{4.98\sigma}{\theta} \right) \qquad (2.2.6)$$

Using this equation it is possible to calculate the fractional volume of air bubbles in sea ice as a function of temperature, salinity and density, as is tabulated in (2.2.i) and shown graphically in figure (2.2.ii).

2.3 The Density of Sea Ice.

From equation (2.2.6) it is seen that:

$$\rho_s = \frac{1 - \nu}{\left(\frac{1 - \sigma}{0.917} + \frac{4.98\sigma}{\theta}\right)} \qquad (2.3.1)$$

Since the second term in the denominator is very small compared with the first, the following approximation is sufficient:

$$\rho_s = \frac{1-\nu}{1-\sigma} \left(1 - \frac{4.57\sigma}{\theta} \right) \times 0.917 \qquad (2.3.2)$$

The second term in the bracket of (2.3.2) is positive because θ is always negative, hence the density appears to increase with salinity, on the assumption that the air bubble content ν, of established ice remains sensibly constant. For a given sample of ice, the density is significantly temperature dependent near to the freezing point. This dependence diminishes considerably at lower temperatures, the change in density of a sample of normal sea ice between -10 and -20^{o}C is only of the order of 0.1%. Never the less, it follows that quotation of more than 3 figures is unjustifiable in the case of a density measurement, whose results are not corrected to a standard temperature.

In nature, because faster growing ice tends to capture more air bubbles as well as more concentrated brine, it follows that an increase in salinity

Table (2.2.i)

Fractional Volume of Air Bubbles in Sea Ice.

Salinity 0‰	Ice Density gm.cm.$^{-3}$				
Temperature, ^{o}C	0.850	0.875	0.900	0.925	0.950
0 to -8.2^{o}C	7.3%	4.6%	1.9%	-	-
Salinity 2‰					
-0.5	9.2%	6.5%	3.8%	1.2%	-
-1.0	8.3	5.6	3.0	0.3	-
-2.0	7.9	5.2	2.5	-	-
-4.0	7.7	5.0	2.3	-	-
-8.0	7.6	4.9	2.2	-	-
Salinity 4‰					
-0.5	11.1%	8.4%	5.8%	3.2%	0.6%
-1.0	9.4	6.7	4.0	1.4	-
-2.0	8.5	5.8	3.1	0.5	-
-4.0	8.1	5.4	2.7	0.0	-
-8.0	7.9	5.2	2.5	-	-
Salinity 8‰					
-0.5	14.8%	12.3%	9.8%	7.3%	4.8%
-1.0	11.4	8.8	6.2	3.6	1.0
-2.0	9.7	7.1	4.4	1.8	-
-4.0	8.9	6.2	3.5	0.9	-
-8.0	8.5	5.8	3.1	0.4	-

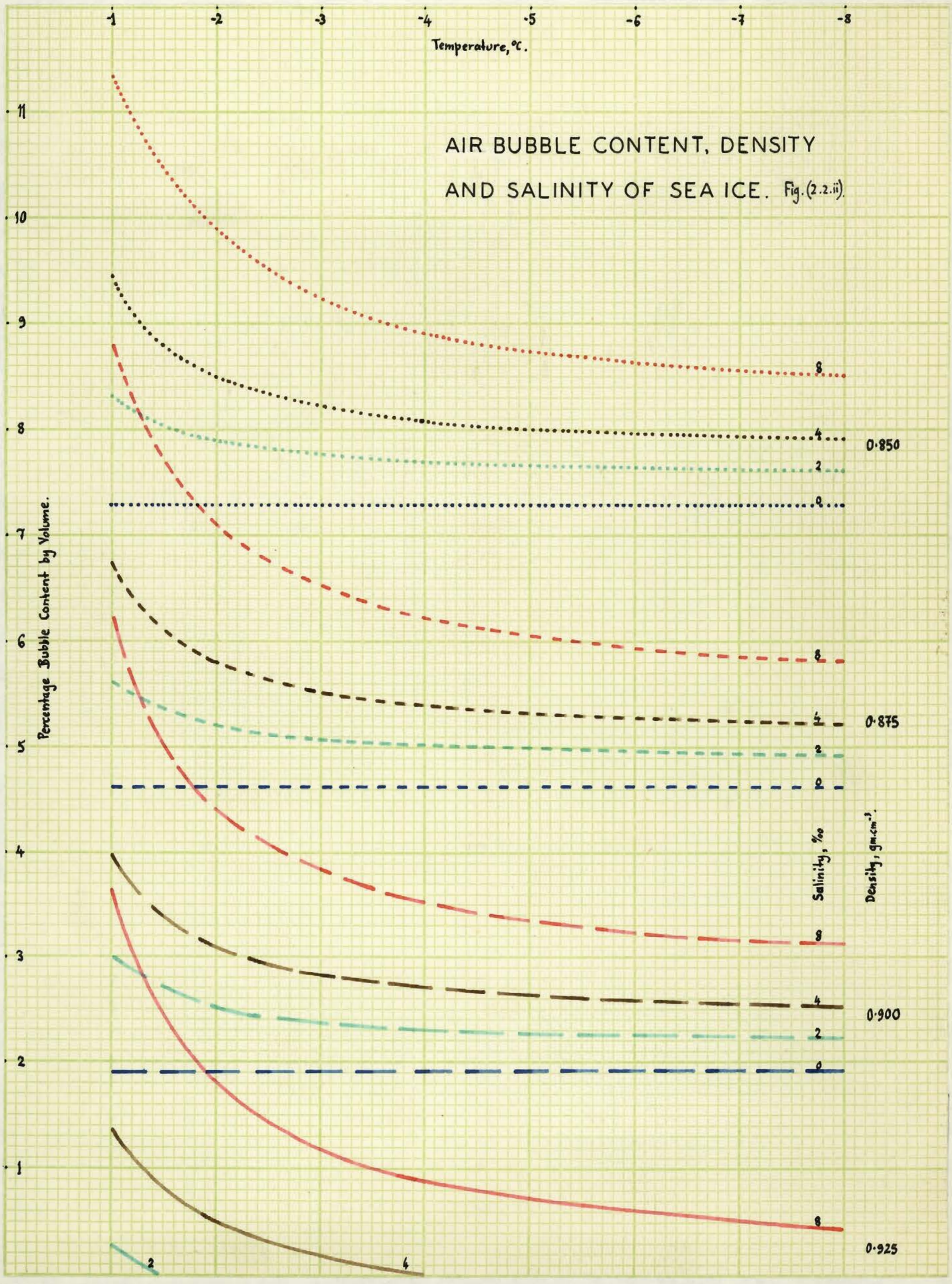
AIR BUBBLE CONTENT, DENSITY
AND SALINITY OF SEA ICE. Fig. (2.2.ii).
Temperature, °C.
-1
-2
-3
-4
-5
-6
-7
-8
Percentage Bubble Content by Volume.
11
10
9
8
7
6
5
4
3
2
1
Salinity, ‰
Density, gm.cm⁻³.
0·850
0·875
0·900
0·925
8
4
2
0

is accompanied by an increase in air bubble content. Since the effect of these two changes is for the former to increase and the latter to decrease the density, this quantity displays a constancy remarkable for a sea ice property.

2.4 Models for the Calculation of the Thermal Conductivity of Sea Ice.

Established sea ice has been shown by Langleben (La60) to consist of pure ice enclosing vertical cylinders of approximately elliptical cross-section of brine, whose lengths, especially at higher temperatures are long compared with their average diameters. Anderson (An60), has preferred to calculate the thermal conductivity on the basis of assuming spherical brine pockets. This assumption may have greater validity at lower temperatures. At these temperatures however, the small amount of brine plays a less significant role in determining the conductivity of the ice than at higher temperatures. It thus seems more reasonable to choose the shape of brine inclusion predominating at those higher temperatures where the brine is more important.

Since the flow of heat occurs along the direction of the cylindrical axes, a short vertical length of sea ice may be considered as a system of parallel connected conductors. It is immaterial for the purpose of calculation, whether the conductors are specially grouped or not; the determining factor for the total conduction being the relative cross-sectional areas of pure ice and brine presented to the heat flux. It is, of course, assumed that no convective movement of brine takes place in the narrow cylinders. It is interesting to note that the thermal conductivity for horizontal heat flow, for which the brine and pure ice appear series connected, is much less than for vertical heat flow. It might thus be expected that non-uniform heating or cooling of a sea ice surface, due to an irregular snow cover, tends to remain a local phenomenon.

Two methods of procedure are now available. One is to consider sea ice as consisting of uniformly bubbly pure ice enclosing vertical cylinders of brine. The other, is to suppose that the brine pockets are more uniformly distributed within the ice than air bubbles. The majority of the air bubbles will have been formed during the initial freezing, and be found throughout the ice. Being more or less spherical in shape, the air bubbles are certainly more uniformly distributed within the bulk of the ice. The method of calculation of the thermal conductivity will thus be to obtain an expression for the thermal conductivity of bubbly pure ice, and then to consider sea ice as a parallel connection of this material and brine.

2.5 The Effect of Air Bubbles on the Conductivity of Ice.

Maxwell (Ma91) obtained an expression for the resistivity r of a compound medium, consisting of a material of resistivity r_1 containing uniformly distributed small spheres of resistivity r_2. If there are n small spheres of radius a_1 contained in a sphere of surrounding material of radius a_2, and

$\nu = \dfrac{na_1^3}{a_2^3}$, then:

$$r = \frac{2r_1 + r_2 + \nu(r_1 - r_2)}{2r_1 + r_2 - 2\nu(r_1 - r_2)} \cdot r_2 \qquad (2.5.1)$$

Since the air bubbles within a body of ice are approximately spherical, (2.5.1) may be used to obtain an expression for the thermal conductivity of bubbly ice. If k_a, k_i, are the conductivities of air and ice respectively, and ν: 1 is the ratio of their volumes, then the conductivity of the compound medium is given by:

$$\frac{1}{k_{bi}} = \frac{\frac{2}{k_a} + \frac{1}{k_i} + \nu(\frac{1}{k_a} - \frac{1}{k_i})}{\frac{2}{k_a} + \frac{1}{k_i} - 2\nu(\frac{1}{k_a} - \frac{1}{k_i})} \cdot \frac{1}{k_i}$$

$$k_{bi} = \frac{2k_i + k_a - 2\nu(k_i - k_a)}{2k_i + k_a + \nu(k_i - k_a)} k_i \qquad (2.5.2)$$

The value of ν under given conditions has been determined in section 2.2. Using c.g.s. value 5×10^{-3} for k_i, it remains for us to assign a value for the conductivity of air.

In the range of interest, i.e. 0 to -20°C, the conductivity of air, (La52), can be taken as $(5.57 + 0.015\ \theta) \times 10^{-5}$ c.g.s., at atmospheric pressure. Assuming the formation of air bubbles immediately before freezing, these will expecience a contration in volume on the formation of pure ice. Accounting also for the hydrostatic pressure at a depth h down from sea level, the air pressure in the bubbles at this point will be given by:

$$p_h = 1.09\ p_o\ (1 + \frac{h}{1.0 \times 10^4})$$

where p_o is atmospheric pressure, and h is the depth in cm. below the surface of normal sea water, i.e. 30 to 40‰ salinity. Supposing that the conductivity of a gas is directly proportional to the pressure, we now have for -30°C:

$$k_a = 6.01 \times (1 + \frac{h}{10^4}) \times 10^{-5} \qquad (2.5.3)$$

This equation completes the information required for the calculation of the thermal conductivity of bubbly fresh water ice, some values of which are shown in table (2.5.i). Calculation shows that the change in thermal conductivity from 6.0×10^{-5} at sea level to 7.2×10^{-5} at a depth of 2 metres of the air bubbles in the ice, is not sufficient to affect the third figure for the conductivity of the compound medium.

Figure (2.5.ii) shows the thermal conductivity of fresh water ice as a function of bubble content and density.

Table (2.5.i)

The Thermal Conductivity of Bubbly Ice.

Fractional Air Bubble Content	Thermal Conductivity at Temperatures between 0^{o} -10^{o}C and Depth 4m.
0%	5.0×10^{-3} cgs.
2	4.85
4	4.70
7.5	4.46
10	4.29
15	3.96

2.6 A Model for Sea Ice Including Air Bubbles.

The nature of brine cells in sea ice has already been discussed in section 2.4, so that we shall now proceed to consider sea ice as a compound bubbly pure ice medium enclosing a number of vertical brine cylinders, whose total cross-sectional area per unit area of sea ice can be specified.

From figure (2.6.i), it may be seen that if A_{bi} and A_b are the cross-sectional areas of bubbly pure ice and brine whose normals are parallel to the heat flow respectively, and J_{bi}, J_b, J_s, represent the heat fluxes through the bubbly pure ice, brine and compound sea ice, then the following

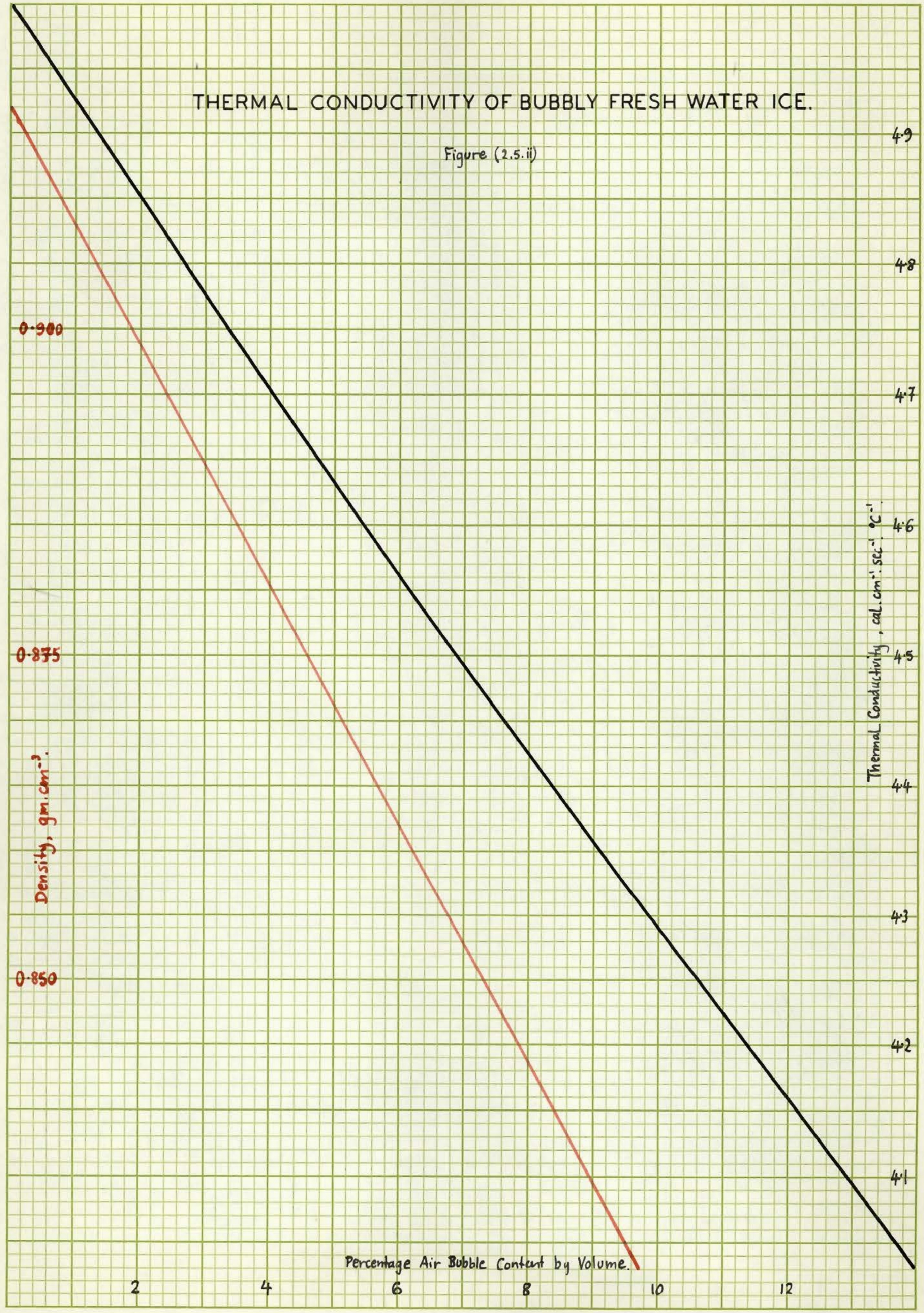
THERMAL CONDUCTIVITY OF BUBBLY FRESH WATER ICE.
Figure (2.5.ii)
0·900
0·875
0·850
Density, gm.cm⁻³.
4·9
4·8
4·7
4·6
4·5
4·4
4·3
4·2
4·1
Thermal Conductivity, cal.cm⁻¹.sec⁻¹.°C⁻¹.
Percentage Air Bubble Content by Volume.
2
4
6
8
10
12

relations hold for a section of sea ice whose ends at a vertical distance x apart, have temperatures θ_1 and θ_2:

$$\left.\begin{aligned} J_{bi} &= k_{bi} \frac{\theta_1-\theta_0}{x} \\ J_b &= k_b \frac{\theta_1-\theta_0}{x} \\ J_s &= A_{bi}J_{bi} + A_bJ_b \end{aligned}\right\}$$

where k_b is the conductivity of brine and k_s that of sea ice.

$$\text{but } J_s = k_s \frac{\theta_1-\theta_0}{x}$$

$$\therefore k_s = k_{bi}A_{bi} + k_bA_b \qquad (2.6.1)$$

The relative cross-sectional area of brine and bubbly pure ice are proportional to their relative volumes, which can be inferred from equation (2.2.3).

$$A_b : A_{bi} = \frac{\sigma\rho_s}{s\rho_w} : 1 - \frac{\sigma\rho_s}{s\rho_w}$$

and since $A_b + A_{bi} = 1$, we have for the conductivity of sea ice:

$$k_s = k_{bi}\left(1 - \frac{\sigma\rho_s}{s\rho_w}\right) + k_b \frac{\sigma\rho_s}{s\rho_w} \qquad (2.6.2)$$

where k_{bi} is given by equation (2.5.2).

Replacing s by $\alpha\theta$ as in section 2.2, we have:

$$k_s = k_{bi} - (k_{bi} - k_b)\frac{\sigma\rho_s}{\alpha\rho_w} \cdot \frac{1}{\theta} \qquad (2.6.3)$$

Although there is no systematic experimental data available on the conductivity of brine, a number of isolated determinations for solutions of several inorganic salts show that the thermal conductivity is strongly dependent on the concentration, and to a lesser extent on the temperature. Assuming that the relation between salt content and conductivity is linear for

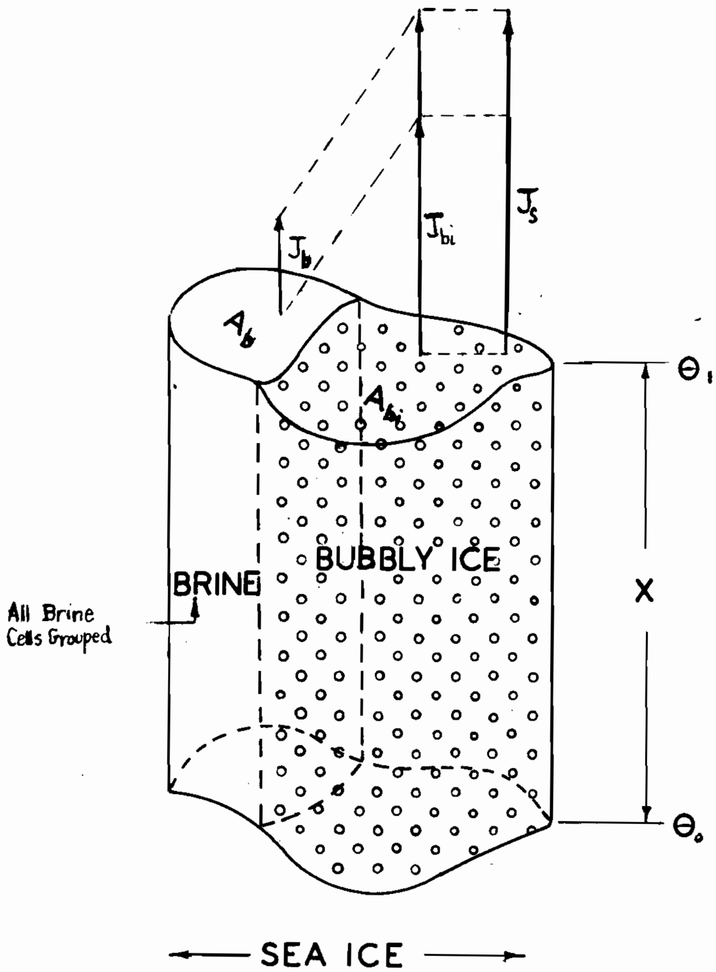

A MODEL FOR SEA ICE.

Figure (2.6.i)

salt content less than 15% at constant temperature, then on the basis of a limited number of isolated conductivity determinations for NaCl and Na_2SO_4 solutions given by Lange (La52), the conductivity of brine at 0°C may be approximated by:

$$k_b = 1.25\ (1 - s) \times 10^{-3} \qquad (2.6.4)$$

Assuming a temperature dependence similar to that for pure water suggested by Lange's data (La52), an additional factor generalizes equation (2.6.4):

$$k_b = 1.25\ (1 - s)\ .\ (1 + 0.006\ \theta) \times 10^{-3} \qquad (2.6.5)$$

Replacing s by $\alpha\theta$ and the known numerical value, i.e. -0.018 for α, we have:

$$k_b = \left(1.25 + 0.030\ \theta + 0.00014\ \theta^2\right) \times 10^{-3} \qquad (2.6.5)$$

It is now possible to calculate the thermal conductivity of sea ice as a function of temperature, salinity and density, using equations (2.6.2) and (2.6.5) in conjunction with (2.6.3), summarized below:

$$k_s = k_{bi} - (k_{bi} - k_b)\ \frac{\sigma \rho_s}{\alpha \rho_w}\ .\ \frac{1}{\theta}$$

where

$$k_{bi} = \frac{2k_i - k_a - 2\nu(k_i - k_a)}{2k_i + k_a + \nu(k_i - k_a)}\ k_i$$

and

$$k_b = \left(1.25 + 0.030\ \theta + 0.00014\ \theta^2\right) \times 10^{-3}$$

The table (2.6.ii) shows the results of calculations based on a value for pure ice at 0°C, of 5×10^{-3} cal. cm.$^{-1}$ °C^{-1} given by Dorsey (Do40). The interesting asymptotic tendencies are shown graphically in figure (2.6.iii).

Fortunately, it can be noted that at lower temperatures where equation (2.6.5) becomes less accurate, the actual value of k_b is of less importance since the relative volume of water present becomes negligible.

Table (2.6.ii)

The Thermal Conductivity of Sea Ice.

Salinity 0‰ Temperature	Density of Ice gm.cm.$^{-3}$				
	0.850	0.875	0.900	0.925	0.950
0°C	4.475 x10^{-3}	4.662	4.857	-	-
Salinity 2‰					
-1°C	4.11	4.27	4.42	4.59	-
-2	4.29	4.46	4.63	-	-
-4	4.37	4.55	4.74	-	-
-8	4.41	4.60	4.79	-	-
Salinity 4‰					
-1°C	3.75	3.89	4.01	4.15	-
-2	4.10	4.26	4.42	4.58	-
-4	4.27	4.44	4.62	4.81	-
-8	4.36	4.54	4.72	-	-
Salinity 8‰					
-1°C	3.05	3.17	3.24	3.31	3.42
-2	3.74	3.86	3.99	4.12	-
-4	4.07	4.23	4.39	4.55	-
-8	4.24	4.41	4.59	4.77	-

These values have been calculated assuming a value of 5×10^{-3} cal. cm.$^{-1}$ sec.$^{-1}$ $^{o}C^{-1}$ for the thermal conductivity of air free pure ice.

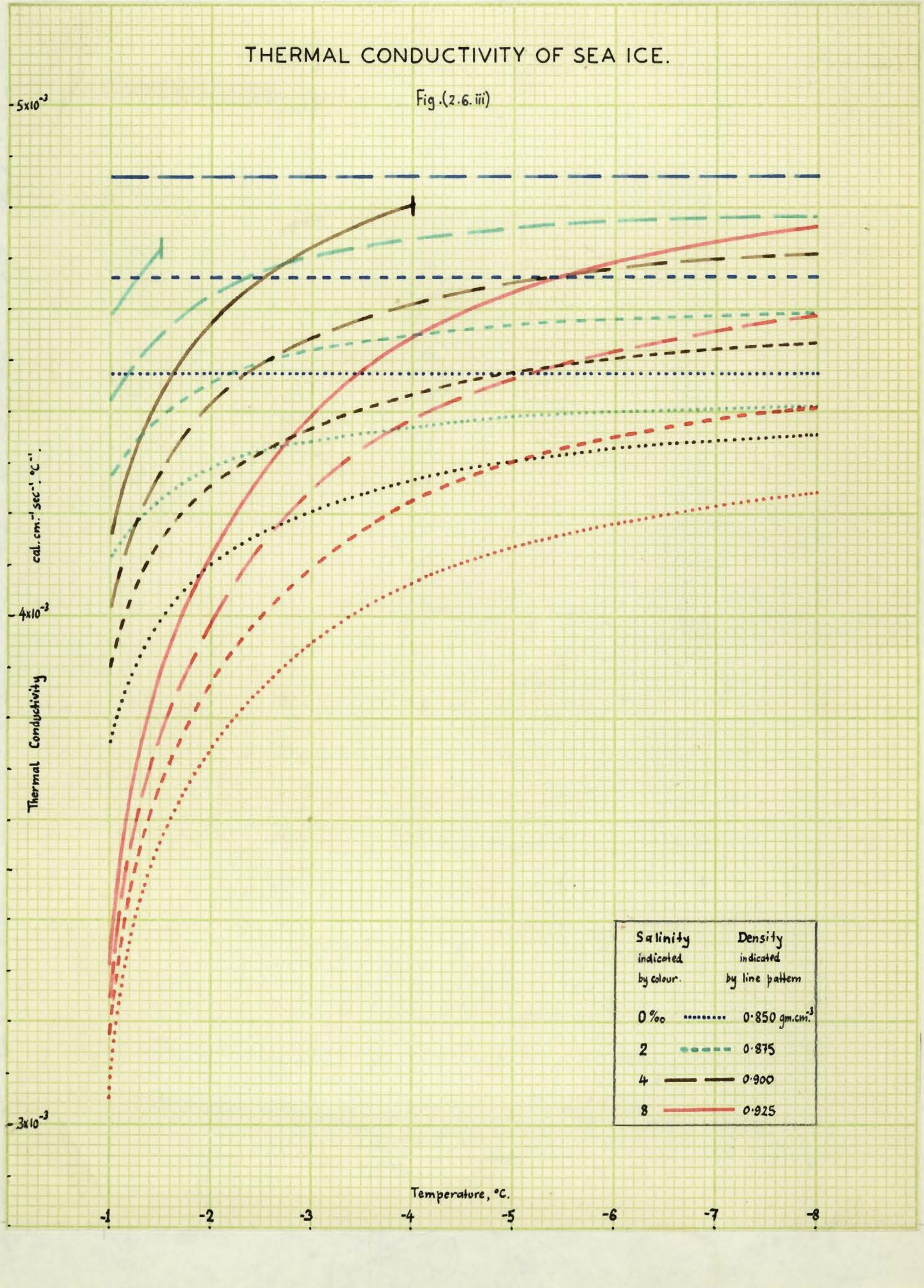
THERMAL CONDUCTIVITY OF SEA ICE.
Fig.(2.6.iii)
5x10⁻³
4x10⁻³
3x10⁻³
Thermal Conductivity cal. cm.⁻¹ sec⁻¹ °C⁻¹.
Temperature, °C.
-1
-2
-3
-4
-5
-6
-7
-8
Salinity indicated by colour.
Density indicated by line pattern
0‰ 0·850 gm.cm.⁻³
2 0·875
4 0·900
8 0·925

2.7 The Thermal Conductivity of Sea Ice below $-8.2^{\circ}C$.

As has been hinted in section 2.1, the commencement of the precipitation of solid hydrates below $-8.2^{\circ}C$, results in a rigorous theory becoming extremely involved. The lack of knowledge of the thermal conductivities of the inorganic hydrates found in sea ice and those of concentrated brines makes it unjustifiable to proceed theoretically from fundamental principles.

Inspection of the curves for the conductivities in figure (2.6.iii) leads to an alternative procedure. Since the salinity of sea ice is rarely greater than 10‰ , it is unlikely that serious discontinuities will occur in the conductivity-temperature function at temperatures where salts begin to precipitate. Already at $-8^{\circ}C$ all the curves shown in figure (2.6.iii) exhibit asymptotic behaviour. At lower temperatures, the conductivity of low salinity ice will tend to the value for fresh water ice. Using equation (2.5.2) for a uniform distribution of a large number of small centres of solid salts in a main body of pure ice, and assuming a low value, 10^{-3} c.g.s., for the conductivity of the solid salts, it is seen that a salinity of 8‰ lowers the conductivity by less than 1%. Almost all salts in the ice are precipitated by $-40^{\circ}C$, it would thus be reasonable to suppose that at this point, the thermal conductivity of a sample of sea ice could be given by the corresponding value for fresh water ice of the same density.

CHAPTER 3

THE DIFFUSION EQUATION

3.1 Introduction.

Surface temperature phenomena on an ice cover can be correlated to the rate of growth of ice at the ice-water boundary. Because the ratio of thermal conductivity to specific heat per unit volume, or thermal diffusivity, is low for ice, the rate of transmission of thermal energy is an appreciably slow process. For the purposes of heat budget calculation, an approximate estimate of the time lapse between related processes at the two boundary surfaces of the ice cover must be obtained. With suitable boundary conditions prescribed, the diffusion equation can formulate this problem. Many solutions have been given for this equation under various restrictions and some basic and more important cases are reviewed in numerous standard texts including Carslaw and Jaegar (CJ59).

3.2 The Single Discontinuous Surface Temperature Change.

This problem is well known and also discussed in general by Carslaw and Jaegar (CJ59). Because this case is the basis for the other more complex cases to be discussed, a brief resume will be given.

Consider an infinitely extending ice cover of thickness h, with the upper surface having been at a temperature θ_o for a time sufficiently long for a uniform temperature gradient to have been established. At time $t = 0$ a discontinuous temperature change to θ_1 occurs at the ice-air surface, $x = 0$.

If this new surface temperature is maintained, a new linear temperature distribution will be approached, and at any time, the temperature distribution is given by the solution of the diffusion equation:

$$\frac{\partial \theta}{\partial t} = K \frac{\partial^2 \theta}{\partial x^2} \qquad , \; K = \frac{k}{\rho c} \tag{3.2.1}$$

With the boundary conditions as shown in figure (3.2.i)

$$\theta(x,0) = \theta_o \frac{h-x}{h} , \; \theta(0,t) = \theta_1 , \; \theta(h,t) = 0 \tag{3.2.2}$$

the solution is:

$$\theta(x,t) = \theta_1 \cdot \frac{h-x}{h} + \sum_{n=1}^{\infty} \left(\frac{2(\theta_o - \theta_1)}{n\pi} \cdot \sin \frac{n\pi}{h} x \cdot e^{-\frac{n^2\pi^2 K}{h^2} \cdot t} \right) \tag{3.2.3}$$

As illustrated in figure (3.2.i), two parameters are chosen to allow equation (3.2.3) to have more general application. Depth in the ice is expressed relative to the thickness, and temperature change at any time is referred to the final temperature change possible. The total temperature change experienced at any point $x = \eta h$ where $0 \leqslant \eta \leqslant 1$ is $(\theta_1 - \theta_o) \cdot (1-\eta)$.

It is useful to calculate the times t_α elapsed when a fraction α of the total temperature change has been completed at a given depth in the ice, and (3.2.3) can be rewritten to give:

$$(1-\eta)(1-\alpha) = \sum_{n=1}^{\infty} \left(\frac{2}{n\pi} \sin \eta n\pi \cdot e^{-\frac{n^2\pi^2 K}{h^2} t_\alpha} \right) \tag{3.2.4}$$

It is interesting to note that for given η, the time t_α taken for a fractional change α to occur in the temperature, is independent of the actual magnitude of the temperature change at the upper surface.

The series of equations (3.2.4) may be calculated for different values of η and the relationship between α and t_α plotted graphically. This has been done for $\eta = \frac{1}{8}$, $\frac{1}{4}$ and $\frac{1}{2}$, the cases $\eta = 0$ and 1 being trivial.

Specification of General Temperature Distribution in Ice.

Figure (3.2.1)

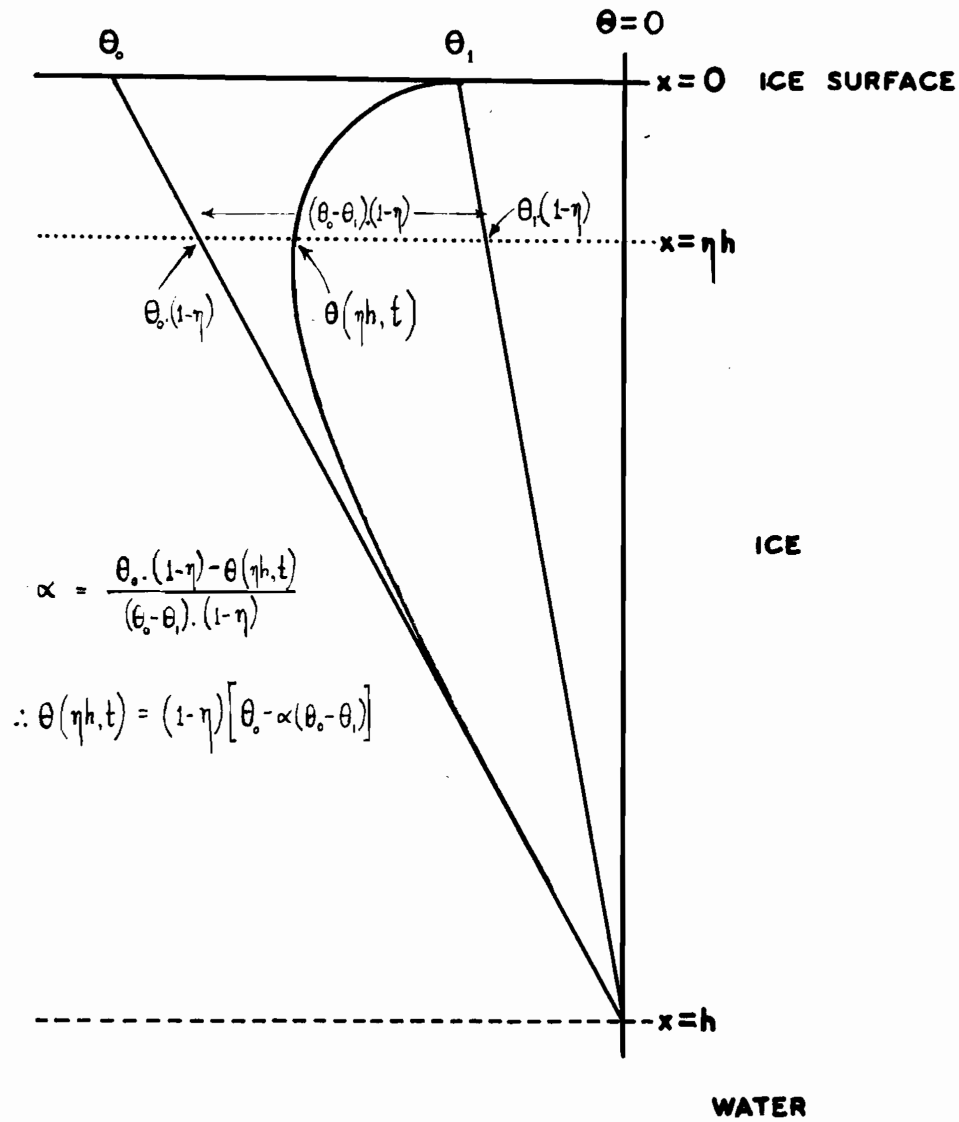

$$\eta = 0\ , \quad \alpha = 1 \quad \text{for} \quad t_\alpha \geqslant 0 \qquad \text{(a)}$$

$$\eta = 1/8\ , \quad \alpha = 1 - \sum_{n=1}^{\infty} \left(\frac{16}{7n\pi} \sin \frac{n\pi}{8} \cdot e^{-\frac{n^2\pi^2 K}{h^2} t_\alpha} \right) \qquad \text{(b)}$$

$$\eta = 1/4\ , \quad \alpha = 1 - \sum_{n=1}^{\infty} \left(\frac{8}{3n\pi} \sin \frac{n\pi}{4} \cdot e^{-\frac{n^2\pi^2 K}{h^2} t_\alpha} \right) \qquad \text{(c)} \qquad (3.2.5)$$

$$\eta = 1/2\ , \quad \alpha = 1 - \sum_{n=1}^{\infty} \left(\frac{4}{n\pi} \sin \frac{n\pi}{2} \cdot e^{-\frac{n^2\pi^2 K}{h^2} t_\alpha} \right) \qquad \text{(d)}$$

$$\eta = 1\ , \quad \alpha \to 1 \quad \text{as} \quad t_\alpha \to \infty \qquad \text{(e)}$$

The graph (3.2.ii) has been plotted for h=100 (cm.) and K=1.01 x 10^{-2} c.g.s. units. Since h and K appear only in the coefficient of t_α in the exponential term, a change in these two constants will merely alter the time scale by a simple factor. It is seen that the time required for a given change in temperature in the ice is proportional to the square of the ice thickness and inversely proportional to the thermal diffusivity.

3.3 Temperature Distributions in an Ice Cover with a Varying Surface Temperature.

The step change in surface temperature discussed in the previous section, can hardly be expected to occur where ice surfaces tend to follow the lower atmospheric temperature. In this section we will discuss the general case of an ice cover experiencing a constantly changing surface temperature not governed by a definite relationship with time. Since the diffusion equation is not separable when a boundary condition is time dependent, it is necessary to consider any continuous change as a series of steps.

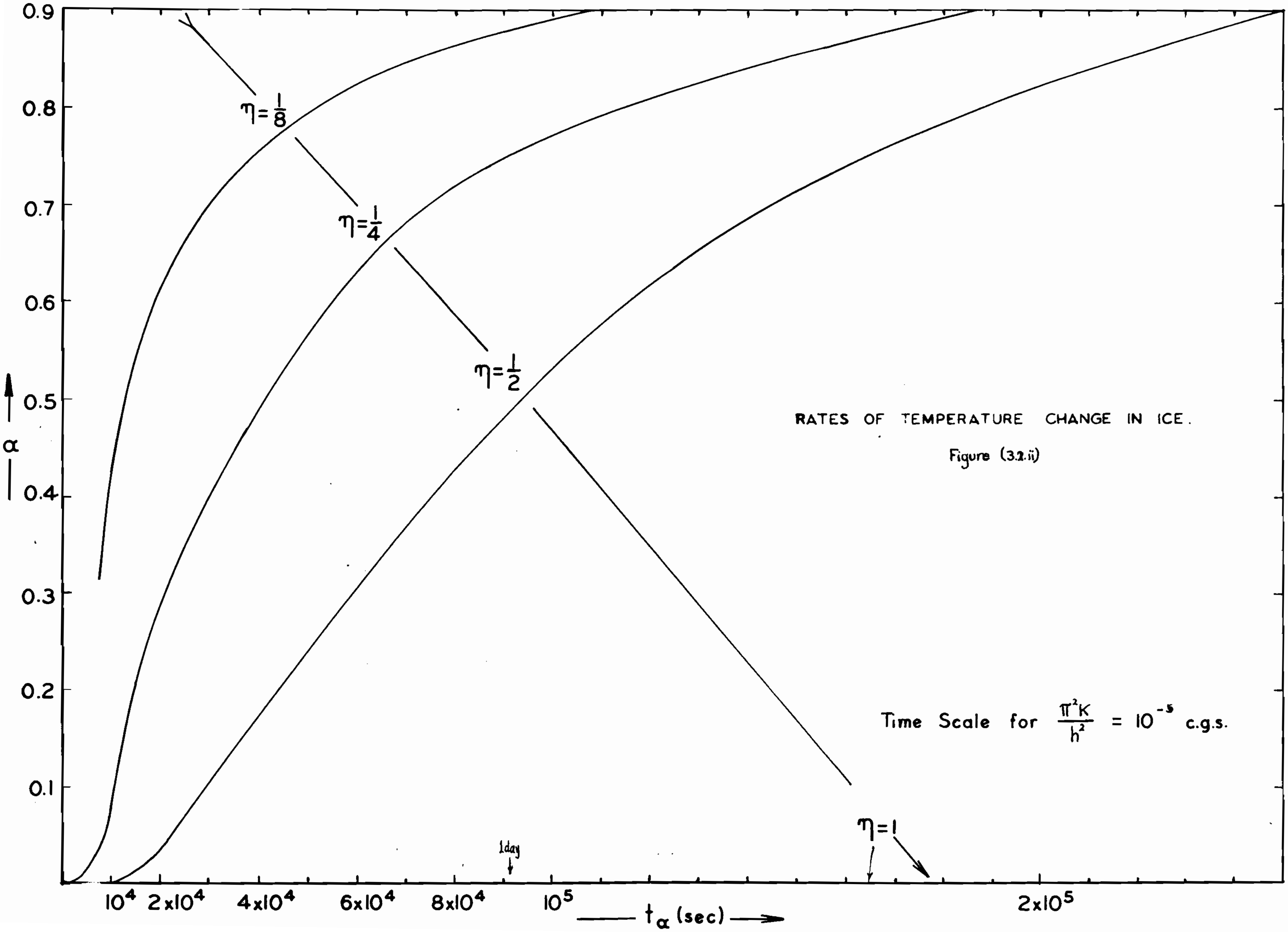

0.9
0.8
0.7
0.6
0.5
0.4
0.3
0.2
0.1
α
$\eta = \frac{1}{8}$
$\eta = \frac{1}{4}$
$\eta = \frac{1}{2}$
$\eta = 1$
1day
10^4
$2x10^4$
$4x10^4$
$6x10^4$
$8x10^4$
10^5
$2x10^5$
t_α (sec)
RATES OF TEMPERATURE CHANGE IN ICE.
Figure (3.2.ii)
Time Scale for $\frac{\pi^2 K}{h^2} = 10^{-5}$ c.g.s.

Suppose that the ice surface temperature changes abruptly from θ_0 to θ_1, θ_2, θ_3 ... θ_n at times $t = T_1$, T_2, T_3, ... T_n. It is convenient to use a special notation for the time variable, in that times between T_1 and T_2 are written $t = T_1 + t'$, and between T_2 and T_3 as $t = T_2 + t''$; in general, times between T_r and T_{r+1} are considered as $t = T_r + t^{ⓡ}$.

In the previous section, the temperature distribution, uniform at time $t = 0$, was found at time t after the surface temperature changed abruptly. It is now considered that this change from θ_0 to θ_1 occurs at time $t = T_1$, so that the solution (3.2.3) of the diffusion equation (3.2.1) is written as:

$$\theta(x,\overline{T_1+t'}) = \theta_1 \frac{h-x}{h} - \sum_{n=1}^{\infty} \frac{2(\theta_1-\theta_0)}{n\pi} \cdot \sin \frac{n\pi}{h} x \cdot e^{-\frac{n^2\pi^2K}{h^2} \cdot t'} \tag{3.3.1}$$

At time $t = T_2$, i.e. $t' = T_2 - T_1$, equation (3.3.1) provides the initial condition for the solution of the equation

$$\frac{\partial\theta}{\partial t''} = K \frac{\partial^2\theta}{\partial x^2} \tag{3.3.2}$$

which gives $\theta(x, \overline{T_2+t''})$.

The boundary conditions relevant to the solution of (3.3.2) are:

$$\theta(x,T_2) = \theta_1 \frac{h-x}{h} - \sum_{n=1}^{\infty} \frac{2(\theta_1-\theta_0)}{n\pi} \cdot \sin \frac{n\pi}{h} x \cdot e^{-\frac{n^2\pi^2K}{h^2}\overline{T_2-T_1}} \quad ;$$

$$\theta(0, \overline{T_2+t''}) = \theta_2 \;;\quad \theta(h, \overline{T_2+t''}) = 0 \tag{3.3.3}$$

In order to enable separation, a change in variable is chosen:

$$\phi(x, \overline{T_2+t''}) = \theta(x, \overline{T_2+t''}) - \theta_2 \frac{h-x}{h} \tag{3.3.4}$$

For this variable, the boundary conditions (3.3.3), become:

$$\phi(x,T_2) = -(\theta_2-\theta_1)\,\frac{h-x}{h} - \sum_{n=1}^{\infty} \frac{2(\theta_1-\theta_0)}{n\pi} \,.\, \sin\frac{n\pi}{h}x \,.\, e^{-\frac{n^2\pi^2K}{h^2}\,\overline{T_2-T_1}} \quad ;$$

$$\phi(0,\ \overline{T_2+t''}) = 0 \ ; \quad \phi(h,\ \overline{T_2+t''}) = 0 \qquad (3.3.5.)$$

Under the latter two of these restrictions, the solution of equation (3.3.2) is required to be of the form:

$$\phi(x,\ \overline{T_2+t''}) = \sum_{k=1}^{\infty} A_k \sin\frac{k\pi}{h}x \,.\, e^{-\frac{k^2\pi^2K}{h^2}\,\overline{T_2+t''}} \qquad (3.3.6)$$

Using the boundary condition for $\phi(x,T_2)$, it is seen that:

$$-(\theta_2-\theta_1)\,\frac{h-x}{h} - \sum_{n=1}^{\infty} \frac{2(\theta_1-\theta_0)}{n\pi} \,.\, \sin\frac{n\pi}{h}x \,.\, e^{-\frac{n^2\pi^2K}{h^2}\,\overline{T_2-T_1}}$$

$$= \sum_{k=1}^{\infty} A_k \sin\frac{k\pi}{h}x \,.\, e^{-\frac{n^2\pi^2K}{h^2}T_2}$$

The orthogonal properties of the sines over the interval h, then enable the evaluation of the constants A_k, in the following manner:

$$\int_0^h \sin\frac{m\pi}{h}x \,.\, \sum_{k=1}^{\infty} A_k \sin\frac{k\pi}{h}x \,.\, e^{-\frac{k^2\pi^2K}{h^2}T_2} \,.\, dx$$

$$= -\int_0^h \sin\frac{m\pi}{h}x \,.\, \left((\theta_2-\theta_1)\,\frac{h-x}{h} + \sum_{k=1}^{\infty} \frac{2(\theta_1-\theta_0)}{n\pi} \sin\frac{n\pi}{h}x \,.\, e^{-\frac{n^2\pi^2K}{h^2}\overline{T_2-T_1}} \right) dx$$

$$A_m \,.\, \frac{h}{2} \,.\, e^{-\frac{m^2\pi^2K}{h^2}T_2} = -\left(\frac{(\theta_2-\theta_1)}{m\pi} \,.\, h \right) - \left(\frac{(\theta_1-\theta_0)}{m\pi} \,.\, h \,.\, e^{-\frac{m^2\pi^2K}{h^2}\,\overline{T_2-T_1}} \right)$$

$$A_m = -\frac{2}{m\pi} \left((\theta_1-\theta_0)\, e^{\frac{m^2\pi^2K}{h^2}T_1} + (\theta_2-\theta_1)\, e^{\frac{m^2\pi^2K}{h^2}T_2} \right) \qquad (3.3.7)$$

Substitution of this expression for A_m in equation (3.3.6) gives:

$$\phi(x,\overline{T_2+t''}) = -\sum_{m=1}^{\infty} \frac{2}{m\pi}\left((\theta_1-\theta_0).e^{-\frac{m^2\pi^2K}{h^2}\overline{T_2-T_1+t''}} + (\theta_2-\theta_1).e^{-\frac{m^2\pi^2K}{h^2}t''}\right)\sin\frac{m\pi}{h}x$$

Again using the transformation (3.3.4), the expression for $\theta(x,T_2+t'')$ follows:

$$\theta(x,\overline{T_2+t''}) =$$

$$\theta_2\frac{h-x}{h} - \sum_{m=1}^{\infty}\frac{2}{m\pi}\left((\theta_1-\theta_0).e^{-\frac{m^2\pi^2K}{h^2}\overline{T_2-T_1+t''}} + (\theta_2-\theta_1).e^{-\frac{m^2\pi^2K}{h^2}t''}\right)\sin\frac{m\pi}{h}x \qquad (3.3.8)$$

Proceeding in this manner, the general solution for n temperature changes may be obtained:

$$\theta(x,T_n+t^{(n)}) = \theta_n\frac{h-x}{h} - \sum_{m=1}^{\infty}\frac{2}{m\pi}\left((\theta_1-\theta_0)\ .\ e^{-\frac{m^2\pi^2K}{h^2}\overline{T_n-T_1+t^{(n)}}} + \ldots\right.$$

$$\left.\ldots + (\theta_r-\theta_{r-1})\ .\ e^{-\frac{m^2\pi^2K}{h^2}\overline{T_n-T_r+t^{(n)}}} + \ldots\right)\sin\frac{m\pi}{h}x$$

which equation can be written as:

$$\theta(x,T_n+t^{(n)}) =$$

$$\theta_n\frac{h-x}{h} - \sum_{m=1}^{\infty}\sum_{r=1}^{n}\frac{2}{m\pi}(\theta_r-\theta_{r-1})\ .\ e^{-\frac{m^2\pi^2K}{h^2}\overline{T_n-T_r+t^{(n)}}}\ .\ \sin\frac{m\pi}{h}x \qquad (3.3.9)$$

3.4 Temperature Distribution in an Ice Cover with a Linear Surface Temperature Change:

The form of equation (3.3.9) can be simplified for certain known temperature conditions. One of the simplest which may be considered is that of a uniform change in the ice surface temperature with time. A paper by Anthony (An51), which this author has been unable to secure, appears to deal with this case directly. However in this section this particular case was chosen as a special form of the general solution (3.3.9), mainly because actual temperature observations were available to illustrate the mathematical solution. It should be noted that in the fore-going analysis, the assumption of a uniform initial gradient is not necessary to enable a solution to the problem. In fact it is only necessary that the functional relationship between θ and x be known.

Under conditions of uniform surface temperature change, it is seen that: $(\theta_r - \theta_{r-1}) = \Delta\theta_r \rightarrow 0$, and $n \rightarrow \infty$

Since all $\Delta\theta$ are equal, the temperature distribution at time $T_n + \Delta T$ is:

$$\theta(x, T_n + \Delta T)_{(\Delta T \rightarrow 0)} = \theta_n \frac{h-x}{h} \lim_{\substack{\Delta T \rightarrow 0 \\ \Delta\theta \rightarrow 0 \\ n \rightarrow \infty}} \sum_{m=1}^{\infty} \frac{2}{m\pi} \Bigg(\ldots\ldots$$

$$\Delta\theta \cdot \left(e^{-\frac{m^2\pi^2 K}{h^2} \overline{T_n + \Delta T}} + e^{-\frac{m^2\pi^2 K}{h^2} T_n} + e^{-\frac{m^2\pi^2 K}{h^2} \overline{T_n - \Delta T}} + \ldots . \; e^0 \right) \sin \frac{m\pi}{h} x \Bigg)$$

Since $\theta(0,t) = \dfrac{\theta_n - \theta_0}{T_n} \cdot t$ i.e. $d\theta = \dfrac{\theta_n - \theta_0}{T_n} \, dt$

where θ_0, θ_n, are the ice surface temperatures at $t = 0$ and T_n respectively, it follows that:

$$\theta(x,T_n) = \theta_n \frac{h-x}{h} - \sum_{m=1}^{\infty} \left(\int_0^{T_n} \frac{2(\theta_n - \theta_0)}{m \pi T_n} e^{-\frac{m^2 \pi^2 K}{h^2} t} dt \right) \sin \frac{m\pi}{h} x \qquad (3.4.1)$$

Integration of (3.4.1) gives:

$$\theta(x,T_n) = \theta_n \frac{h-x}{h} - \sum_{m=1}^{\infty} \frac{2h^2(\theta_n - \theta_0)}{m^3 \pi^3 K T_n} \left(1 - e^{-\frac{m^2 \pi^2 K}{h^2} t} \right) . \sin \frac{m\pi}{h} x \qquad (3.4.2)$$

To suit this particular type of case, the quantity α which appears in equation (3.2.5) is redefined as the ratio of the temperature change experienced for a given value of t at a given x, and the temperature change which would have been experienced had the thermal diffusivity of the ice been infinite. It is clear that the above definition of α leads to no change, and is equally valid in the case of a single step change in temperature, but that the earlier, simple definition could not be applied to the present case, owing to the continuous change in surface temperature with time. As before, for equation (3.2.5), the distance within the ice sheet is written as: $x = \eta h$. The temperature at a distance $x = \eta h$ down in the ice at a time T_n, after referring to figure (3.2.i), is seen to be given by:

$$\theta(\eta h, T_n) = (1 - \eta) \left(\alpha \theta_n + (1 - \alpha) \theta_0 \right)$$

$$= \theta_n \cdot \frac{1-\eta}{1} - \sum_{m=1}^{\infty} \frac{2h^2(\theta_n - \theta_0)}{m^3 \pi^3 K T_n} (1 - e^{-\frac{m^2 \pi^2 K}{h^2} T_n}) \sin \frac{m\pi}{h} x \qquad (3.4.3)$$

Hence the following relation is obtained:

$$(1-\eta)(1-\alpha) = \sum_{m=1}^{\infty} \frac{2h^2}{m^3 \pi^3 K T_n} (1 - e^{-\frac{m^2 \pi^2 K}{h^2} T_n}) \sin \frac{m\pi}{h} x \qquad (3.4.4)$$

For a number of values of η, this equation becomes:

$$
\left.
\begin{aligned}
&\eta = 0 \qquad \alpha = 1 \quad \text{for all values of } T_n. && \text{(a)}\\
&\eta = \tfrac{1}{8} \qquad \alpha = 1 - \sum_{m=1}^{\infty} \frac{16h^2}{7m^3\pi^3 K\, T_n}\left(1 - e^{-\frac{m^2\pi^2 K}{h^2} T_n}\right)\sin\frac{m\pi}{8} && \text{(b)}\\
&\eta = \tfrac{1}{4} \qquad \alpha = 1 - \sum_{m=1}^{\infty} \frac{8h^2}{3m^3\pi^3 K\, T_n}\left(1 - e^{-\frac{m^2\pi^2 K}{h^2} T_n}\right)\sin\frac{m\pi}{4} && \text{(c)}\\
&\eta = \tfrac{1}{2} \qquad \alpha = 1 - \sum_{m=1}^{\infty} \frac{4h^2}{m^3\pi^3 K\, T_n}\left(1 - e^{-\frac{m^2\pi^2 K}{h^2} T_n}\right)\sin\frac{m\pi}{2} && \text{(d)}\\
&\eta = 1 \qquad \alpha \text{ has no meaning, but } \alpha \to 1 \text{ as } K \to \infty && \text{(e)}
\end{aligned}
\right\} \quad (3.4.5)
$$

Since α is easily obtained from temperature profile observations, K may be calculated from one or more of the equations (3.4.5), by means of systematic trial substitutions. For normal ice thicknesses, i.e. of the order of 1 metre, one term of the series (3.4.5) is sufficient for all practical purposes when T_n is greater than about 10^5 second.

The above data would best be employed in processing ice temperature data covering a period of the order of months. Due to the requirement of constant ice thickness, application is restricted to permanent pack ice.

3.5 A Theoretical Analysis of Permanent Ice Pack Temperature Records.

It was found that the temperature records reported for a Russian floating ice island by Iakovlev (Ia55), showed the mean monthly ice surface temperature to have varied approximately linearly over two periods of six months, with stationary values occurring during January and February, and July and August. The change in surface temperatures between August and January exhibited greater linearity than that between February and July, hence the former records were chosen for analysis, and reproduced in figure (3.5.i), the surface temperature as a function of time being superimposed.

The value of α, as defined in section 3.4 was measured for $\eta = \frac{1}{2}$, at 2,3,4 and 5 months after the initial uniform temperature gradient in August. Owing to the fact that the exponential term becomes very small and all terms except for m = 1 in (3.4.5 d) are of negligible importance for the large values of T_n involved in this case, the trial and error process for finding the appropriate value of the diffusivity K becomes a simple mathematical operation.

The value of h in the equation is taken as the mean thickness of ice during the time T_n. The figure for the mean ice temperature is arrived at similarly.

In order to provide a basis for comparison, the specific heat was calculated from the value of the thermal diffusivity obtained. Since no record of salinity and density was given by Iakovlev, average values of 4.7×10^{-3} for the thermal conductivity and 0.915 for the density were assumed. Similarly, due to the absence of a salinity profile, it was necessary to assume that the ice, after extensive summer draining with negligible new ice growth by October, would have had a mean salinity of about 2‰ between August and October. It is clear from the temperature records that ice of greater salinity could hardly have existed during this time. With the gradual addition of new ice, the mean salinity of the cover was reasonably expected to have increased, thus the approximate values shown in table (3.5.ii) were used to obtain the specific heat of the ice at the mean temperature obtained from

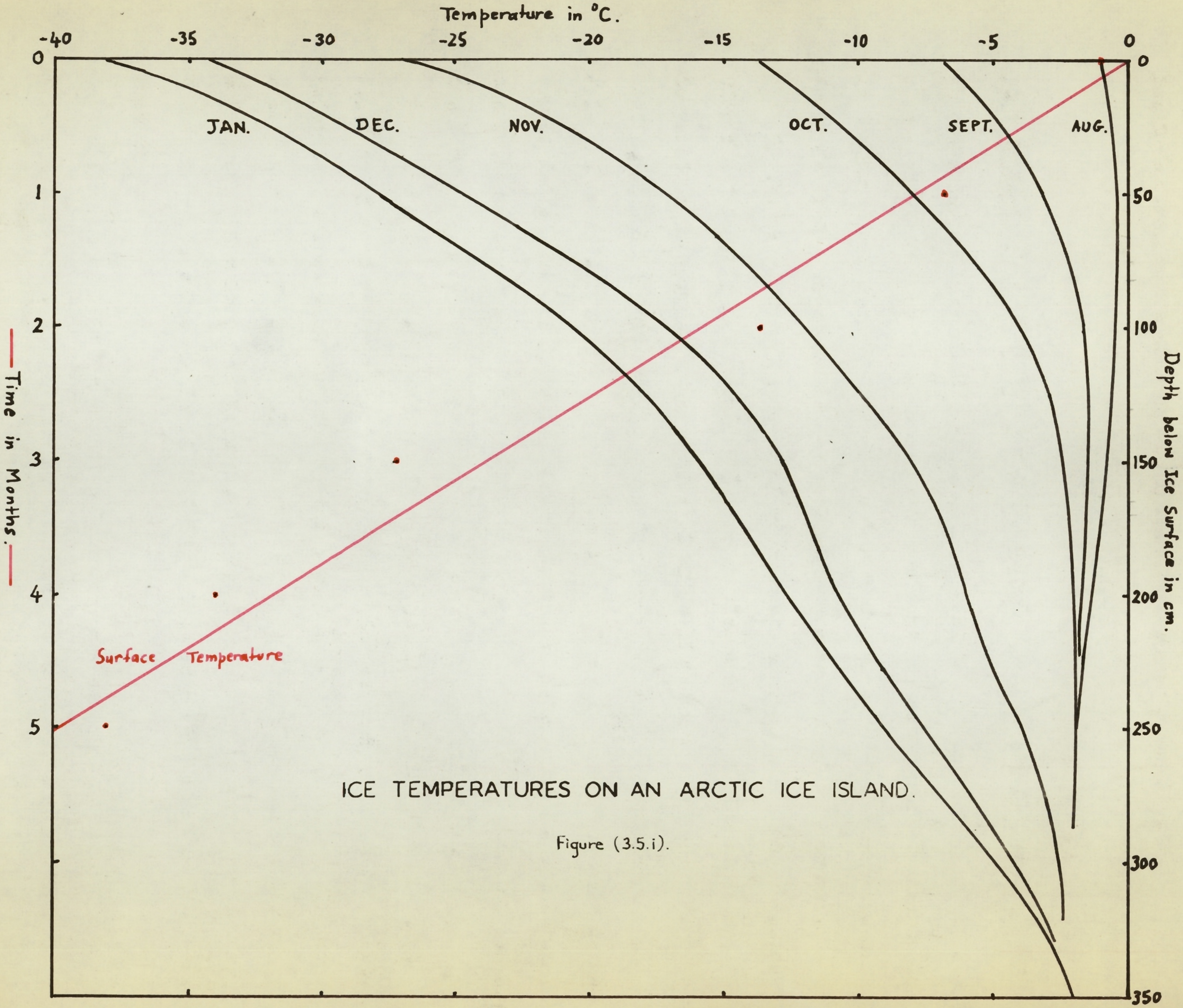

ICE TEMPERATURES ON AN ARCTIC ICE ISLAND.

Figure (3.5.i).

Table (3.5.ii)

Analysis of Long Term Ice Temperature Records.

Time Elapsed since Initial Uniform Gradient in August. Months	Seconds	Average Ice Thickness $\bar{h}$ in cm. during Elapsed Time.	Experimentally Determined Value of α	Value of K giving Experimental Value for α when subs. in Equation (3.4.5)	Mean Ice Temperature at $\eta = \frac{1}{2}$	Calculated Mean Value of Specific Heat.	Estimated Salinity (Mean) of Ice in ‰	Accepted Value of Specific Heat.
2 (Oct.)	0.52×10^{7}	260	0.28	0.23×10^{-2}	$-2.0^{\circ}C$	2.2	2	2.6
3 (Nov.)	$0.79 \times$ "	300	0.50	0.32 "	-3.6	1.8	3	1.7
4 (Dec.)	1.06 "	330	0.64	0.38 "	-5.4	1.4	4	1.2
5 (Jan.)	1.32 "	340	0.71	0.53 "	-7.1	1.3	5	1.0

figure (1.4.ii) to allow comparison with the calculated values.

Table (3.5.ii) summarizes the steps undertaken in the calculations. A definite correlation between the values obtained from the temperature diffusion theory and the accepted specific heats is evident. In view of the many uncertainties and approximations introduced, it would have been surprising to find closer agreement. It does appear however, that even in its present form, the theory can account for the temperature profiles found in an ice cover.

CHAPTER 4

THE GROWTH OF SEA ICE

4.1 Methods of Study.

The first solution to the mathematical problem of analysing ice growth was given by Stefan (St91). Stefan discussed the growth of Arctic sea ice initially by neglecting the specific heat, followed by a more complete analysis involving this term also. The assumption of a constant, fresh-water value for the specific heat was not serious when applied to the permanent ice cover, but leads to inaccuracies when applied to an annual ice cover.

Neglect of the specific heat of the ice implies a uniform temperature gradient in the cover. Thus, if the surface temperature of ice of thickness h is given by θ relative to the water at the freezing temperature below, the flux of heat through the ice is given by:

$$J = k \frac{\theta}{h} \tag{4.1.1}$$

At the ice-water interface, this heat is supplied entirely by the latent heat of freezing of additional water, so that:

$$J = \rho L \frac{dh}{dt} \tag{4.1.2}$$

where ρ is the density and L the latent heat of formation of ice. Elimination of J from (4.1.1) and (4.1.2) gives:

$$h \frac{dh}{dt} = \frac{k}{\rho L} \theta$$

Integration of this expression results in the relation known as Stefan's simple ice growth equation:

$$h_2^2 - h_1^2 = \frac{2k}{\rho L} \int_{t_1}^{t_2} \theta \, dt \qquad (4.1.3)$$

where h_2 and h_1 are the ice thickness at times t_2 and t_1 respectively.

Inclusion of the specific heat led Stefan to the following relation:

$$h_2^2 \left(1 + \frac{c\theta_2}{3L}\right) - h_1^2 \left(1 + \frac{c\theta_1}{3L}\right) = \frac{2k}{\rho L} \int_{t_1}^{t_2} \theta \, dt \qquad (4.1.4)$$

where c is the specific heat of the ice and θ_2 and θ_1 are the ice surface temperatures at times t_2 and t_1 respectively.

Using the data obtained by a number of British and German Arctic expeditions, Stefan used equation (4.1.4) in the first calculation of the thermal conductivity of sea ice. Referring to chapter 2, the value of 4.2×10^{-3} cal. cm.$^{-1}$ sec.$^{-1}$ $^{o}C^{-1}$ obtained by Stefan is acceptable for drained Arctic sea ice.

More recent work such as that of Kolesnikov offers no advantages over the rigorous mathematical treatment of Stefan. Kolesnikov (Ko58) in simultaneously considering the effect of surface snow, atmospheric convection and radiation, achieved a complex almost unwieldly expression. The simpler approach of treating the fluxes of conduction, convection and radiation separately has been adopted in the later chapters of this thesis.

The most serious error involved in the application of equation (4.1.4), is that the expression in itself does not take account of the time taken by a temperature effect to travel through the ice. In section 3.1 it has been shown that several days may be involved for ice thicknesses of the order of one metre. Stefan was aware of this and theoretically calculated the time taken by a surface temperature disturbance to be noticed in terms of ice growth, a value of almost 9 days being obtained for ice of two metre thickness. This calculation however was made on the assumption of a constant value of 0.5 cal. $gm.^{-1}$ for the specific heat of the ice, and becomes inconveniently complex when true sea ice of non-uniform specific heat is involved. Because of this, section 6.5 describes an experimental method of determining these times.

Supposing that the freezing exposure from the initial time of formation is being correlated with ice thickness, it is clear that there will be no initial delay between surface temperature and ice growth effects. When the ice thickness reaches 1.5 metres however, the delay may be of the order of twenty days, so that the freezing exposure integral should be bounded many days before the time of the final ice thickness. Without this correction, errors of up to 25% may be introduced in measurements taken over a 90 day period.

Observations reported by Barnes (Ba28) to support a simple Stefan type equation actually show that the effect of finite temperature diffusion is important even in the analysis of ice whose thickness is only of the order of a millimetre. Barnes made rapid measurements on river ice formed in areas cleared by an ice breaker. Invariably, the theoretically calculated ice thickness tended to exceed the observed value, this error progressively increasing for greater ice thicknesses.

4.2 Practical Corrections to Stefan's Simple Ice Growth Equation.

As a result of the high values for the specific heat of annual sea ice especially at temperatures near to the freezing point, Stefan's equation corrected for a constant value of the specific heat (4.1.4) is in general not sufficiently accurate. The simple formula (4.1.3) needs two corrections, the first involving the specific heat is developed below; the other, necessary because of the finite temperature diffusion in the ice, is discussed in section 6.5.

Figure (4.2.i) shows the temperature distribution in an ice cover initially of thickness h, before and after an additional thin layer of thickness Δh has been formed, assuming continued uniformity of temperature gradient. It is seen that the temperature of the ice at a distance x below the surface is given by:

$$\theta = (\theta_0 - \theta_F)\,\frac{h-x}{h} + \theta_F = \theta_0 - (\theta_0 - \theta_F)\,\frac{x}{h} \qquad (4.2.1)$$

The change in temperature of the ice at this point after freezing of the layer Δh is:

$$\Delta\theta = (\theta_0 - \theta_F)\,\frac{x}{h} - (\theta_0 - \theta_F)\,\frac{x}{h+\Delta h} \doteq (\theta_0 - \theta_F)\,\frac{x.\,\Delta h}{h^2} \qquad (4.2.2)$$

where θ_0 is the ice surface temperature and θ_F is that of the ice-water interface.

The change in heat content of a volume Δx of ice at a depth x is thus

$$\Delta Q_i = (\theta_0 - \theta_F)\,\frac{x\ \Delta h}{h^2}\cdot\Delta x\cdot\rho\cdot c_{sx} \qquad (4.2.3)$$

where c_{sx} is the specific heat of the sea ice at a depth x. Substituting the expression for the specific heat (1.3.7) modified by equation (4.2.1) to eliminate θ, the total change in heat content of the ice cover for unit increase in thickness is found to be given by:

$$Q_i = \rho\cdot\overline{c_s\Delta\theta} = -\int_0^h (\theta_0-\theta_F)\,\frac{x}{h^2}\,\rho\,\frac{\sigma L_i}{\alpha}\,\frac{dx}{\left(\theta_0-(\theta_0-\theta_F)\,\frac{x}{h}\right)^2}$$

$$+\int_0^h (\theta_0-\theta_F)\,\frac{x}{h^2}\,\rho\,\frac{\sigma(c_w-c_i)}{\alpha}\,\frac{dx}{\left(\theta_0-(\theta_0-\theta_F)\,\frac{x}{h}\right)} + \int_0^h (\theta_0-\theta_F)\,\frac{x}{h^2}\,\rho\,c_i\,dx \qquad (4.2.4)$$

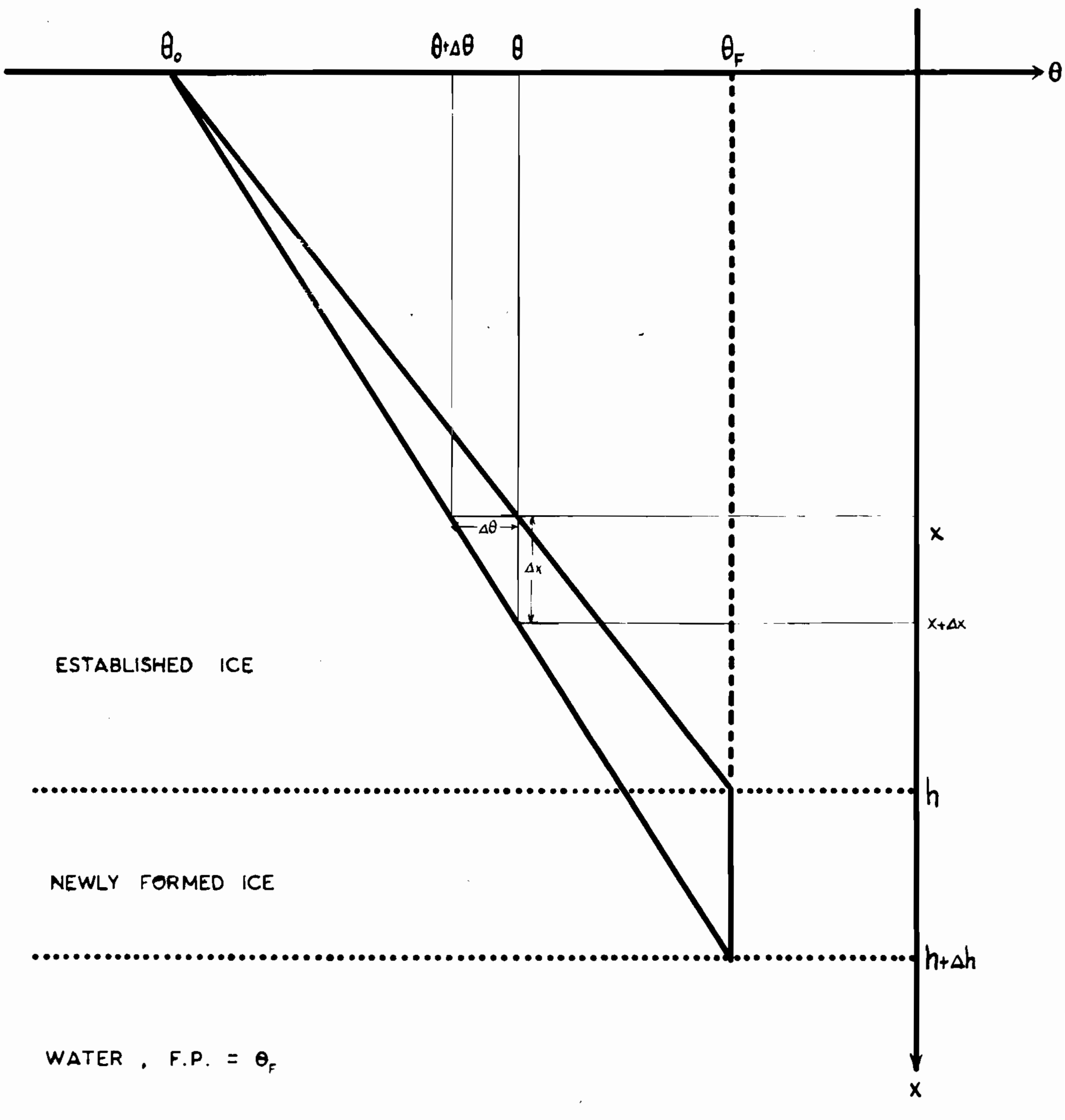

TEMPERATURE CHANGES DURING ICE GROWTH.

Figure (4.2.i).

Integration of this expression leads to:

$$Q_i = \rho \cdot \overline{c_s \cdot \Delta\theta} = \left(\left(\frac{L_i + (c_w - c_i)\theta_0}{(\theta_0 - \theta_F) \cdot \alpha} \cdot \sigma \cdot \ln \frac{\theta_0}{\theta_F} \right) - \left(\frac{L_i + (c_w - c_i)\theta_F}{\theta_F \cdot \alpha} \sigma \right) + \frac{\theta_0 - \theta_F}{2} c_i \right) \rho \tag{4.2.5}$$

The term $\overline{c_s \cdot \Delta\theta}$ is a convenient notation for the mean value of the product of the specific heat and temperature change in the ice cover.

At the same time, the heat involved in the freezing of the unit layer of ice only is:

$$Q_F = -L_s \rho$$

which from equation (1.4.1) becomes:

$$Q_F = -(1 - \sigma - \frac{\sigma}{s}) \rho L_i \tag{4.2.6}$$

It is seen that for $\theta_0 \rightarrow \theta_F$, $\frac{Q_i}{Q_F} \rightarrow 0$ and for $\theta_0 \rightarrow -\infty$, $\frac{Q_i}{Q_F} \rightarrow +\infty$, substantiating Stefan's observation that equation (4.1.3) holds most accurately for ice surface temperatures near to the freezing point.

Using the values for the constants quoted in section 1.2, $\frac{Q_i}{Q_F}$ may be calculated for different salinities and surface temperatures of an ice cover. The graph (4.2.ii) shows these values for ice frozen from sea water having a -1.8°C freezing point.

4.3 Analogue Circuits for Ice Growth and Temperature Analysis.

Three equations are of fundamental importance in specifying the thermal conditions existing in an ice cover at any time. They are:

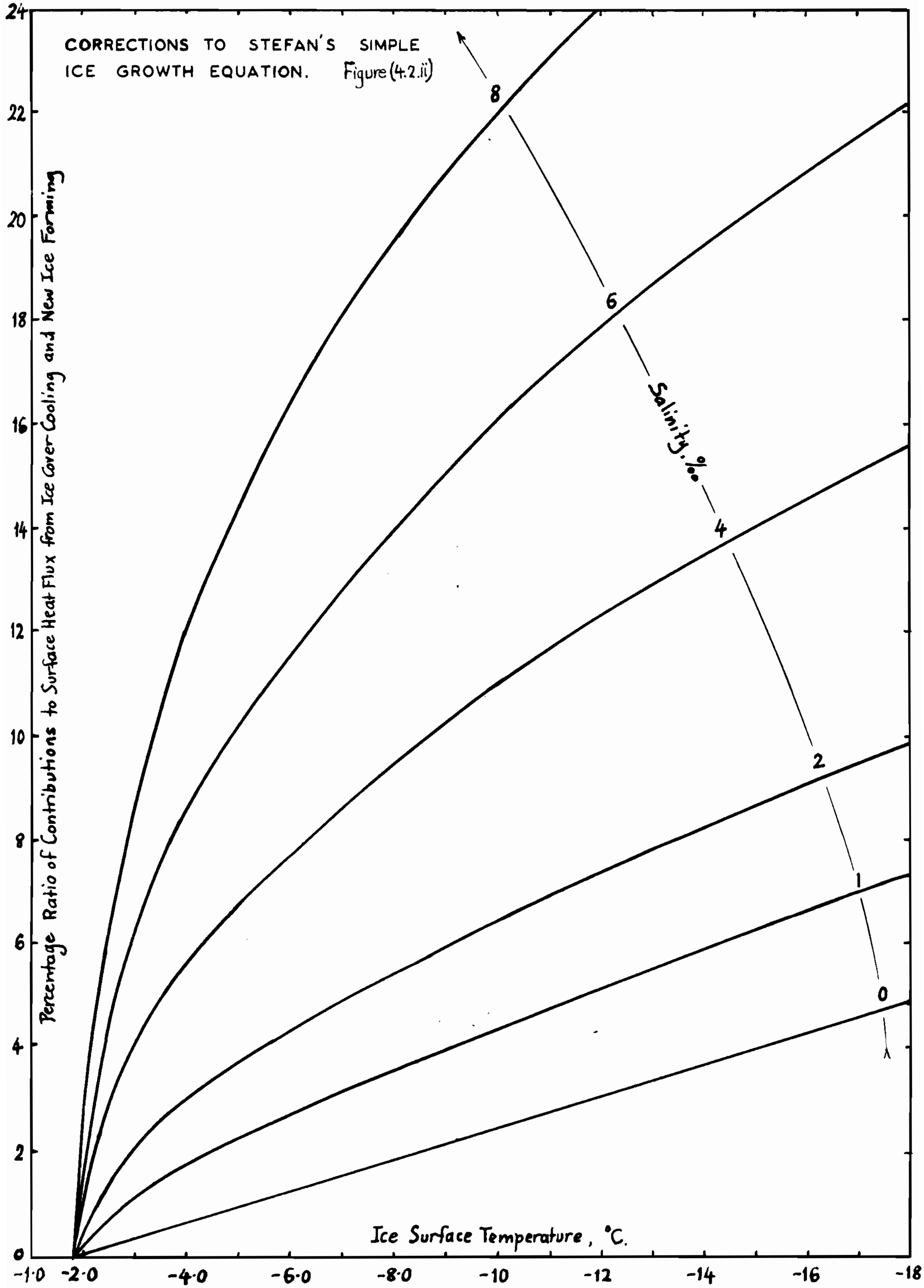
CORRECTIONS TO STEFAN'S SIMPLE ICE GROWTH EQUATION. Figure (4.2.ii)
Percentage Ratio of Contributions to Surface Heat Flux from Ice Cover Cooling and New Ice Forming
Ice Surface Temperature, °C.
Salinity ‰
8
6
4
2
1
0
0
2
4
6
8
10
12
14
16
18
20
22
24
-1·0
-2·0
-4·0
-6·0
-8·0
-10
-12
-14
-16
-18

$$\frac{\partial \theta}{\partial t} = \frac{k}{\rho c} \frac{\partial^2 \theta}{\partial x^2} \tag{4.3.1}$$

$$J = k \frac{\partial \theta}{\partial x} \tag{4.3.2}$$

$$\dot{h} = \frac{k}{\rho L} \left(\frac{\partial \theta}{\partial x}\right)_{(x=h)} = \frac{1}{L\rho} J_{(x=h)} \tag{4.3.3}$$

where θ is the temperature at a point in the ice cover of thickness h at time t. k, c and L are the thermal conductivity and capacity and latent heat of the ice of density ρ. J is the heat flux in the x-direction, and $\dot{h}$ is the rate of advance of the lower boundary. Equation (4.3.1) is the diffusion equation, whose solution as we have seen in chapter 3, becomes a difficult operation as soon as boundary conditions become time dependent.

Electrical analogues are finding increasing application to thermal problems of this type. Two main types of analogue circuit are found described in the literature. A direct analogue is possible with resistive-capacitive networks and these basically similar circuits have been extensively reviewed by Lawson and McGuire (LM53). An entirely different system has been described by Liebmann (Li55). This latter circuit is purely resistive and the transient flows which occur in a capacitive system are simulated by a progressive adjustment of potentiometers. Whilst this method allows the analogue current to be accurately measured at any time before further change is introduced in the circuit currents, the earlier direct analogue is more easily applicable to complete automation.

No reference has been found to the problem of a growing plane boundary in a thermal medium such as an ice cover. Thus in the following sections, a resistive-capacitive analogue circuit for a growing ice cover will be discussed.

4.4 Scaling Factors in Analogue Analysis.

A true analogue for one dimensional heat flow consists of a conductor with continuously distributed resistance and capacitance. Whilst these are properties of any electrical conductor, the preparation of an electrical cable with capacity high enough for the observation of long term transient effects would be a major undertaking. The usual practical solution to these requirements as indicated in the literature (LM53), makes use of a chain of resistors bypassed at intervals with capacitors to ground, as is shown in figure (4.5.i). The resolution of the analogue is improved by more frequent intervals of capacitive bypassing. In all circuits, the resistance r, and capacity γ, per unit length remain the important quantities. Ice temperatures are replaced by voltages V, in the network and heat fluxes are observed as currents i.

The three thermal equations of section 4.3 are shown with their electrical analogues below:

$$\frac{\partial \theta}{\partial t} = \frac{k}{\rho c}\frac{\partial^2 \theta}{\partial x^2} \qquad (4.3.1) \qquad \frac{\partial V}{\partial t} = \frac{1}{r\gamma} \cdot \frac{\partial^2 V}{\partial x^2} \qquad (4.4.1)$$

$$J = k\frac{\partial \theta}{\partial x} \qquad (4.3.2) \qquad i = \frac{1}{r} \cdot \frac{\partial V}{\partial x} \qquad (4.4.2)$$

$$\dot{h} = \frac{k}{L\rho}\left(\frac{\partial \theta}{\partial x}\right)_{(x=h)} = \frac{1}{L\rho} J_{(x=h)} \qquad (4.3.3) \qquad \dot{\ell} = \frac{1}{r\gamma}\left(\frac{\partial V}{\partial x}\right)_{(x=\ell)} = \frac{1}{\lambda} i_{(x=\ell)} \qquad (4.4.3)$$

Equation (4.4.3) expresses the electrical equivalent of growth, merely by providing for extension to the circuit of length ℓ.

A scaling factor can be defined to connect each of the pairs of analogues appearing in the equations above, even though some of these factors may be chosen to be of unit magnitude or even dimensionless. Consideration shows that the potential analogue to temperature in $^{\circ}C$ is conveniently measured in volts, so that when we write:

$$\theta = \int V$$

the units of the scaling factor $\int$ are $^{\circ}C$. volt^{-1}, and its magnitude is unity. Other scaling factors are conveniently assigned non-unit magnitudes. For example, for ice of 1 metre thickness, and initially having a uniform temperature gradient, the centre of the ice will experience half of the total temperature excursion when the surface temperature is suddenly changed to a new fixed value, in about 10^5 seconds. Clearly a much shorter observation time, say 10 seconds would be desired in the laboratory analogue. This means that the rate of change of potential, as given by equation (4.4.1) should be 10^4 times that of the rate of change of temperature given by (4.3.1). Hence the chosen value of $\frac{1}{r\gamma}$ should be made 10^4 times that of the factor $\frac{k}{\rho c}$. Similarly, the heat flux through an ice cover having a uniform temperature gradient of $0.2^{\circ}C$. cm.$^{-1}$, (i.e. $20^{\circ}C$ across 1 metre), is about 10^{-3} cal. cm.$^{-2}$ sec.$^{-1}$ which represents far too high a current flow in the analogue circuit, if the current in amperes simulates the heat flux in cal. cm.$^{-2}$ sec.$^{-1}$ directly.

Two non-unit scaling factors are now introduced:

$$\frac{1}{\int t} \cdot \frac{k}{\rho c} = \frac{1}{r\gamma} \qquad (4.4.4)$$

$$\int c \cdot k = \frac{1}{r} \qquad (4.4.5)$$

$$\therefore \int c \cdot \int t \cdot \rho c = \gamma \qquad (4.4.6)$$

The time scaling factor is of course dimensionless, and it has been shown that a suitable magnitude is 10^{-4}. The scaling factor for the conductivities $\int_c$, has the units: coulomb cal.$^{-1}$ volt^{-1} $^{\circ}C$ cm.^{2} and its magnitude remains to be chosen. Since for ice, $\frac{k}{\rho c} = 10^{-2}$, it is seen from (4.4.4) that $\frac{1}{r\gamma} = 10^{2}$. If γ is chosen as 0.05 μF cm.$^{-1}$, then: $r = 2 \times 10^{5}\,\Omega$ cm.$^{-1}$ so that the analogue of a one metre thick ice cover having a conductivity of 5×10^{-3} cal. cm.$^{-1}$ $^{o}C^{-1}$ sec.$^{-1}$ would have a total resistance of 20MΩ, and conduct 1 μA in the steady state on application of a 20 volt potential.

It is then seen from equation (4.4.5) that:

$$\int_c = 10^{-3}$$

This implies that a thermal medium of conductivity 1 cal. sec^{-1} cm.$^{-1}$ $^{o}C^{-1}$ would be simulated by a circuit having a resistivity of $10^{3}\Omega$ cm.$^{-1}$.

The advantage of the scaling factors suggested, is that they combine analogous observation times and quantities with simple decimal conversion factors.

4.5 The Simulation of Ice Growth in an Analogue Circuit.

At any time, the rate of growth of an ice cover is given by the equation (4.3.3). In the analogue circuit, the potential gradient at the lower boundary, approximated by the potential gradient in the lowest resistor, prescribes the rate at which resistors should be added to the existing chain. Owing to the discontinuous nature of the analogue, the simplest method of determining the rate of ice growth, is to measure the charge passing through the lowest resistor; when this totals the amount simulating the quantity of heat released per cm.^{2} during the growth of 10 cm. of ice, a further resistor-capacitor element representing this new 10 cm. of ice, is added to the circuit.

A unit scaling factor between depth in the ice and length in the analogue circuit has of course been chosen, so that from equation (4.3.3) and (4.4.3) we have:

$$\dot{\ell} = \frac{1}{\int_t} \dot{h} \qquad (4.5.1)$$

and since from (4.4.5),

$$\frac{1}{r} = \int_c k, \quad \text{we have} \quad \frac{1}{\int_t} \frac{k}{L\rho} = \int_c \frac{k}{\lambda}$$

because the temperature - voltage scaling factor is of unit magnitude;

$$\lambda = \int_c \cdot \int_t L\rho = 10^{-7} L\rho \qquad (4.5.2)$$

The units of λ are coulomb cm.$^{-1}$, compared with $L\rho$ in (cal. cm.$^{-2}$) cm.$^{-1}$. Thus whereas $L\rho$ cal.cm.$^{-3}$ are released during the formation of new ice, the corresponding amount of charge in the analogue circuit will be 10^{-7} $L\rho$ coulomb cm.$^{-1}$.

If the circuit of figure (4.5.i) is used, a pair of probes can supply the voltage signal to a current integrator which measures the total charge through the circuit element. Since the circuit shown enables the "ice" to be added to in 10 cm. steps, when the integrator registers 10^{-6} $L\rho$ coulomb, i.e. about 7 x 10^{-5} coulomb, it is arranged to discharge and trigger the probes to the next resistor-capacitor element on the stepping switch mounted chain.

The elements below the lower probe do not contribute to the circuit's behaviour, as no current flows in them and the fact that they have a discharge path prevents them from accidentally becoming charged.

A table of analogues and scaling factors has been compiled in (4.5.ii).

Present limitations of the analogue are chiefly due to the fixed values of the electrical components, which do not follow the behaviour of their thermal analogue's temperature dependence. In the case of the resistors, this

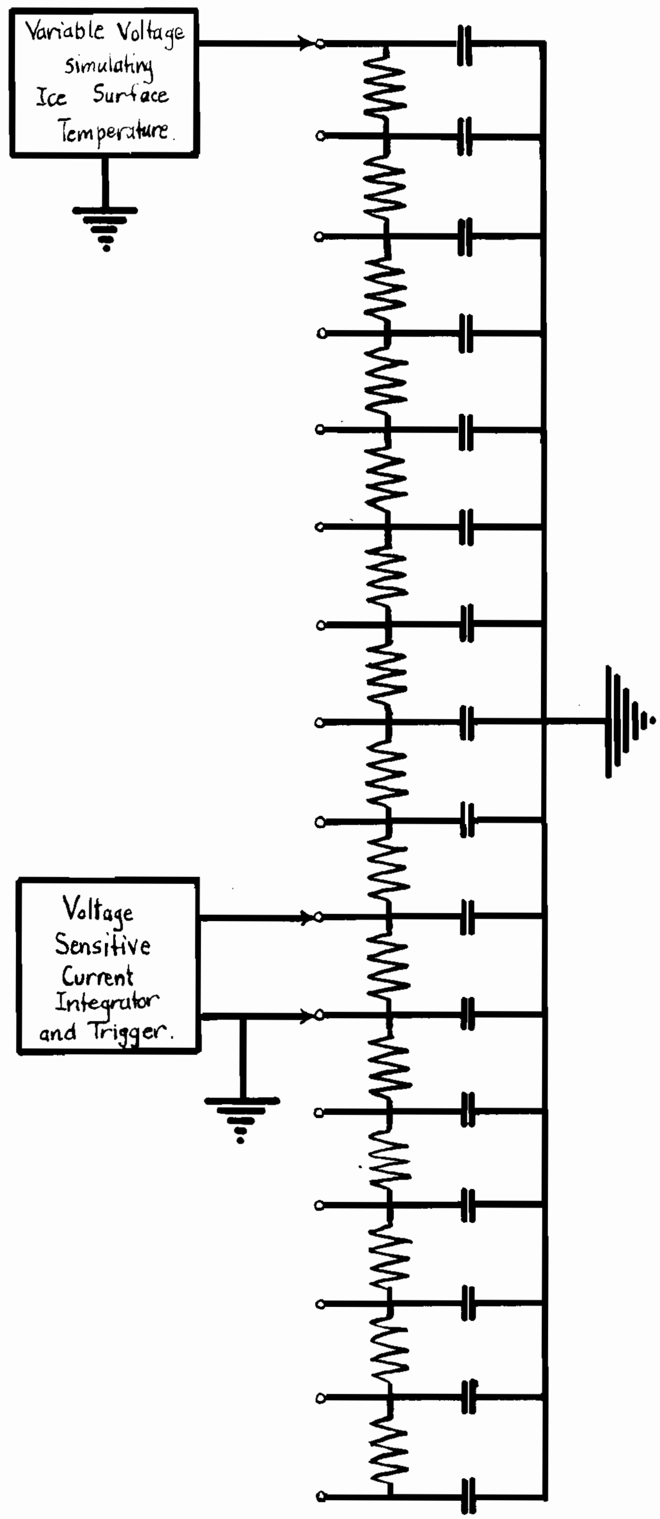

ANALOGUE CIRCUIT FOR AN ICE COVER

Figure (4.5.i)

Table (4.5.ii)

Thermal and Electrical Analogues.

Thermal		Scaling Factor		Electrical	
Quantity	Units			Quantity	Units
Temperature	$^{\circ}C$	1	volt $^{\circ}C^{-1}$	Potential	volt
Heat Flux	cal.$cm.^{-2}sec.^{-1}$	$\int_c$	coul.$cal.^{-1}volt^{-1}cm.^{2}$ $^{\circ}C$	Current	amp. (coul.$sec.^{-1}$)
Heat Content per Unit Vol.	cal.$cm.^{-2}cm.^{-1}$	$\int_c \int_t$	coul.$cal.^{-1}cm.^{2}$	Charge per Unit Length	coul.$cm.^{-1}$
Conductivity	cal.$cm.^{-1}$ $^{\circ}C^{-1}sec.^{-1}$	$\int_c$	coul.$cal.^{-1}volt^{-1}cm.^{2}$ $^{\circ}C$	Reciprocal Resist. per Unit Length.	cm.Ω^{-1} (coul.$volt^{-1}sec.^{-1}$cm.)
Capacity per Unit Volume.	cal.$cm.^{-2}cm.^{-1}$ $^{\circ}C^{-1}$	$\int_c \int_t$	farad $cal.^{-1}$ $volt^{-1}$ $^{\circ}C$ $cm.^{2}$	Capacity per Unit Length	farad $cm.^{-1}$ (coul.$volt^{-1}cm.^{-1}$)
Time	sec.	$\int_t$	dimensionless	Time	sec.
Length	cm.	1	"	Length	cm.

could be overcome by means of regular adjustment by the operator. The capacitors however, which introduce the most serious error could be replaced by circuit elements whose capacity is dependent on the potential difference.

A simple network, without ice growth simulation was built, with which the transmission of "temperature pulses" was easily observed. The broadening and flattening of the potential pulse as it travelled down the circuit was similar to the analogous thermal phenomenon observed over long periods of time, or calculated with difficulty.

CHAPTER 5

THE FLUXES OF THERMAL ENERGY AND THEIR MEASUREMENT

5.1 Introduction.

The radiant energy of the sun when incident on the earth's surface, is the cause of a number of secondary fluxes transporting this energy. A complete understanding of the earth's heat budget demands an accurate knowledge of all of these fluxes as well as of any stored energy due to the specific and latent heats of the absorbing materials. In the case of terrestial areas in the temperate and tropical latitudes, the fluxes consequent to solar radiation being absorbed in the upper layers of the soil are caused by heating of the surface. Heat is then conducted down into the earth and convection occurs upwards into the lower atmosphere. Evaporation of moisture at the surface may result in considerable loss of heat, in some regions this may even be the chief mechanism of losing the energy received from the sun. In addition to direct reflection and diffusion of short wave sunlight, all surfaces radiate energy of longer wavelengths characteristic of their temperatures and to a lesser extent of their nature.

In oceanic regions, convection in the water is an important factor in attaining equilibrium, and the stored heat is of great importance because of the large specific heat of water. After a summer of heating, this stored energy is so vast, that the oceans can lose energy throughout the following winter, supplying the surface layers with heat at a rate which may be large compared with the net noon solar radiation. Should the water freeze, as in polar regions, the flux of heat to the surface greatly increases. Thus the conditions peculiar to a growing ice cover are the existence of two independent sources of heat for the surface: firstly, as in all regions, solar radiation (and some atmospheric radiation), and secondly, the conducted flux of heat derived mainly from the freezing process at the ice-water boundary. For most other regions of the earth's crust, it is only nocturnally that the sign of the conducted heat flux is such as to heat the surface layers.

After the initial formation of ice, convection in the water ceases to be of any importance. Prior to this stage, convective circulation occurs until the water reaches a uniform temperature of from $4^{\circ}C$ to $-1.9^{\circ}C$, depending on the salinity, which may vary from zero in fresh water to about 35‰ in the oceans. Further cooling of a fresh water surface is necessary for freezing, but for water whose salinity exceeds 24.7‰ the density monotonically increases with decreasing temperature, so that the entire body of water reaches the freezing point before ice forms. In the oceans, the compressibility of water leads to somewhat greater temperatures at lower depths. A profile taken by Milne (Mi60) in the Barrow Strait near Cornwallis Island under annual ice, showed that the water temperature increased with depth by $0.5^{\circ}C$ and the salinity by 2‰ , over 100 metres, the net result being a small increase in density with depth. Under these conditions, no thermal convection occurs, and in the absence of forced vertical currents, the sole mechanism for heat transfer remaining is that of conduction. With temperature gradients of the order of 10^{-5} $^{\circ}C$ $cm.^{-1}$, this effect is completely negligible in water.

On an annual ice cover, the fluxes of radiation and conducted heat are the most important. However, for an accurate assessment of the distribution of energy, convection and evaporation at the upper surface must also be considered. Under certain conditions the sign of the evaporative flux may also reverse and actually be an additional mechanism for surface heating. In temperate climates, this is seen in the formation of dew and under freezing conditions a frost deposit. It is important to distinguish between these processes which involve a change of state at or near to the ice cover surface, and the precipitation which results from a change of state far from the cover. The former directly changes the heat content of the cover by extracting or supplying heat, whilst the latter adds to the heat content only to the extent of its own heat capacity.

Late in the history of an annual ice cover, surface melting will also account for much of the incident solar energy. Surface flooding during the winter, may occur on occasion and be an important source of heat for the surface layers. It is clear that the complete assessment of the energy budget involves observation of all changes of state at the cover boundaries, knowledge of the heat capacity of the total cover and records of the fluxes of radiation, conduction and convection.

The convention of signs for a particular flux of energy was chosen to be dependent on direction only. Hence any downward flow of heat or one resulting in a gain of heat energy for the ice cover was considered positive, and an upward flux resulting in heat loss from the cover, negative.

5.2 Short Wave and Long Wave Radiation and their Measurement.

The sun may be regarded as a black body whose surface radiates at about $6000^{\circ}K$. Wien's displacement law, which relates the wavelength of maximum energy in an emitted spectrum to the emitting body's temperature, indicates that the wavelength of maximum intensity in solar radiation is about $5000^{\circ}A$ or 0.5μ (micron). A similar calculation for the surface of the earth, which emits radiation at a much lower temperature, shows a maximum for about 10μ.

This subject has been extensively reviewed by Sutton (Su53). The important facts are that direct solar radiation is essentially confined to the range between 0.15 and 4μ, and terrestial radiation to between 3 and 80μ. Because of this virtual non-overlapping of the two spectra, a simple instrumental distinction between short wave solar radiation and long wave terrestial and atmospheric radiation is possible. In practice it is convenient to measure short wave and total or all wave radiation, the long wave component can then be found as a difference.

Four radiometers were employed in the monitoring of radiation above the Hudson Bay annual ice cover near Churchill. Two Kipp solarimeters, each sensitive over a hemisphere, were set up to measure incident and reflected short wave radiation. A hemispherical and a net radiometer, both of Gier and Dunkle design (GD51), were used to measure all wave radiation. The four quantities measured were thus: short wave incident, S_i; short wave outwards from the cover, S_o; all wave (short wave plus long wave) incident, $A_i = S_i + L_i$; net inward all wave, $A_i - A_o = S_i + L_i - S_o - L_o$. These quantities are illustrated vectorially in figure (5.2.i).

The quantity of direct interest in the analysis of the balance of energy is the net all wave radiation. This term indicates the actual radiant energy balance. When it is positive, the ice cover gains heat, when it is negative, more heat is lost by radiation than absorbed.

The Kipp short wave radiometers are relatively simple devices, consisting essentially of a black painted thermopile under twin glass hemispherical envelopes. They are superior to the Eppley type, which has been described by Kimball and Hobbs (KH23), in that the latter's large glass envelope allows convection over the element leading to a calibration factor depending on whether the instrument is facing up or down. The temperature dependence of

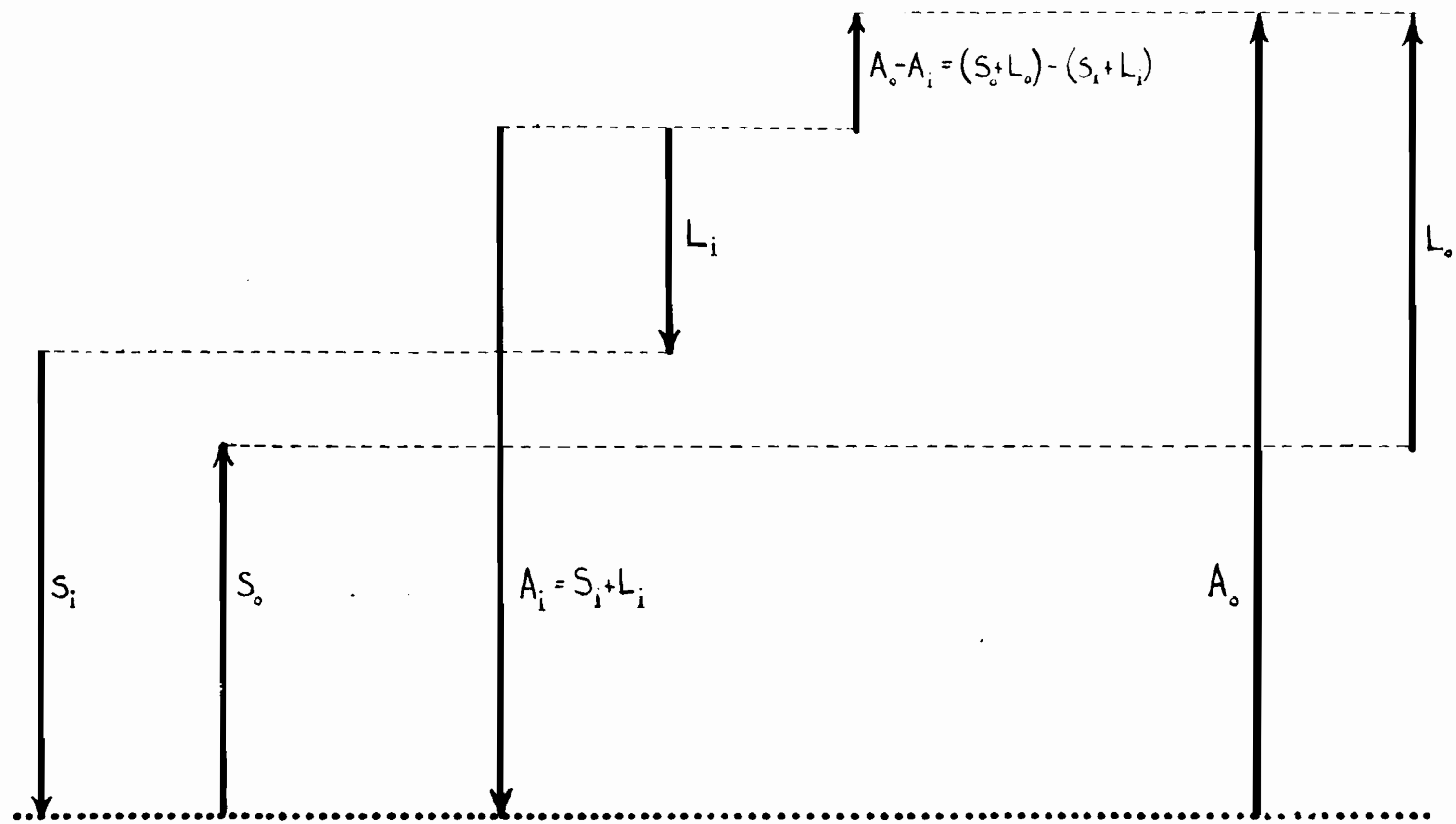

RADIATION DIAGRAM.

Figure (5.2.i)

the Kipp calibration factor being about 0.2% $^{o}C^{-1}$ is down by approximately a factor of four from that for the Eppley instruments.

The Gier and Dunkle all wave radiometers, unlike those developed by the Commonwealth Scientific and Industrial Research Organization in Australia, have no envelopes and depend on eliminating the effects of convectively transported heat on the sensitive elements by means of a collimated draft of air from a blower mounted on the instruments. Unfortunately the calibration factor of these devices is sensitive to the air speed over the thermopiles, a fact which becomes increasingly serious under windy conditions. Portman (Po54), has shown that the output of this type of radiometer changes by +2%, -6% and -16% in an approximately 20 m.p.h. wind, blowing with, across and against the blower air stream respectively. These instruments could certainly be improved by arranging for small ducts from the blower to form side air curtains to protect the sheet flow of air over the horizontal thermopiles from external winds.

There being no emission of short wave radiation at the temperature of the short wave radiometer elements, it is not necessary to be informed as to their temperature, except perhaps as a small correction in the calibration factor. In the case of the hemispherical all wave radiometer, the temperature of the element must be known in order to calculate the radiation from it. The temperature does not enter the net radiometer reading except in a correction to the calibration factor, as the net radiation is proportional to the temperature difference across the horizontally mounted black reference plate or element. The temperature difference across this is small, so that within experimental accuracy, it is assumed that the element radiates equally upwards and downwards, hence making computation of these terms unimportant for the net radiometer.

There are a number of sources of serious error in the radiometer outputs. Because of the reflectivity of the black paint coating all the radiometer elements, the output at glancing angles of incidence from a point source is less than would be expected from the cosine law. The low angle of the sun above the horizon in polar regions may result in this effect being very important. Liljequist (Li56) examined this angular dependence of the calibration factor of his short wave radiometers, which incorporated the Moll type thermopiles also used in the Kipp instruments, in considerable detail. A different calibration will be required under conditions of diffuse lighting as on an overcast day or from a smooth snow surface. On days with a partial cloud cover, it is almost impossible to assign an accurate calibration factor. Because the automatic recording station near Churchill was too remote, it was not possible to have accurate information regarding the cloud cover over the site at the time of each measurement. Thus no correction was made for the calibration factor in the results. Care was taken, however, in choosing only data obtained on completely overcast days and completely clear days for comparison throughout the season. This means, of course, that accurate values of the albedo could be found only on completely overcast days when both the upward and the downward facing radiometer were facing sources of diffuse radiation.

A further effect peculiar to cold climates leading to error in the outputs of all radiometers is caused by the occasional deposit of hoar frost. In the case of the glass domed short wave radiometers, a small cap of frost forming on top of the dome acts as a collector when the sunlight has a low angle of incidence, thus giving the instrument a false high reading. The same frost forming on the Gier and Dunkle type all wave radiometers deposits directly on the elements and thus acts as a reflector for the short wave component leading to a reduction in output. The frost does not affect the black body characteristics of the element in the long wave region, so that the instrument is still functional at night. Because the effect of hoar frost is opposite on the short and all wave instruments, it is usually easily detected during the evaluation of the records. As the frost rarely forms on a downward facing surface, the output of the short wave radiometer measuring reflected radiation can be used to determine the incident solar radiation provided the snow cover albedo is known.

The limitation on the accuracy of the all wave radiometers due to the variation in air speed over the elements has been discussed earlier in this section. At a remote automatic station, the blower type radiometers are more speedily cleared of hoar frost than the blowerless C.S.I.R.O. type.

A further source of uncertainty appears when radiation is measured discontinuously. Under clear sky conditions one might expect little advantage in continuous monitoring of outputs, but a varying partial cloud cover will lead to occasional non-representative values. Although these can often be detected by a sharp deviation from the general trend, the results on this type of day must be treated with caution.

5.3 Thermal Conduction in Sea Ice and its Measurement.

The conducted heat flux in the ice was found by measuring the temperature gradient in a suitable reference block buried in the ice cover. The ice in the cover itself is not suitable because of the continuous change in thermal properties. The device used will be referred to as an ice flux meter. Its construction involved chiselling a pit 1.5 metre^2 in area and 35 cm. deep, which over a period of two days was gradually filled with pure (tap) water, freezing in a vertical thermocouple probe. This probe, illustrated in figure (5.3.i), consists essentially of a vertical waterproofing support for the conductors, whose junctions are located in polythene sheaths.

From a knowledge of the thermal conductivity of the reference ice and the temperature gradient as indicated by thermocouples spaced at 5 cm. intervals, the heat flux could be calculated at any time. This type of device has the necessary advantage of being similar in most properties to the surrounding sea ice, especially in its transparency to short wave radiation, which most available flux meters, being designed for soil burial, are not. The non-salinity of the reference ice was verified shortly after installation, and at the close of the season, indicating that the physical properties had remained essentially constant throughout the course of the measurements.

The thermal conductivity of the flux meter ice was obtained from the theoretically based graph (2.4.i). Only the density must be measured in this determination, most conveniently by a simple process described in section 6.9. The density of two samples from a 3 inch diameter core extracted from the reference ice was found to be as shown below:

Depth	Density	Salinity	Bubble Content	Thermal Conductivity
0 to 10 cm.	0.901_1 gm.cm^{-3}	0	1.13%	$4.91_5 \times 10^{-3}$ cal.cm^{-1}°C^{-1}sec^{-1}
15 " 25	0.909_5	0	0.82%	4.93×10^{-3}

The inaccuracy in temperature measurement is the most significant source of error in the flux determination, compared with which the uncertainty in the conductivity of pure ice and its variation over the temperature range experienced, 5.04 ± 0.05 cal. cm.$^{-1}$ sec.$^{-1}$ $^{o}C^{-1}$, for 0^{o} to -15^{o}C according to Dorsey (Do40), is quite small. The maximum temperature measured over the 10cm. interval chosen for temperature gradient reference was about 2^{o}C; the accuracy

ICE FLUX METER.

Figure (5.3.i).

(Full Scale).

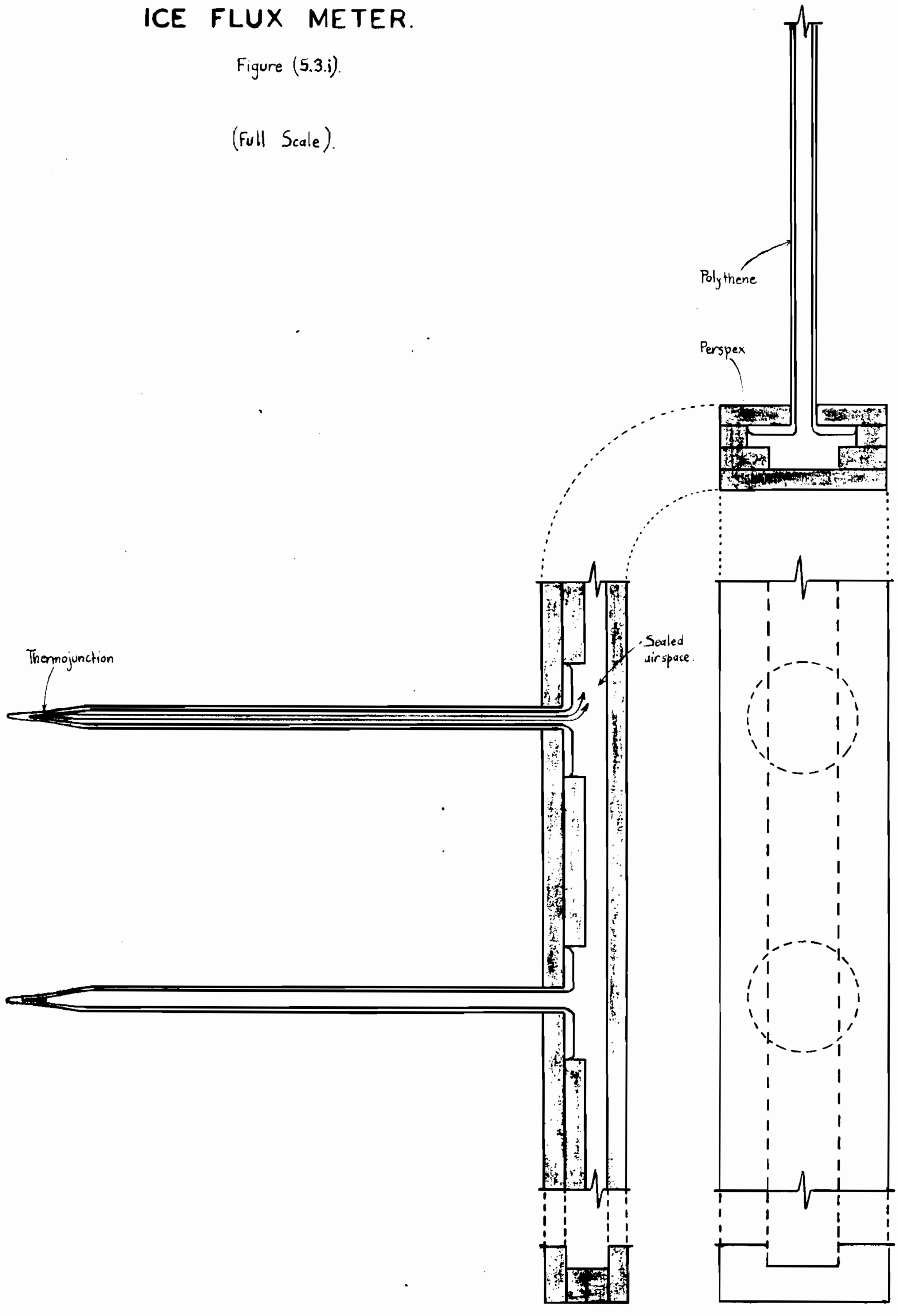

of this measurement being no better than to within 0.05°C or 2.5%. However, the average temperature difference across the 10 cm. reference interval was about 0.7°C, the corresponding heat flux having an error of less than 8%.

A further use for the ice flux meter involved the comparison of temperature gradients within the reference ice and the neighbouring sea ice at the same depth, enabling a determination of the thermal conductivity of the sea ice at this depth for a number of temperatures.

5.4 Convective Heat Flow from the Earth's Surface.

Convective heat flow is a transfer phenomenon of extreme meteorological importance in the first 500 to 1000 metres of the earth's atmosphere, in which two main mechanisms are involved. Firstly there is the process of buoyant energy transfer, which is actually true convection; secondly the mechanism of turbulent transfer, which as will be seen is a process whereby the effectiveness of conduction is greatly increased. The former mechanism is important when significant surface heating takes place and according to Geiger (Ge61) its magnitude can be computed if the radiation balance and conducted surface flux are known. In the polar regions, large temperature gradients are usually the result of nocturnal radiation cooling of the surface, resulting in a density gradient not conducive to buoyant convection. Atmospheric heat transfer thus appears to depend chiefly on turbulence over an ice cover, which latter process will be discussed in this section.

It is a practical experience that the rate of cooling of a body increases with relative motion of surrounding cooler air, so that the experimental study of convective heat loss or gain of a body involves the measurement of both temperatures and wind speeds in its neighbourhood. In general, in nature, and especially in the case of a large plane ice cover, the wind moves horizontally, and a temperature gradient, if at all, exists in the vertical direction. When the wind speed is sufficiently low, the organized molecular flow is laminar, and vertical heat transfer takes place in the same manner as in horizontally motionless air, which in the absence of a density gradient is by conduction.

Under higher wind speed conditions, the onset of turbulence causes a distortion in the air flow layers. No matter how chaotic the motion of a gas may appear on a given scale, the motion appears smooth or laminar if a magnified view is taken of a sufficiently small section. On this basis, it can be seen that the effect of turbulence is to increase the horizontal areas of gas layers by distortion, providing greater opportunities for transfer of momentum across these layers than in the case of laminar flow.

Over a smooth horizontal surface there is always a region immediately adjacent to it namedalaminar sublayer, in which the flow is smooth. Because of the limited transfer opportunities across this layer compared to the turbulent areas above, a rough surface whose projections into the air stream disrupt the laminar flow enables greater heat flow to occur.

The basis of theoretical attempts to calculate heat transfer in the air depends on the determination of the thickness of the laminar sublayer and the temperature gradient across it whence calculation of the heat flux is a simple operation since the transfer constant is the thermal conductivity.

A comprehensive paper by Halstead (Ha54) shows how the measurement of wind speed and temperature at two points separated vertically provides all the information necessary to determine heat flow across the laminar sublayer which, because of the demand for continuity, continues unchanged on through turbulent layers above.

The author has generalized Halstead's equations developed for work in a temperate climate, and introduced the necessary changes to enable their application to arctic temperature conditions. For air with no organized velocity, the heat flux J can be given as:

$$J = K \frac{d(\rho c_p \theta)}{dx} \qquad (5.4.1)$$

where K is the thermal diffusivity.

If the air is in turbulent motion, Halstead has shown that the effective surface area of the layers of air exchanging energy can be given by:

$$A_x = A_\delta \frac{r}{\delta} x \qquad (5.4.2)$$

where $x = \delta$ is the height of the laminar sublayer, and r is a constant. Introducing this factor into (5.4.1), we have:

$$J = K r \frac{x}{\delta} \frac{d(\rho c_p \theta)}{dx} \qquad (5.4.3)$$

Integration from δ to x:

$$\theta_x - \theta_\delta = \frac{J}{K \rho c_p r} \ln \frac{x}{\delta} \qquad (5.4.4)$$

Since δ and θ_δ are both common to the turbulent and laminar layers:

$$J = K \rho c_p \frac{\theta_\delta}{\delta} \qquad (5.4.5)$$

From (5.4.4) and (5.4.5) is obtained:

$$\theta_x = \theta_\delta \left(1 + \frac{1}{r} \ln \frac{x}{\delta}\right) \qquad (5.4.6)$$

An equation of similar form was obtained by Halstead for the horizontal air speed u:

$$u_x = u_\delta \left(1 + \frac{1}{r} \ln \frac{x}{\delta}\right) \qquad (5.4.7)$$

For turbulent flow over a rough surface, the horizontal air speed at height x may be given by:

$$u_x + u_r = u_\delta \left(1 + \frac{1}{r} \ln \frac{x}{\delta}\right) \qquad (5.4.8)$$

where u_r represents the decrease in velocity in the turbulent region due to surface roughness. Under rough conditions the concept of the laminar sublayer is fictitious, and kept for mathematical convenience only.

Halstead has also shown that:

$$u_\delta \,.\, \delta = 121 \nu (1 + 0.0067\ \theta) \qquad (5.4.9)$$

where ν is the kinematic viscosity of air.

As a mean value for the winter months at Button Bay, air temperature of -20°C was taken so that:

$$u_\delta \,.\, \delta = 105 \nu \qquad (5.4.10)$$

Substituting the values of θ_a, θ_b and u_a, u_b for the temperatures and air speeds at heights x = a and b above the surface, the following expression for the convective heat flux may be obtained from (5.4.6), (5.4.8) and (5.4.10)

$$J = \frac{K \rho c_p}{105 \nu} \cdot \frac{r^2 (\theta_a - \theta_b)(u_a - u_b)}{(\ln \frac{a}{b})^2} \qquad (5.4.11)$$

The following numerical values were inserted:

$\rho = 0.0013$ gm. cm.$^{-3}$

$c_p = 0.24$ cal. gm.$^{-1}$ $^\circ$C^{-1}

$\frac{K}{\nu} = 1.4$

$r = 4.65$ (according to Halstead)

giving the equation:

$$J = 0.90 \left(\ln \frac{a}{b}\right)^{-2} . (\theta_a - \theta_b)(u_a - u_b) . 10^{-4} \qquad (5.4.12)$$

where the units of J are cal. cm.$^{-2}$ sec.$^{-1}$.

At the Button Bay site, the anemometers were mounted 270 and 100 cm.

above the ice surface. Periodic adjustments of the constant 0.90 $(\ln \frac{a}{b})^{-2}$ in equation (5.4.12) were necessary because of the accumulation of a snow cover.

The anemometers used were of the Canadian Department of Transport type 51, having three cups spinning on a vertical axis whose geared down rotation closed a pair of contacts once for each nautical mile of wind. Closing of the contacts was used to actuate an electrical pulse, recorded on a strip chart recorder. The same recorder movement and chart were used to record the information from both anemometers, the instruments causing deflections in opposite directions. This procedure eliminated all timing errors between the two instruments. Counting of the recorded pulses gave the wind speed directly in knots, a conversion factor equal to 5.12 enabled the speed to be expressed in cm. sec.$^{-1}$.

Air temperature was measured by copper-constantan thermocouples. The elements were protected from corrosion by a thin layer of polythene drawn over the junction during the application of heat. Radiation shielding was necessary of course, and was accomplished by mounting individual thermocouples along the axis of an aluminium cylinder polished on the outside, and painted matt-black inside. The figure (5.4.i) shows how the cylinders were cut to increase their angle of wind acceptance.

The same multichannel self balancing potentiometric recorder was used for sea ice and air temperature as well as radiation monitoring.

5.5 Evaporation and Condensation.

The large latent heats of vaporization of water and ice lead to important exchanges of energy at surfaces where these substances vaporize or

THERMOCOUPLE MOUNTING AND RADIATION SHIELD.

Figure (5.4.i).

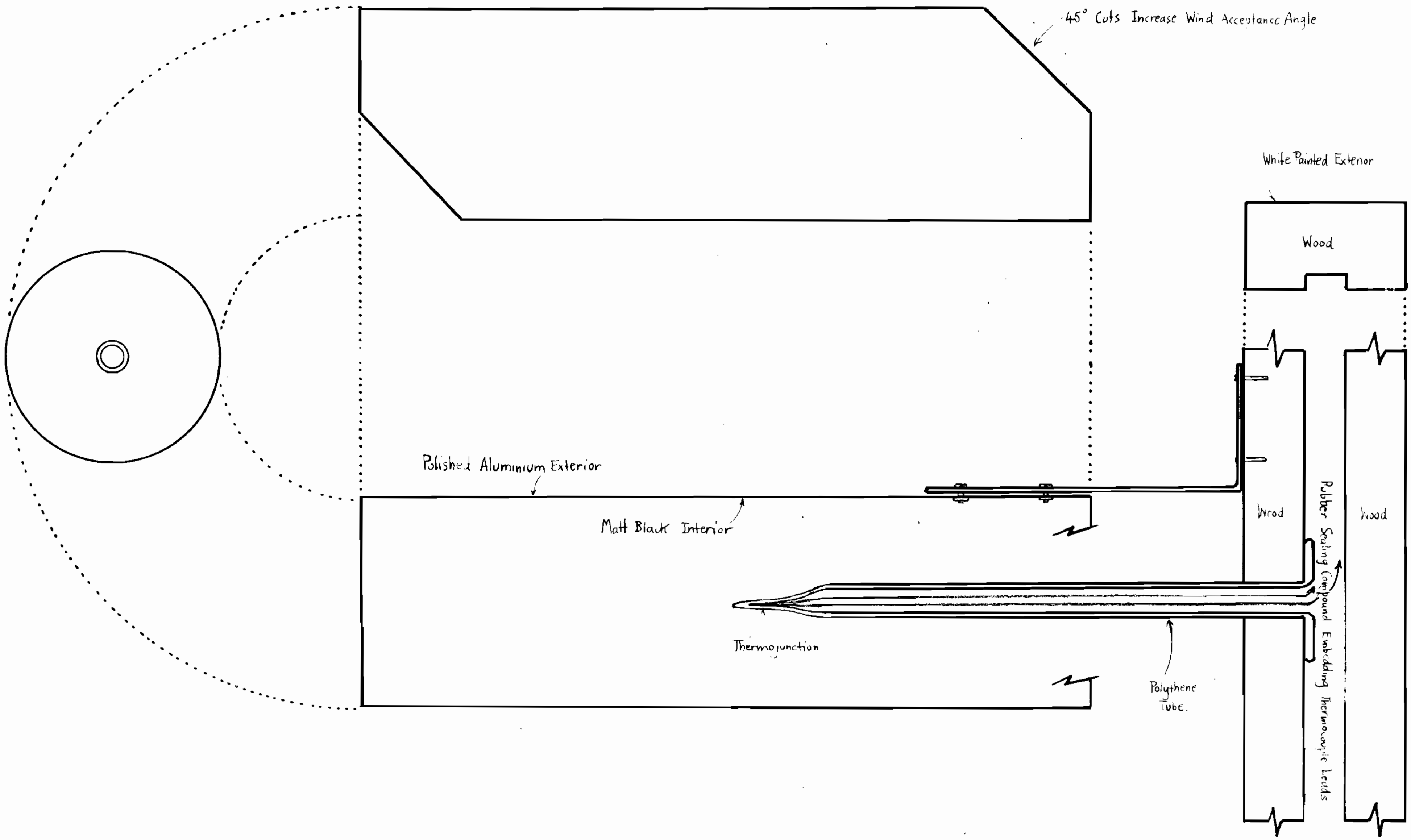

condense. It is important to distinguish between condensation on a surface and precipitation from clouds above, as the latter affects the energy budget of the surface only to the extent of its relatively small heat content. Because condensation may be considered as negative evaporation, the latter term will be used to cover both cases in the general discussion.

As in the case of convective heat transfer, two mechanisms may be recognized as causing evaporation. Firstly that of surface heating by both radiation and the conducted surface heat flux and secondly, the turbulent motion of air over the evaporating surface which prevents the formation of an equilibrium layer of water vapour near to the surface. The fact that both processes may occur independently or act together, causes the analysis of evaporation, as that of convective heat transfer, to become complex and not reliable under all conditions. Geiger (Ge61) has discussed the relation between evaporation and convection in some detail.

Halstead (Ha54) has developed an expression for the evaporative flux on similar lines to that for convective heat transfer. Equation (5.4.12) becomes changed only by the substitution of humidity gradient for temperature gradient and a different constant. Just as equation (5.4.12) predicted no convective heat transfer during wind calm, the evaporative equation leads to a value of zero for the latter term also. Under these conditions the equations are not valid. A wind tends to prevent a large temperature gradient in the air, but during calms, negative temperature gradients may reach a magnitude sufficient to cause significant buoyant convection. At the same time evaporation might also be expected to continue.

According to Hofmann (Ho56), the relative importance of surface heating and air turbulence in influencing evaporation is greatly dependent on the relative humidity. His study led to the following equation for the evaporative heat flux over a surface having an unlimited supply of water substance:

$$E = E_R + E_w = - L \left(\omega_R (R - K) - \omega_w \omega \frac{V-v}{V} \right) \qquad (5.5.1)$$

E_R is the component caused by radiation and conducted surface heat, and E_W is that due to the wind. L is the latent heat of evaporation of water, or ice, depending on the state of the surface water substance. ω_R and ω_w are temperature dependent constants, and ω depends on the wind speed. V is the saturation vapour pressure for the temperature of the air and v is the actual vapour pressure. R and K are the radiation balance and the surface conducted heat respectively. According to the convention of heat flux signs selected in section 5.1, the energy flux of positive evaporation, in absorbing energy from the surface, is given a negative sign. Over an ice and snow cover, the relative humidity generally being high, the latter term in equation (5.5.1) may often be neglected. Particularly as the empirical constants for this term are unreliable for the temperatures experienced over Hudson Bay, only the first term was used in the actual calculation of the evaporative heat flux, using a mean value of 0.25 gm. cal.$^{-1}$ for ω_R. This procedure was partially justified when approximate calculations of the evaporative energy flux using Halstead's equation, which actually gives the E_W term of (5.5.1) only, yielded negligible values. This fact would be reflected in equation (5.5.1) by low values for ω_w and ω. Many examples may be given to illustrate the importance of the E_R term when E_W is negligible because of a saturated atmosphere. Two extreme cases are the "steaming" of wet surfaces after rain, and the formation of fogs over open leads of water in polar regions; in both instances, further vaporization is forced to proceed in a saturated atmosphere.

Measurement of the evaporative flux is extremely difficult under freezing conditions as either the humidity gradient (for Halstead's equation) or the relative humidity (for Hofmann's equation) must be determined. Lithium chloride film hygrometers appear to be the type most applicable for an automatic unmanned recording station. The author has tested these devices, whose resistance decreases monotonically with increase in water vapour content of the surrounding air, but a number of limitations are evident. Chief of these is that the sensors become unreliable and require servicing after condensation or deposition of hoar frost. For this reason, direct continuous monitoring of the evaporative heat flux was not attempted at the Hudson Bay site.

5.6 Timing and Programming a Multichannel Recorder.

A Brown-Honeywell multichannel recorder was connected to monitor 24 sources of e.m.f.. Automatic repeated scanning is accomplished essentially by an input-selecting rotary stepping-switch. Unless manually or otherwise controlled, the recorder normally repeats its cycle of measurements indefinitely.

The potentiometer may be left on stand-by operation with only its electronic components, i.e. the continuous balance amplifier, in operation. Operation of the chart driving motor results in the clutch, which allows operation of the micro switch controlling the stepping-switch impulses by the recorder printing arm, coming into operation. Hence control over the function of the chart drive motor by means of a single contact essentially allows complete control of the instrument.

The simplest method of programming merely requires an electric or clockwork timer whose contacts control either directly, or indirectly by a relay, the running of the chart motor. The cam operating the timer contacts is designed so that the latter are closed for a period of time sufficiently long to allow completion of the longest cycle possible. Considerable disadvantages in this method are evident, since it is laborious to determine which interval of measurement a given printed reading belongs to, because in general an integral number of complete cycles, plus an incomplete one, will be recorded. Thus any one of the e.m.f. channels may be the first to be scanned during a given sampling period. This latter fact is serious when it is recalled that the radiometer outputs were also measured by the recorder. Since these instruments require about 20 seconds to come to equilibrium after their fans are turned on, the outputs are best scanned at the end of a cycle. A further disadvantage lies in the considerable waste of chart paper due to the unnecessary multiplication of the printed record in repeated cycles.

Accordingly, a circuit was designed which would respond to the current pulses triggering the rotary, multiposition stepping-switch. Its ease of installation is such that only one lead to the stepping-switch position, corresponding to the channel after whose monitoring a cycle is completed, requires connection. This means that the expensive recorder need not in itself be irreversibly modified.

Reference is now made to the circuit diagram shown in figure (5.6.i).

Closing of the timer contacts causes the discharge of C_1, which has been charged through R_1, through K_1, and thus momentarily closes K_{11}. This allows K_{21} to be pulled in permanently, so that the instruments are connected to power through K_{23} and K_{24}. K_{22} also being in, C_2 commences to become charged through R_2. On receiving power, the recorder commences a cycle of 25 scans and recordings, each channel being connected in turn by a stepping-switch which receives pulses from the main unit. When a cycle has been completed, the switch is in the final channel; the pulse received in this position

RECORDER PROGRAMMING CONTROL UNIT

Figure (5.5.i)

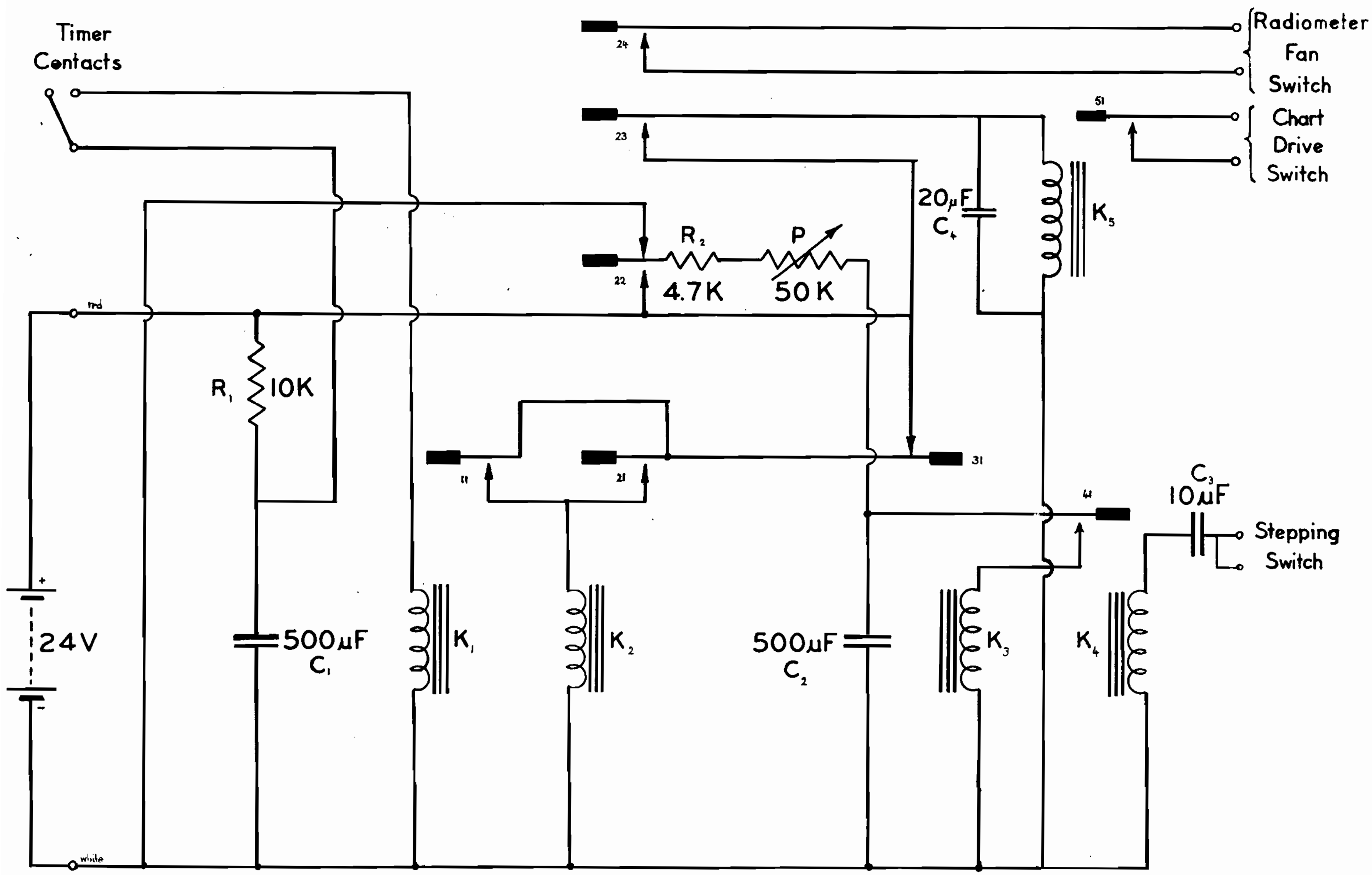

to return the switch to the first channel is caused to switch the instrument off with a slight delay so that the stepping switch coasts into the first channel position by the following means: The signal pulse received through C_3 pulls in K_{41}, thus discharging C_2 through K_3, so that K_{31} opens, disconnecting the power from K_2 for a short interval, so that it then remains open permanently, and the instrument is switched off through K_5, whose contacts K_{51} open after a short delay when C_4 is discharged. C_2 now slowly discharges through R_2, and the instrument cannot be restarted for a controllable time interval of the order of 1 minute. The delaying relay K_5 is necessary to enable the printing mechanism of the recorder to complete its action. Without it, the printing channel number lags an additional stage after each complete cycle, and the last channel reading is not printed.

In spite of the many relay contacts, this control unit operated continuously for three months without breakdown.

5.7 An Automatic Recording Station.

The recording equipment consisted of a Brown-Honeywell multichannel recorder monitoring 24 temperature and radiation channels, and a single channel Esterline Angus 1 mA. recorder. The latter was connected to a simple circuit causing it to undergo deflection to the left and right for each nautical mile of wind recorded by the upper and lower anemometer respectively. This type of recorder is continuously operating, and being clock work, is independent of the timing system required for the self balancing potentiometer.

The programming unit described in the previous section received its starting impulse once every two hours from a clock driven by a d.c. motor and

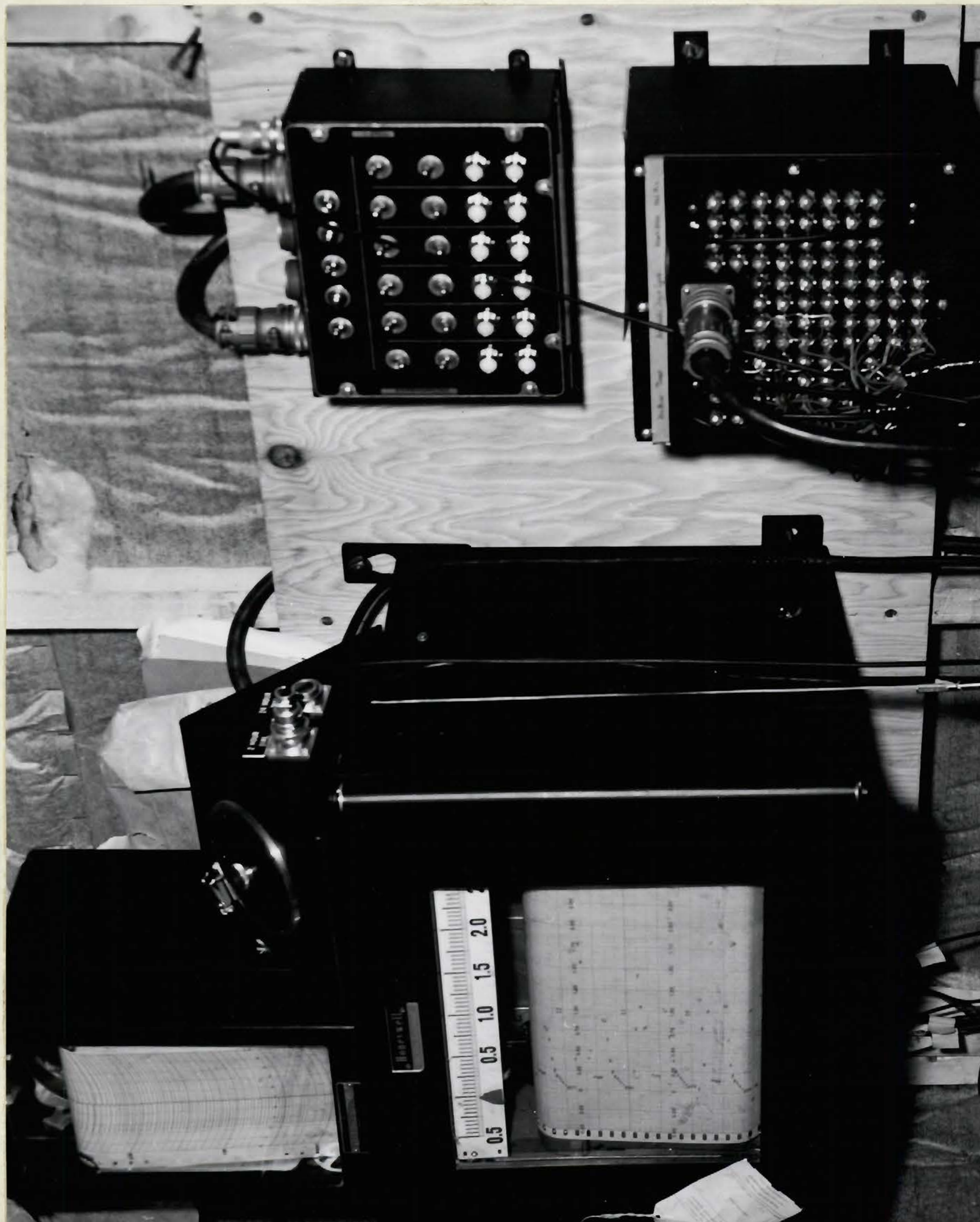

Recording and Timing Equipment.
Figure (5.6.1).

controlled by mechanical escapement. All these units were housed in a 7' x 7' x 7' wooden hut and kept at an operating temperature by a propane stove.

Electrical power was supplied by a 32 volt d.c. wind generator. Because of the frequent high winds during the winter, this type of generation is most reliable and economic in the Canadian Arctic. Charge was stored in heavy duty accumulators with a total potential of 24 volt, using only a simple relay type voltage regulator. A transistorized voltage regulator allowed the satisfactory operation of the electric clock as well as the continuous balance amplifier of the recorder on 21 volt.

The Brown-Honeywell recorder is shown in photograph (5.7.i), with the Esterline Angus recorder and the electric clock above the main unit. The programming unit is contained within the switching box seen in the lower right. The prefabricated wall mounting for the instruments allowed maximum use of the limited space available.

Exterior views of the station taken in May 1961 are shown in the photographs (5.7.ii) and (5.7.iii), taken from the south west and north respectively. In the former, viewed from left to right, are seen the wind generator, the hut and vehicle, the thermocouple pole with two junctions remaining above the snow surface, two Gier and Dunkle all wave radiometers, and two Kipp solarimeters sharing the same monopod. The photograph (5.6.iii) shows, in addition, the two anemometers.

Button Bay Site, 1961
Figure (5.6.ii)

Button Bay Site with Anemometers in Foreground

Figure (5.6.iii)

CHAPTER 6

THE RESULTS OF A WINTER'S RECORDS ON HUDSON BAY ANNUAL ICE

6.1 The Ice Cover and the Site.

The field station which was operated during the winter months of January, February, March and April, with supplementary visual observations in May, 1961, was located approximately two miles from the nearest land, on the frozen surface of Button Bay. The exact location was established by compass bearing observations of three known landmarks. Button Bay, as the accompanying map (6.1.i) shows, is an approximately semi-elliptical indentation in the south western Hudson Bay shoreline, occupying an area of some 50 square miles. This bay is fed directly only by one minor stream whose watershed does not extend for more than 20 miles, and the large volume of water from the Churchill River is deflected away eastwards by the Eskimo Point peninsula. Aerial reconnaissance has shown that Button Bay is generally completely covered by ice between early December and June. Aerial photographs taken in 1957-58 are shown in figures (6.1.ii,iii,iv,v,vi). This area, being landlocked on three sides and free of the danger of mechanical breakup of the cover as well as being essentially free of low salinity water currents, provides an almost ideal site for vertical energy transfer studies at sea. The linear dimensions of the Button Bay ice cover being of the order of 10,000 metres, may be considered practically infinite when compared to an ice thickness of 1.5 metre, and is even large compared to the height of the turbulent boundary layer in the atmosphere.

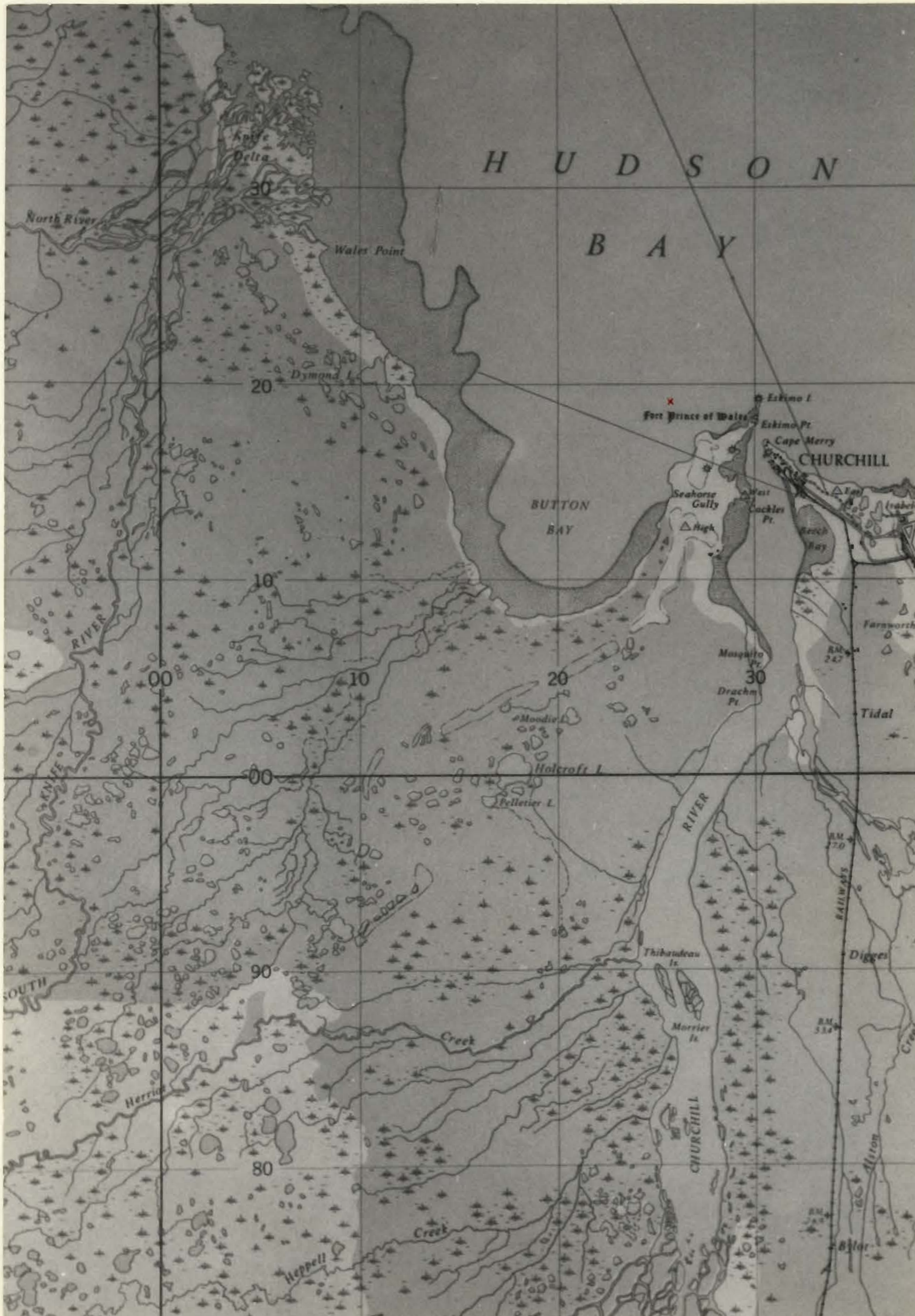

BUTTON BAY.
1961 Site marked in red, Approximate limits of field of view in photographs (6.1.ii-vi) indicated. Side of Grid Square = 10 Km.
Figure (6.1.i).

Button and Hudson Bay

December 1957

Figure (6.1.ii).

January 1958
Figure (6.1.iii)

February - March 1958
Figure (6.1.iv)

April 1958
Figure (6.1.v)

May 1958
Figure (6.1.vi)

The thickness of the ice cover is shown as a function of time in early 1961 in figure (6.1.vii). This graph will frequently be referred to in the following sections of this chapter, as will figure (6.1.viii) which shows the air and ice surface temperatures as a function of time.

The sea water below the cover was used as a reference for all temperature measurements, necessitating monitoring of the salinity. Water samples taken from four metres below the ice surface on five occasions between February and April were determined to be of salinity 29.1, 30.0, 29.8, 29.6 and 29.4‰ respectively. The mean being 29.6‰ ; 30‰ was used in most calculations. The graph (1.1.i) shows that a freezing point of about -1.6_5°C is to be expected for water of this salinity, a fact verified by direct temperature measurements.

As a matter of convenience and conciseness, an abbreviation has been adopted for the recording of dates. The months of January, February, March and April are denoted by the letters J, F, M and A respectively. Using this notation, the 27th. of February, for example, would be written as 27F.

6.2 The Fluxes of Radiation.

The examples selected from the daily records obtained are from two representative periods of the ice cover's history. These are in February, when the daily radiation balance is negative, and in April when it is positive. Figures (6.2.i...v) show the components of radiation and the four main energy fluxes for at least one clear and a completely overcast day for each of the two periods.

All the radiation components have peak values occuring shortly after noon on the time scale. Apart from timing inaccuracies, this is because true

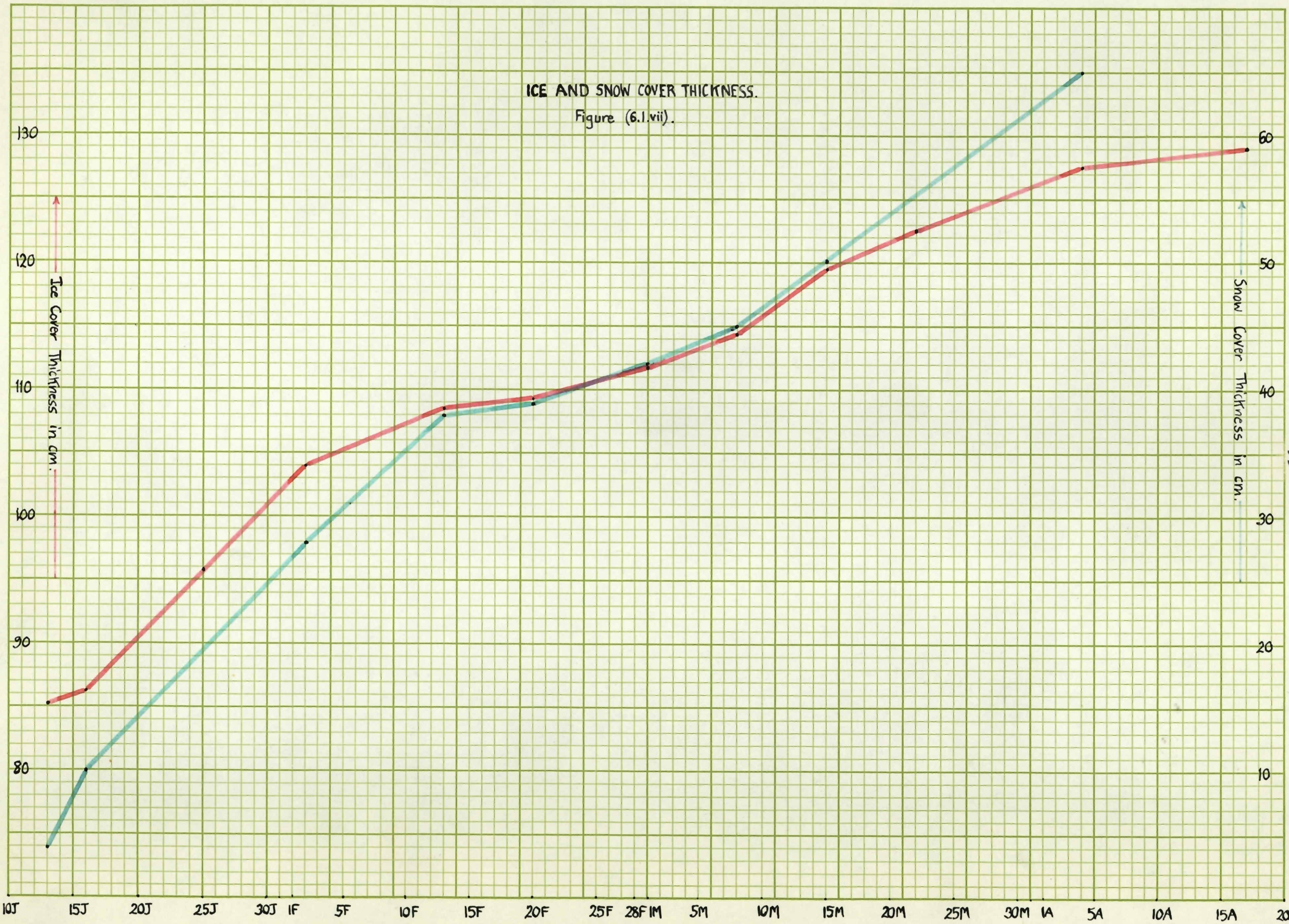

ICE AND SNOW COVER THICKNESS.
Figure (6.1.vii).
130
120
110
100
90
80
Ice Cover Thickness in cm.
60
50
40
30
20
10
Snow Cover Thickness in cm.
10J
15J
20J
25J
30J
1F
5F
10F
15F
20F
25F
28F
1M
5M
10M
15M
20M
25M
30M
1A
5A
10A
15A
20A

Figure (6.1.viii)

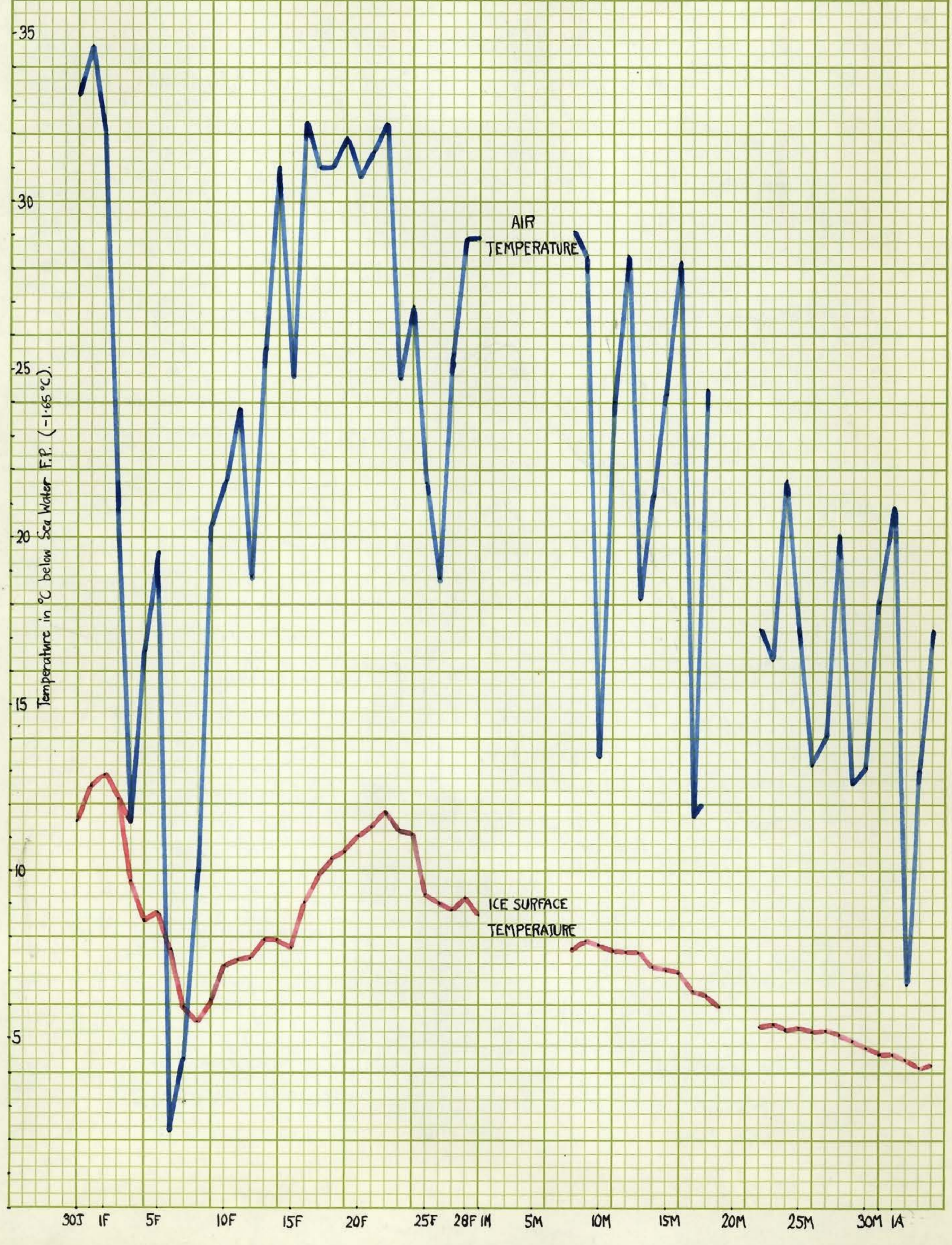

local time at Churchill on average lags local standard time, to which the timer was set, by 16 minutes.

The most conspicuous feature of the records in this sub-arctic region, was the high transparency of the atmosphere to solar radiation. At noon, approximately 90% of the solar energy was transmitted to the earth's surface. A similar degree of transparency is evident in the records of Liljequist (Li56), obtained at Maudheim, about 71°S.

In general, less short wave and all wave radiation reached the surface on overcast than on clear days. This reduction in intensity of short wave radiation was less than might be expected to be absorbed by or reflected from the upper surface of the cloud cover, an observation also made by Diamond and Gerdel (DG58) on the Greenland ice cap. This maintenance of a high value for incident solar radiation on overcast days can be explained on the basis of multiple reflection and scattering between the snow cover and lower cloud surface. It was interesting to observe a progressive increase of the fraction of radiation reaching the earth's surface on overcast days, as the solar angle above the horizon increased. Using the short wave records for pairs of one overcast and one clear day, not separated by more than three days, the relative transmission at noon on overcast days was calculated to be 73%, 75% and 81% for 24F, 9M and 6A respectively. Although no accurate quantitative conclusions can be drawn, this effect is almost certainly due to the cloud thickness which the radiation passes through becoming less at angles of incidence closer to the normal, as well as to the change in instrumental calibration.

An important consequence of an overcast sky is the considerable increase in long wave radiation. This is to be expected, as carbon dioxide and water vapour are the only atmospheric gases which are significant absorbers and emitters of radiation at these wavelengths. The dependence of long wave

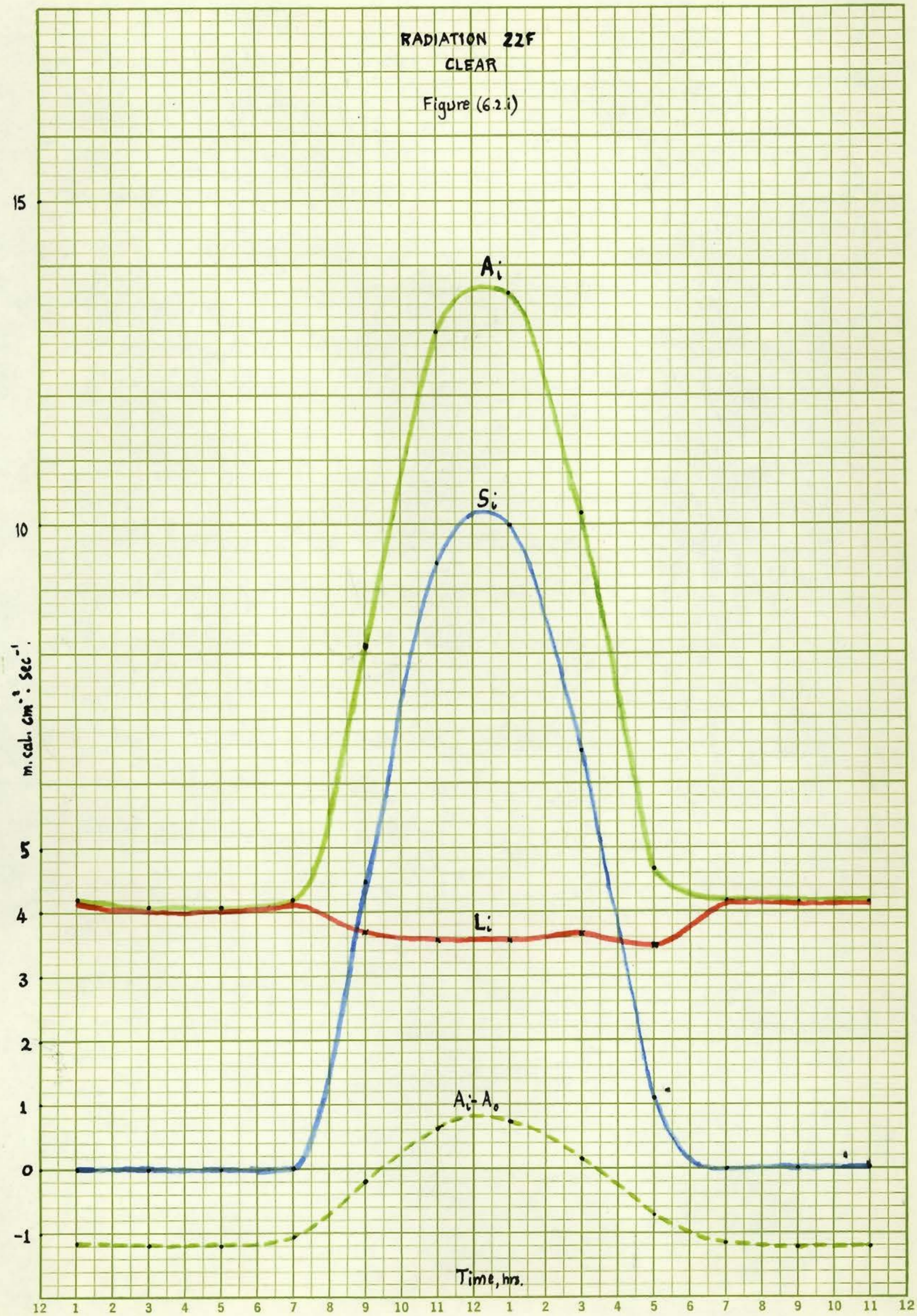

K+E 1 DAY BY HOURS X 100 DIVISIONS KEUFFEL & ESSER CO. 358-130 MADE IN U.S.A.

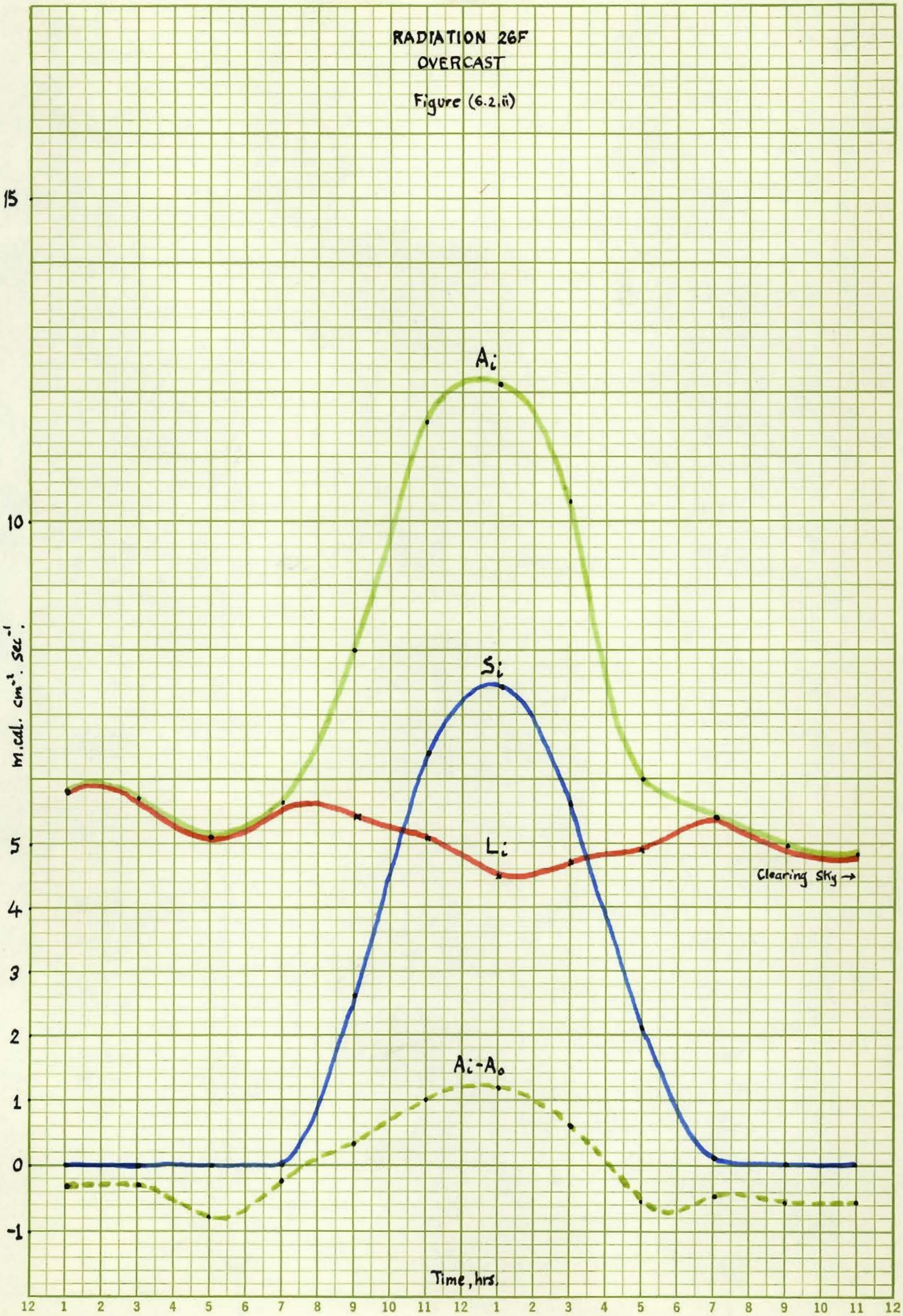
RADIATION 26F
OVERCAST
Figure (6.2.ii)
m.cal. cm⁻². sec⁻¹
15
10
5
4
3
2
1
0
-1
Aᵢ
Sᵢ
Lᵢ
Aᵢ-A₀
Clearing Sky →
Time, hrs.
12 1 2 3 4 5 6 7 8 9 10 11 12 1 2 3 4 5 6 7 8 9 10 11 12

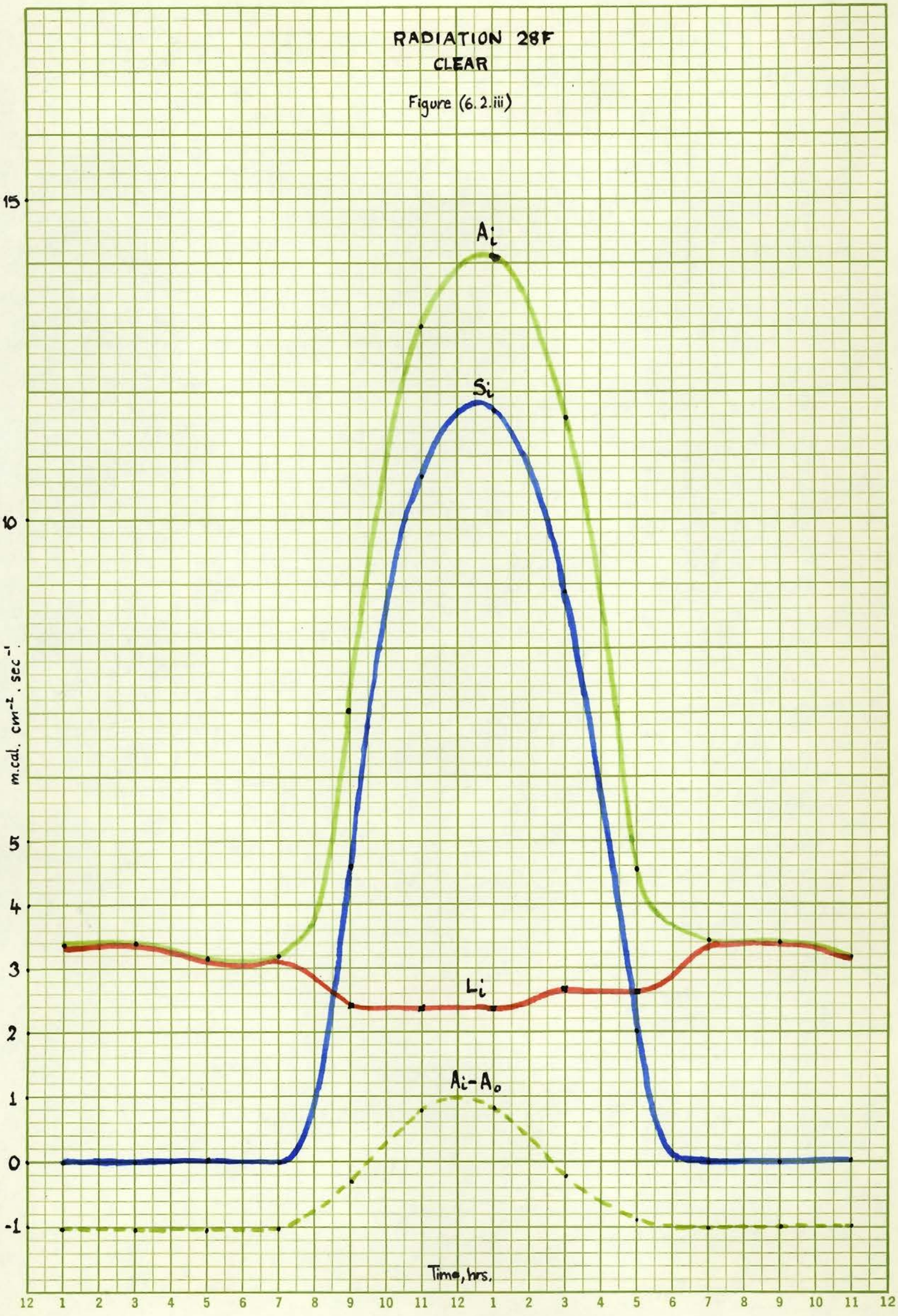
RADIATION 28F
CLEAR
Figure (6.2.iii)
A_i
S_i
L_i
$A_i - A_o$
m.cal. cm^{-2}. sec^{-1}
15
10
5
4
3
2
1
0
-1
Time, hrs.
12 1 2 3 4 5 6 7 8 9 10 11 12 1 2 3 4 5 6 7 8 9 10 11 12

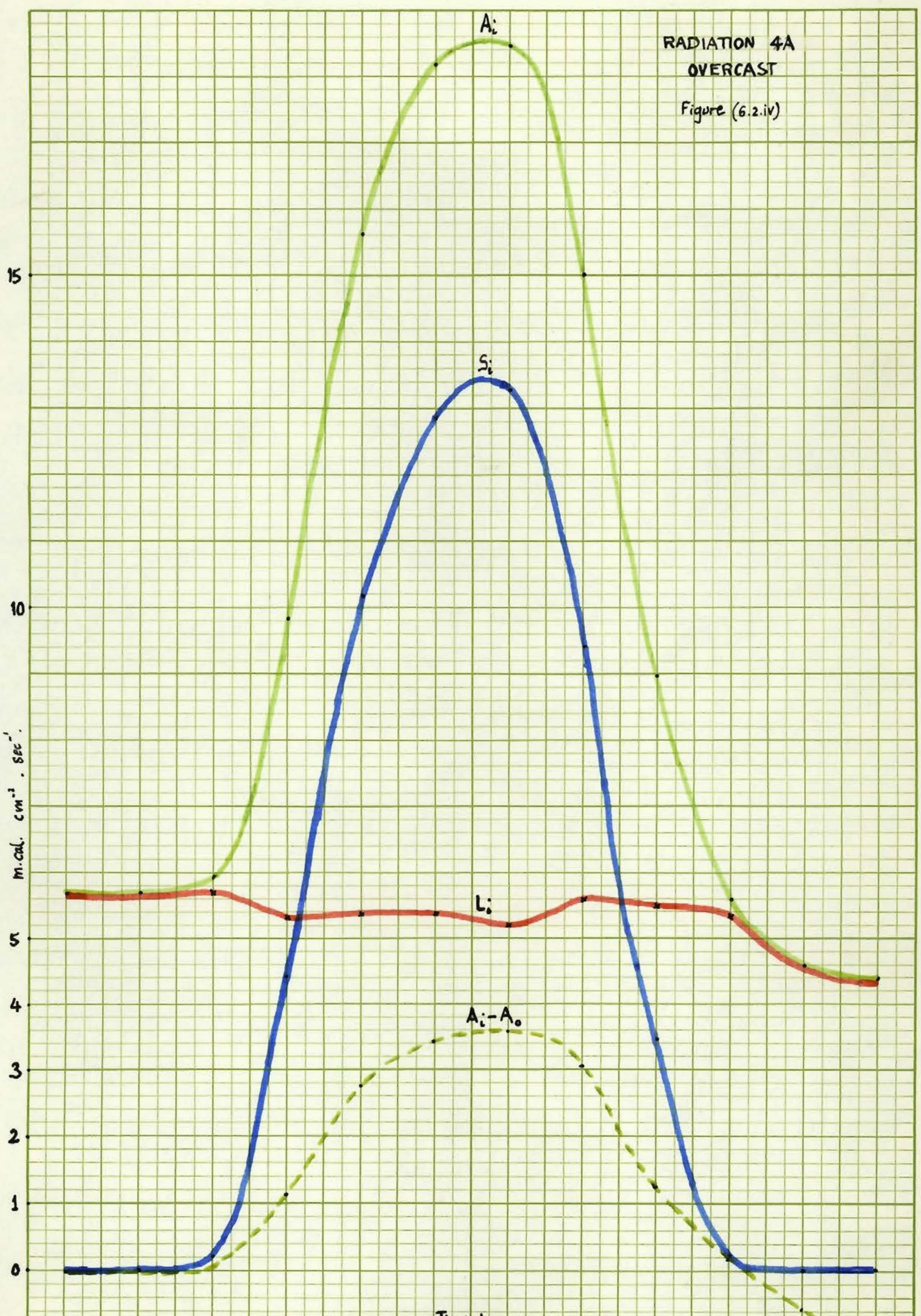
RADIATION 4A
OVERCAST
Figure (6.2.iv)
A_i
S_i
L_i
$A_i - A_o$
m.cal. cm⁻². sec⁻¹.
Time, hrs.
15
10
5
4
3
2
1
0
12 1 2 3 4 5 6 7 8 9 10 11 12 1 2 3 4 5 6 7 8 9 10 11 12

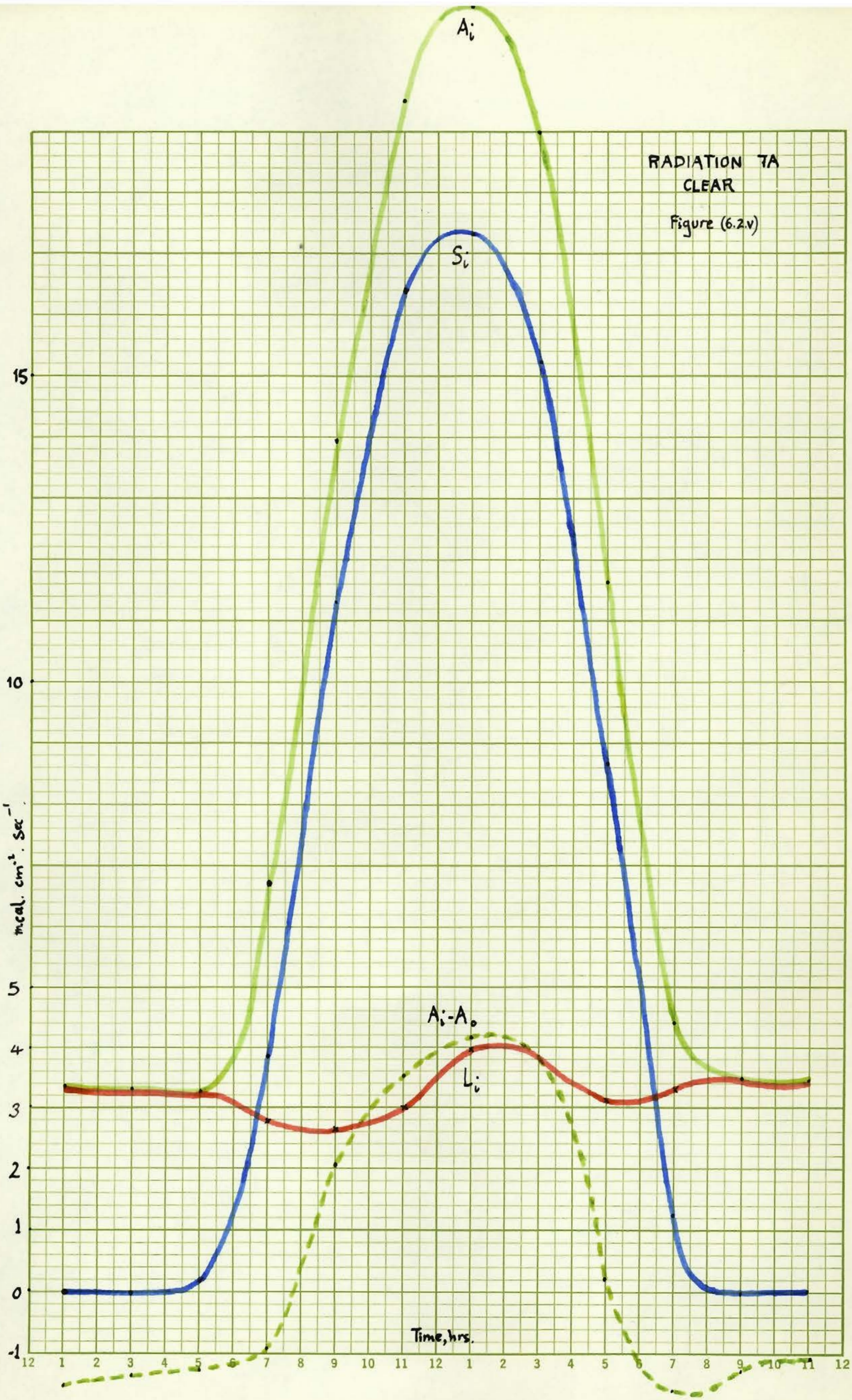

RADIATION 7A
CLEAR
Figure (6.2.v)
A_i
S_i
$A_i - A_o$
L_i
mcal. cm^{-2}. sec^{-1}
Time, hrs.

radiation on these quantities has been investigated by Elsasser, who has devised a practical diagram (El40) which enables the estimation of radiant flux at any level, including the surface, if the humidity and temperature profiles are known. No comparisons of instrumental readings with the semi-empirical values derived from an Elsasser or similar diagram appear to have been made in polar regions. Untersteiner (Un61) made use of the Elsasser diagram to compute long wave radiation, but awaiting the calibration of his radiometers, has published no instrumental results covering these wavelengths. The author had no facilities for obtaining the temperature and humidity profiles at the atmospheric heights needed for the empirical calculations. The measured values cannot be compared with Untersteiner's empirical determinations as the latter were obtained during the melting season on permanent pack ice. The increase in long wave radiation on the overcast 4A is particularly evident when compared to the clear 7A, but the value on 22F is high for a clear day at this time. On the clear 28F, long wave radiation remained below 4 m. cal.-cm.$^{-2}$ sec.$^{-1}$. This illustrates the danger of making quantitative generalizations, as a warmer upper atmosphere can lead to high values of long wave radiation even on clear days. However, the long wave radiation was invariably less on clear than on overcast days. The irregular tendencies exhibited by the long wave radiation curves are certainly instrumental in origin. The incident long wave radiation would not be expected to change significantly on a clear day and a decrease during the hours of daylight would be unexpected. Since the long wave radiationis obtained by subtraction of short and all wave radiometer measurements, the irregularity displayed by this computed curve is a reflection on the reliability of all the radiation values.

It is interesting to calculate the black body temperature of the upper atmospheric layers emitting the long wave radiation. From figure (6.2.vi), it

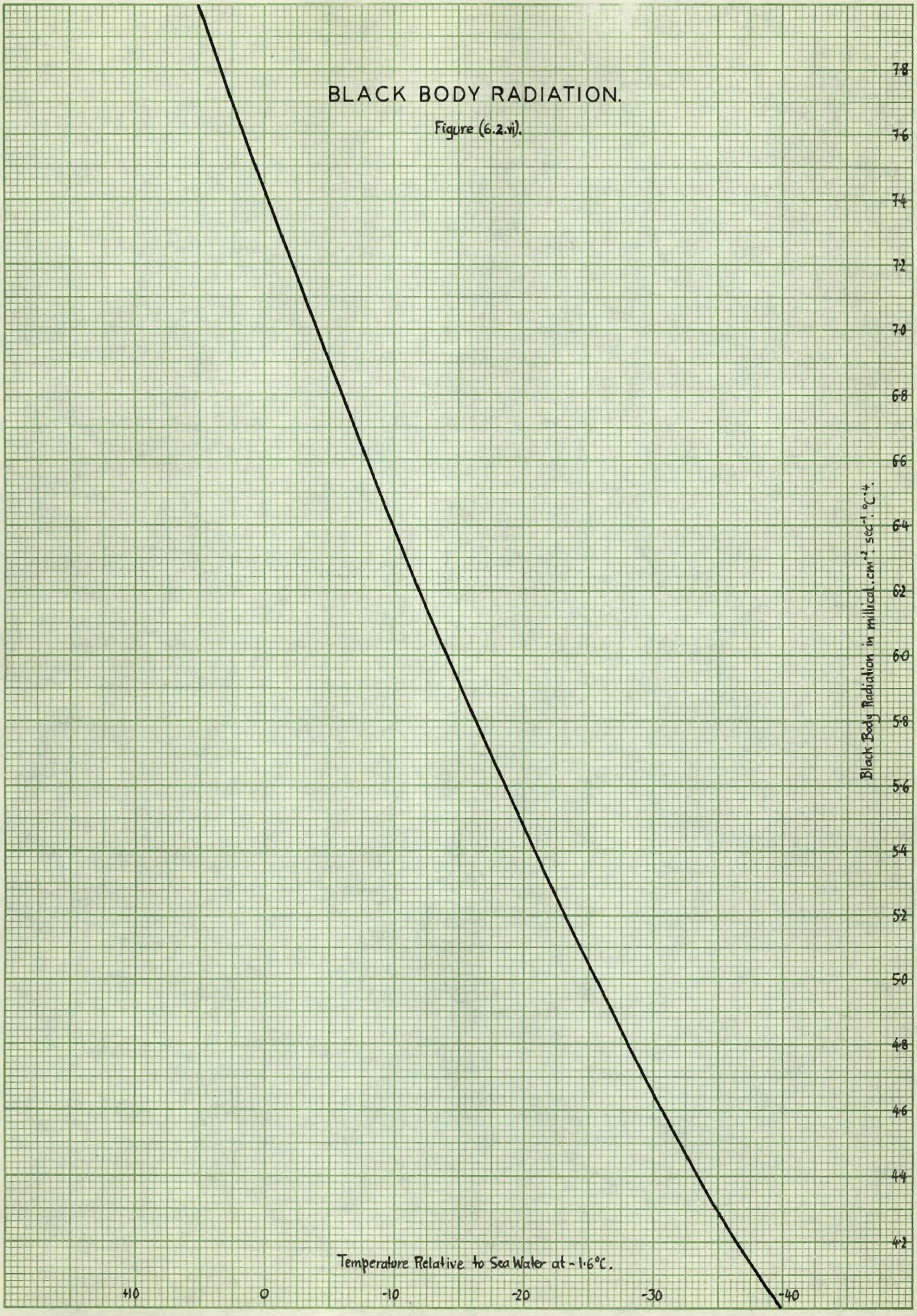
BLACK BODY RADIATION.
Figure (6.2.vi).
Black Body Radiation in millical. cm⁻². sec⁻¹. °C⁻⁴.
7·8
7·6
7·4
7·2
7·0
6·8
6·6
6·4
6·2
6·0
5·8
5·6
5·4
5·2
5·0
4·8
4·6
4·4
4·2
Temperature Relative to Sea Water at -1·6°C.
+10
0
-10
-20
-30
-40

may be seen that on the overcast day 4A, the 5.4 ± 0.2 m.-cal. cm.$^{-2}$ sec.$^{-1}$ of long wave radiation corresponded to a cloud temperature of some -22.5 $\pm$ 2.2°C. By comparison, the mean air temperature 2 metres above the cover shown in figure (6.1.viii) was -18.5°C. Although an inversion might have been expected to predominate on such overcast days, the measurements of convective heat transfer support these black body temperature figures. The air above the cover was colder even on overcast days and as will be discussed later, the inversion was a nocturnal event only. Because nocturnal net radiation loss was low with an overcast sky, even these inversions tended to be small. Calculations for clear days, of course, show that the upper atmosphere was even colder.

The net radiation at noon was negative only during one clear day in early March, when some surface flooding of the ice cover took place. This indicates that constant negative net radiation might be expected during the initial formation of the ice cover. The summed daily records shown in figure (6.3.v) show that the daily radiation balance was consistently negative until the latter half of March, when a sudden transition to continuous daily positive net radiation became evident. Unfortunately, inaccessibility of the recording instruments for their periodic servicing at this time meant that the actual transition stage was not monitored. The period of positive net radiation was interrupted only once, when a period of high radiation absorption which caused melting and relatively warm surface temperatures, was followed by increased radiation from the cover and hence a negative radiation. balance.

The short wave albedo could be measured reliably only on overcast days, because of the change in calibration factor with angle of incidence discussed in section 5.2. The falling off in sensitivity of the radiometers was illustrated by the apparent decrease in albedo with increase in solar angle above the horizon, provided the snow surface was quite smooth. The short wave albedo determined on overcast days, when both upper and lower facing radiometer faced sources of diffuse radiation, remained essentially constant at 0.85 from February to April.

A number of observers have stressed the importance of radiant energy penetrating the ice cover. According to Iakovlev (Ia58), 80% of all solar radiation is absorbed in the upper 15 to 20 cm. of an ice cover. This corresponds to an extinction coefficient of some 0.1 cm.$^{-1}$. Untersteiner holds that radiation is much more penetrating and has determined the extinction coefficient to be approximately 0.015 cm.$^{-1}$ which value is supported by Ambach's and Mocker's determination of 0.018 cm.$^{-1}$ for glacier ice (AM59). Because sea ice would be expected to be less transparent than glacier ice, it is possible that the extinction coefficient for the former lies between the values quoted by Iakovlev and Untersteiner. Both Iakovlev (Ia58) and Dorsey (Do40) are in agreement as to the much greater absorptivity of snow, 20 cm. of which is stated to absorb more than 95% of the incident radiation. In view of this fact, the presence of a substantial snow cover at the Button Bay site, meant that the radiant heating of the upper ice cover layers could be neglected. It is unlikely that ice is significantly transparent to long wave radiation, as this would imply radiant heat loss from the ice-water interface and consequently a rate of ice growth greater than that prescribed even by Stefan's simple equation. Examination of estuary ice at Churchill by the author (Sc60) and the measurements on the St. Lawrence river on very thin ice by Barnes (Ba28) both show that the rate of ice growth is actually less than predicted by Stefan's equation. A result of the transparency of ice to short wave radiation is discussed at the close of the following section.

6.3 The Fluxes of Conduction, Convection and Evaporation.

Although the water below the ice cover is a source of heat independent of winter solar radiation, the magnitude of the conducted flux of heat through the ice is influenced by radiation absorbed at the surface. This is because the ice surface temperature, and hence the temperature gradient in the ice, is largely determined by solar radiation and the two atmospheric heat exchange processes. Convection and evaporation are of course greatly dependent on the radiation, a fact which is reflected in the results.

The ice flux meter measuring the conducted heat through the ice being 20 cm. below the surface of the ice, which was covered by a substantial snow cover, no diurnal variations in the flux were detected. Apart from the effects of changes in the heat content of the established ice, the magnitude of the conducted heat flux was related to the rate of growth of ice. As the ice thickness increased, the rate of growth tended to decrease, a trend recorded by the flux meter, whose summed daily readings are also shown in figure (6.3.v). Many of the determinations of the energy budget of an ice cover, including those of Iakovlev (Ia58) and Untersteiner (Un61) did not involve measurement of the conducted flux of heat directly. Rather the total exchange of heat energy at the cover surface calculated from measurements of net radiation, convective and evaporative energy transfer and surface melting were correlated to the change in total heat content of the cover. So many terms, some of poor accuracy, being involved in the net surface energy transfer, the latter term is not sufficiently reliable for any conclusions to be drawn as to the thermal capacity and latent heat of the ice. Readings from a conducted surface flux meter give a direct value for net energy exchange at that level, and are of sufficient accuracy to enable a useful calculation of thermal properties of the ice below. Because the flux meter was separated from the air and ice-water interface by snow and ice respectively of considerable thermal capacity, related phenomena at these three levels do not occur simultaneously. This rate of energy transfer by conduction will be discussed in the following section.

The dominant feature of the convective heat flux is its dependence on the net radiation. The diurnal inversion is clearly seen in figures (6.3.i... ..iv), in which the same colour coding as in figure (6.3.v) is employed with the letters R, K, C and E denoting net radiation, conduction, convection and evaporation respectively. Surface heating by solar radiation by day leads to convective loss of heat, and radiation cooling of the upper surface by night leads to an inversion. Thus in addition to the curves for heat gained by radiation and convection being opposite in sign, a short time lag, whilst the surface responded by heating or cooling, would also be expected for the convective process. In addition to the diurnal dependence of convective heat loss on the radiation, the same phenomenon may be observed to a less pronounced extent on a larger time scale, as may be seen in figure (6.3.v).

Evaporation having been determined by the semi-empirical method described in chapter 5, the dependence of this energy flux on the sign and magnitude of the net radiation is clear, because of the relative constancy of the conducted surface heat flux during any one day. The records in figure (6.3.v) show that in February, the conducted heat flux was still of sufficient magnitude to frequently determine the sign of the evaporative flux. There can be no doubt that evaporation is a more important mechanism of heat loss early in the history of an ice cover as well as later in the season under the influence of prolonged solar radiation. For example the author's examination of ice from the Churchill River estuary (Sc60), indicated a rate of ice growth of some 12 cm. per day during the first two days of the cover's existence.

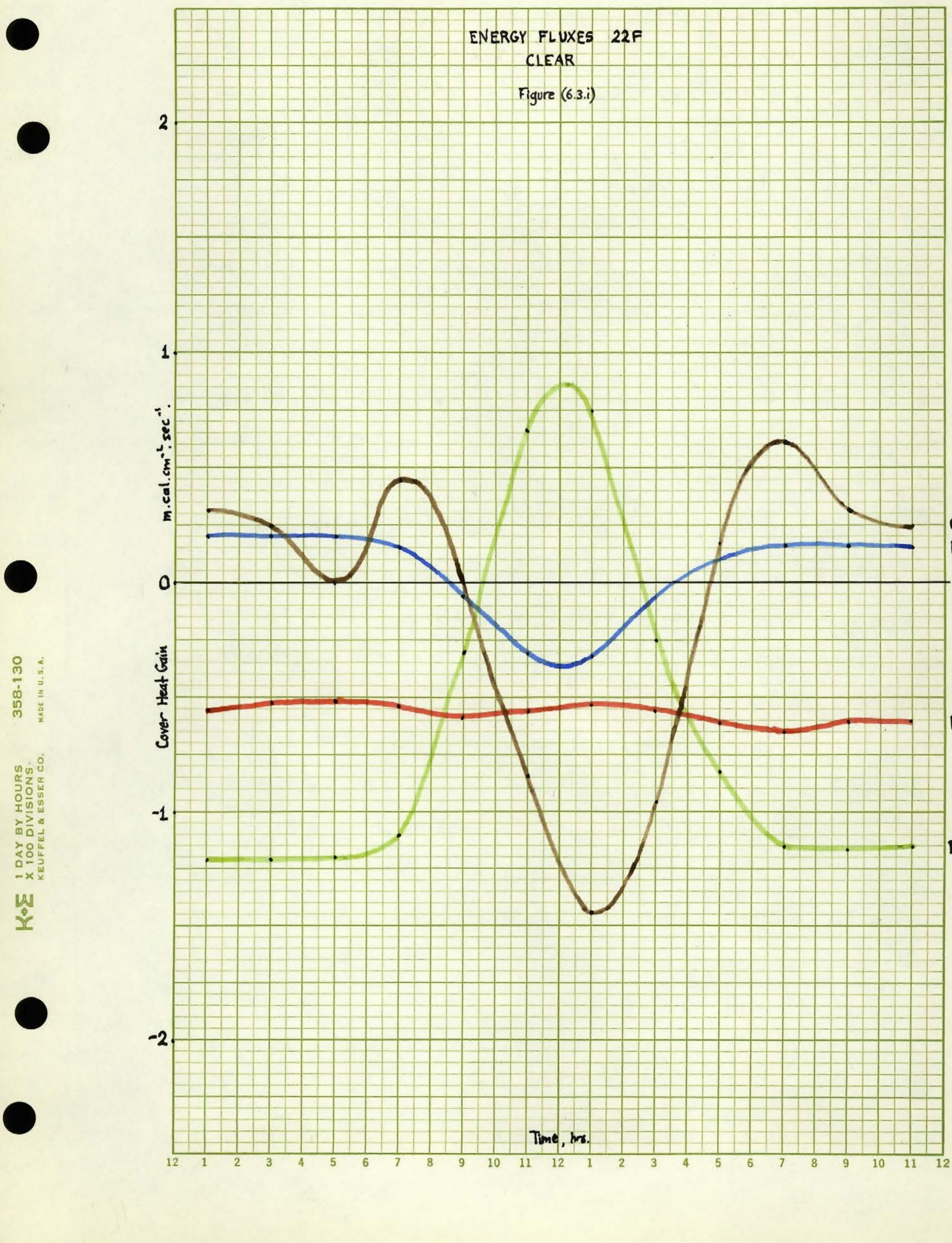
ENERGY FLUXES 22F
CLEAR
Figure (6.3.i)
Cover Heat Gain m.cal.cm⁻².sec⁻¹.
2
1
0
-1
-2
C
E
K
R
Time, hrs.
12 1 2 3 4 5 6 7 8 9 10 11 12 1 2 3 4 5 6 7 8 9 10 11 12
K+E 1 DAY BY HOURS X 100 DIVISIONS KEUFFEL & ESSER CO. 358-130 MADE IN U.S.A.

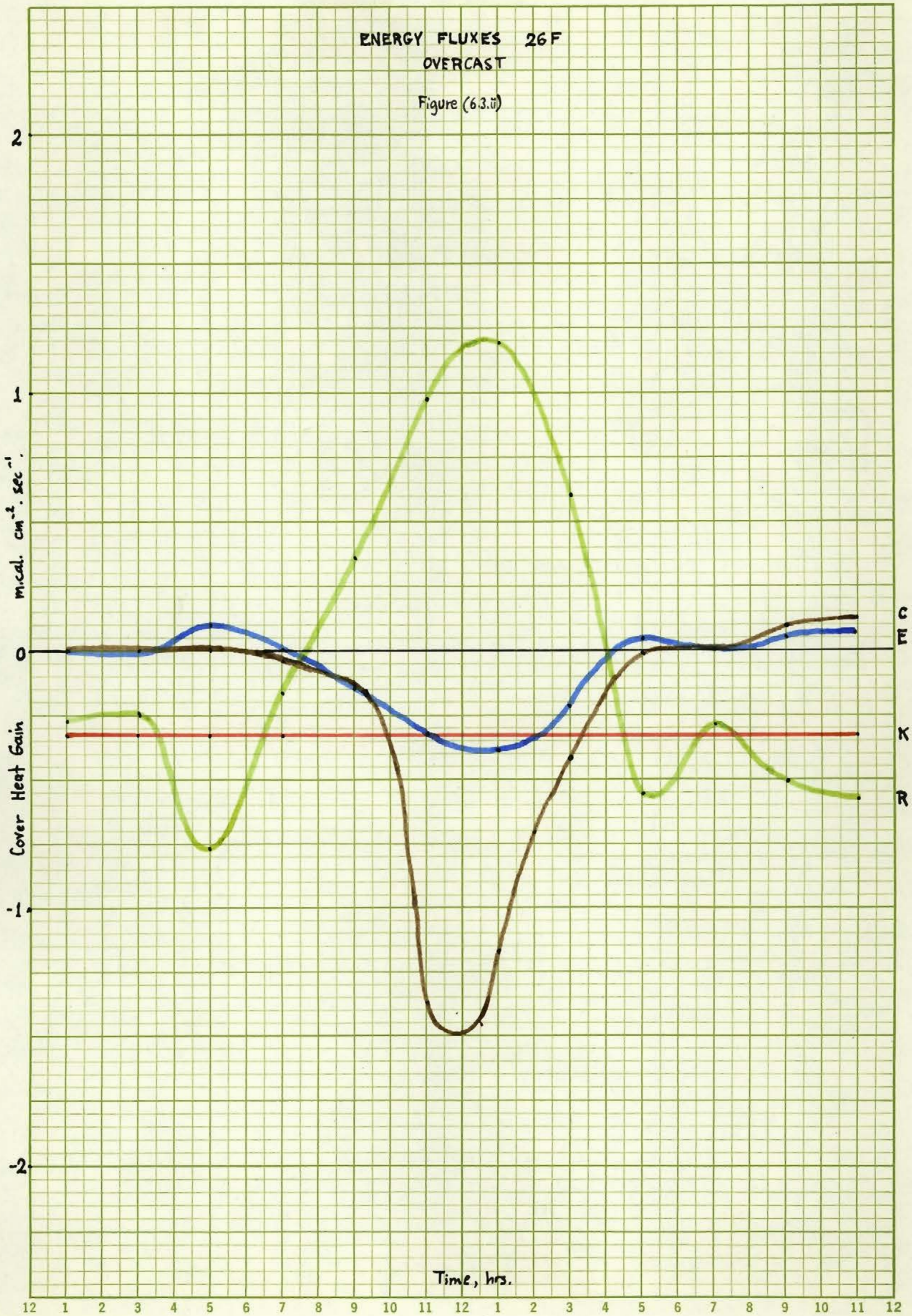
ENERGY FLUXES 26F
OVERCAST
Figure (6.3.ii)
2
1
0
-1
-2
Cover Heat Gain m.cal. cm^{-2}. sec^{-1}.
C
E
K
R
Time, hrs.
12 1 2 3 4 5 6 7 8 9 10 11 12 1 2 3 4 5 6 7 8 9 10 11 12

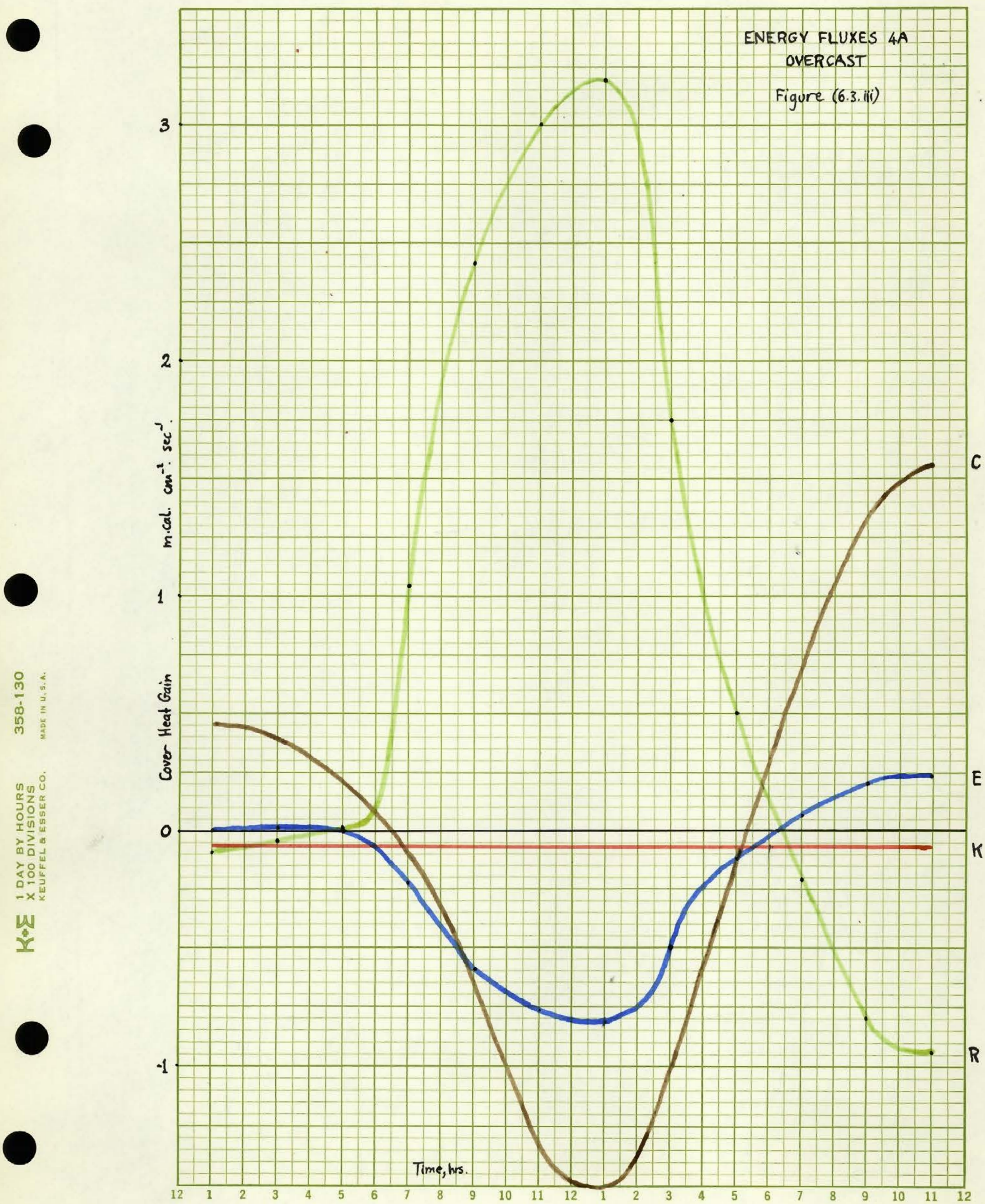
ENERGY FLUXES 4A
OVERCAST
Figure (6.3.iii)
Cover Heat Gain m.cal. cm⁻¹. sec⁻¹.
3
2
1
0
-1
C
E
K
R
Time, hrs.
12 1 2 3 4 5 6 7 8 9 10 11 12 1 2 3 4 5 6 7 8 9 10 11 12
K+E 1 DAY BY HOURS X 100 DIVISIONS KEUFFEL & ESSER CO. 358-130 MADE IN U.S.A.

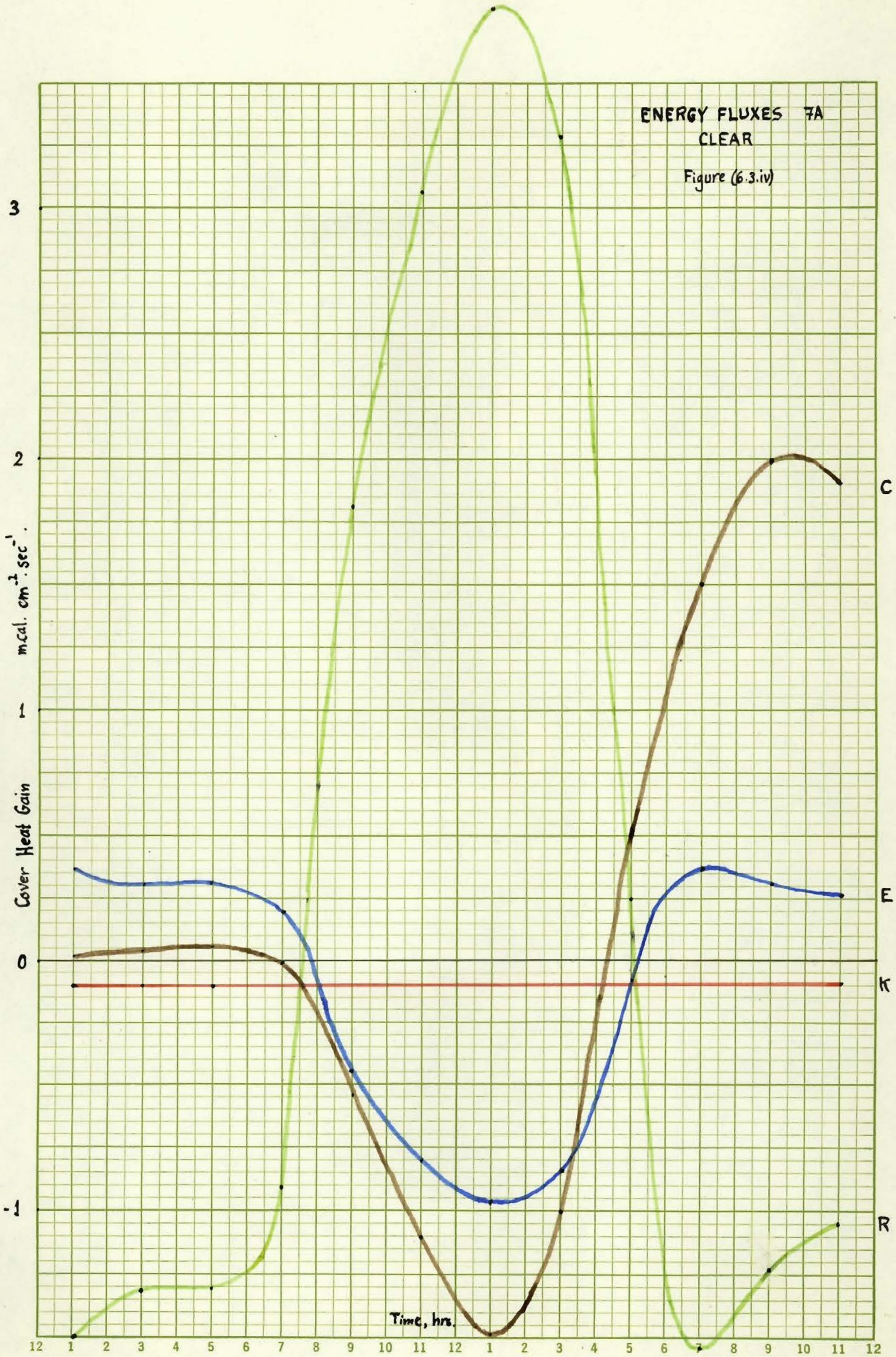
ENERGY FLUXES 7A
CLEAR
Figure (6.3.iv)
Cover Heat Gain m.cal. cm^-2. sec^-1.
3
2
1
0
-1
C
E
K
R
Time, hrs.
12 1 2 3 4 5 6 7 8 9 10 11 12 1 2 3 4 5 6 7 8 9 10 11 12

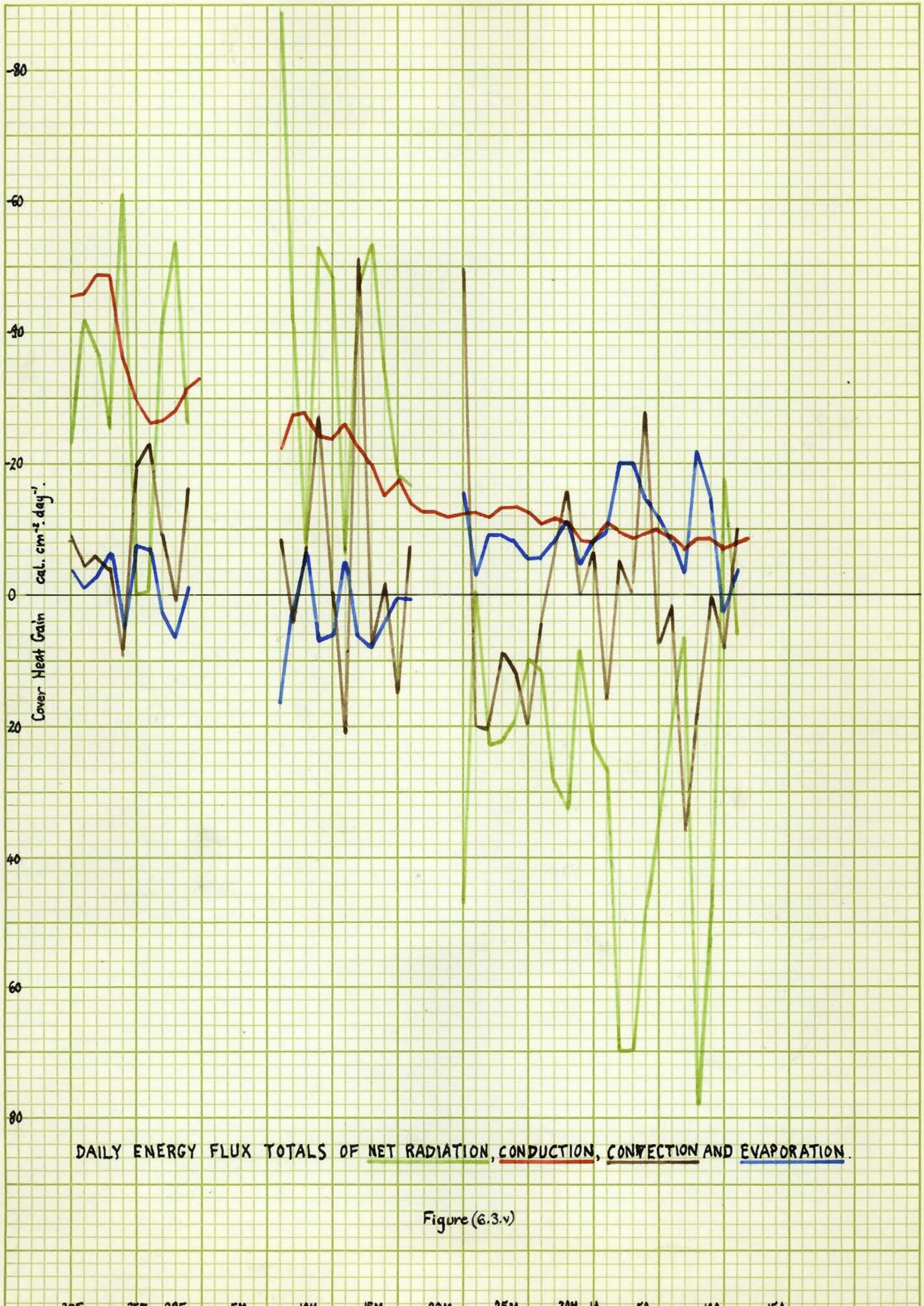
-80
-60
-40
-20
0
20
40
60
80
Cover Heat Gain cal. cm⁻². day⁻¹.
20F
25F
28F
5M
10M
15M
20M
25M
30M
1A
5A
10A
15A
DAILY ENERGY FLUX TOTALS OF NET RADIATION, CONDUCTION, CONVECTION AND EVAPORATION.

Figure (6.3.v)

This rate of growth required a loss of approximately 10 m.-cal. cm.$^{-2}$ sec.$^{-1}$ from the upper ice surface. Because of the low albedo of a new ice surface, radiation could account for little of this heat loss during the day, and for not more than 7 m.-cal. cm.$^{-2}$ sec.$^{-1}$ during the night. The perfectly flat and smooth surface of the ice indicated the absence of a wind sufficient to have caused turbulent heat transfer to be important. It is thus probable that buoyant convection and evaporation were the chief energy loss processes. The alternate layers of fresh and sea ice, each having grown in about 6 hours, showed no diurnal variation in thickness. This could be due to increased evaporation during the daytime as well as transparency of the ice to solar radiation. If Ambach's and Mocker's (AM59) value for the extinction coefficient of 0.018 cm.$^{-1}$ for glacier ice is assumed for the remarkably clear estuary ice, then over 80% of incident solar radiation penetrated through 12 cm. of the ice. Since the all wave radiation at noon during the November freeze-up did not exceed 12 m.-cal. cm.$^{-2}$ sec.$^{-1}$, only about 2.5 m.-cal. cm.$^{-2}$ sec.$^{-1}$ were absorbed in the new ice. This left approximately 3 m.-cal. cm.$^{-2}$ sec.$^{-1}$ at night and 5.5 m.-cal. cm.$^{-2}$ sec.$^{-1}$ at noon, to be lost in the atmosphere by convection and evaporation.

The interdependence of the two atmospheric heat transfer processes was clearly shown on calm clear nights. The inversion set up at these times precluded any buoyant energy transfer, and in the absence of turbulence, evaporation, or rather condensation, was the only remaining available process. Hoar frosts of about 0.2 mm. thickness were found deposited only after calm relatively clear nights. A 0.2 mm. layer of frost of density 0.4 corresponds to a heat transfer of about 5 cal. cm.$^{-2}$. Averaged over a 14 hour February night, an energy flux of 1.2 m.-cal. cm.$^{-2}$ sec.$^{-1}$ may be calculated. By comparison the average condensation energy empirically determined for the nocturnal hours of 22F is 1.8 m.-cal. cm.$^{-2}$ sec.$^{-1}$.

6.4 The Rate of Transfer of Energy through an Ice Cover.

Correlation of temperature exposure at the ice cover surface and the rate of ice formation is of considerable importance, hence it is necessary to be able to calculate at least approximately, the rate of transmission of a temperature disturbance through the ice.

In section 3.2, it was shown that the time taken for a given degree of completion of a temperature change initiated by a sudden discontinuity in surface temperature is directly proportional to the square of the ice thickness, and inversely so to the diffusivity, i.e.

$$t_\theta \propto \frac{h^2}{K} \qquad (6.4.1)$$

Similarly the theory of section 3.4 has indicated that for sufficiently long time intervals, this relation holds true for ice covers whose surface temperature is continually changing with time.

It is difficult to include the diffusivity changes in any practical application, as the observation of time lag in temperature change is most conveniently made on peaks or valleys in the growth and temperature curves, so that a significant change in diffusivity occurs during one single interval of measurement. Since the mean diffusivity over the period of time in which a maxima or minima occurs is approximately equal in both cases, it is convenient to consider K as a constant in equation (6.4.2) and write:

$$t_\theta = \chi h^2 \qquad (6.4.2)$$

The calculation of the rate of growth of ice is shown in table (6.4.i), and

Table (6.4.i)

Ice Thickness and Rate of Growth at Button Bay.

Time	Thickness	Mean Growth Rate	Mean Time for Rate
13J	85.2 cm.		
		0.37 cm.day^{-1}	14.5J
16J	86.3		
		1.07	20.5J
25J	95.9		
		1.01	29J
2F	104.0		
		0.41	7.5F
13F	108.5		
		0.11_4	16.5F
20F	109.3		
		0.28	24.5F
1M	111.8		
		0.38_6	4.5M
8M	114.5		
		0.71	11.5M
15M	119.5		
		0.43	18.5M
22M	122.5		
		0.38_5	28M
4A	127.5		

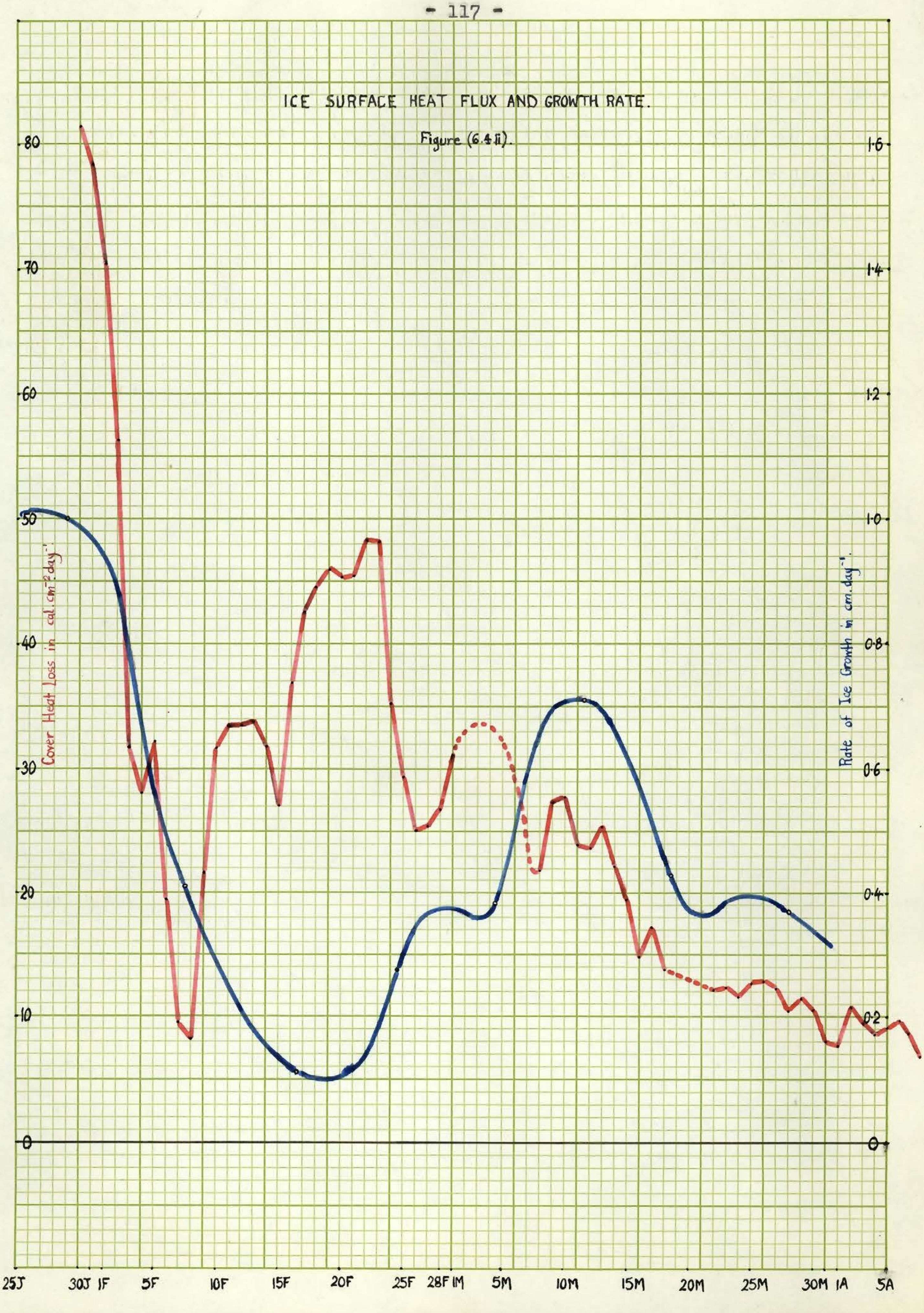
ICE SURFACE HEAT FLUX AND GROWTH RATE.
Figure (6.4 ii).
Cover Heat Loss in cal.cm⁻².day⁻¹
Rate of Ice Growth in cm.day⁻¹
80
70
60
50
40
30
20
10
0
1.6
1.4
1.2
1.0
0.8
0.6
0.4
0.2
0
25J
30J
1F
5F
10F
15F
20F
25F
28F
1M
5M
10M
15M
20M
25M
30M
1A
5A

is reproduced graphically in figure (6.4.ii) which also shows the measured heat flux at a depth of 20 cm. in the ice cover. Although the former curve necessarily lacks detail, owing to the limited number of observations, the main features are visible and similar on both curves. The predominant minimum and maximum in the heat flux, occurring between 8F and 9F, and 22F and 23F respectively, are reproduced particularly clearly on the growth curve, but other minor trends also appear to be followed. The ratios of the two valleys and the two peaks are approximately 80 and 70 (cal. $cm.^{-3}$) respectively. As these values are reasonable approximations to the latent heat of formation and cooling of the existing ice, it is reasonable to assume that the information from the graph is a suitable basis for further deduction.

Table (6.4.iii) below summarizes the method of calculating χ from the observations.

Table (6.4.iii)

Date of Flux Max. or Min.	Date of corresponding ice growth max. or min.	Time diff. in days, t	Mean ice depth below flux met. during time int.	χ day $cm.^{-2}$
7.5F	19F	11.5	86	$1.6^{\pm 0.3} \times 10^{-3}$
22.5F	11M	16.5	93.5	$1.8^{\pm 0.3} \times 10^{-3}$
Mean value of the transfer constant:				$1.7^{\pm 0.3} \times 10^{-3}$

The general application of equation (6.4.2) requires an expression for the mean thickness $\bar{h}$ over the time interval t_θ. Since h is monotonically increasing with time during the winter, we can write:

$$\bar{h} = \frac{2h_0 + t_\theta \frac{dh}{dt}}{2}$$

where h_0 is the initial ice thickness below the meter, and $\frac{dh}{dt}$ is the mean rate of increase during the time t_θ.

$$\bar{h}^2 = h_0^2 + h_0 t_\theta \frac{dh}{dt} \qquad (6.4.3)$$

the term containing t_θ^2 being quite small. Substituting (6.4.3) in equation (6.4.2), we have:

$$t_\theta = \frac{\chi h_0^2}{1 - \chi h_0 \frac{dh}{dt}} \qquad (6.4.4)$$

Table (6.4.iv) indicates the application of this equation.

Table (6.4.iv)

Time of Flux Measurement	Depth of Ice below Meter at that time, h_0	Mean growth Rate $\frac{dh}{dt}$	t_θ days	Time Surface Flux is shown in Growth
30J	81 (cm.)	0.6 (cm. day^{-1})	12 ± 2	11F
19M	101	0.3	18 ± 3	6A

When the surface temperature rather than the heat flux at a depth of 20 cm. is compared with the rate of growth of ice, χ is found to be equal to 1.2 ± 0.2 and the values for t_θ calculated by means of (6.4.4) are found to be 13 ± 2 and 18 ± 3 respectively, thus being in accord with the values calculated in table (6.4.iv).

On examination of the records showing ice temperature as a function of depth and time, it is interesting to observe that the above conclusions are supported. In figure (6.4.v) the ice temperature is shown at five 25 cm. separated points along a vertical axis in the cover. It is seen that the time

130

ICE TEMPERATURES. Figure (6.4.v).

lag becomes longer between the lower levels where the temperatures are higher and hence mean diffusivity is lower. Similarly the time lag for transmission of a minimum in temperature is greater than for a maximum, for the same reason. This is of course also why the mean value for χ is less for the entire cover than for the portion below the 20 cm. level.

6.5 The Balance of Thermal Energy.

At the cover surface, the algebraic sum of the net radiation and the atmospheric heat fluxes must equal the total heat supplied by conduction in the cover, except when melting or freezing occurs at the surface. Thus in this section, the four energy fluxes of radiation, conduction, convection and evaporation will be considered. The conducted heat flux, and its relation to change in heat content of the ice cover and the heat released by freezing, will be discussed in later sections.

The heat budget for three periods of eight days is shown in table (6.5.i). Because the ice flux meter was not at the snow surface at which heat exchanges occurred, the readings after a relative delay of 1 day in February and March, and 2 days in April were used. Choice of suitable delay times can be estimated from the time separation of corresponding maxima and minima in air and ice surface temperature curves shown in figure (6.1.viii).

During the February period shown, the measured heat losses above the cover total 317.4 cal. cm.$^{-2}$ compared with a sub-surface total heat flow of 287.8 cal. cm.$^{-2}$. Considering the latter to have been the more accurately determined quantity, the tally is correct to within 10%. This discrepancy is easily covered by the possible errors for the radiation and conduction measurements alone, discussed in chapter 5. Noteworthy are the relatively small

Table (6.5.i)

Total Heat Flux in $cal.cm.^{-2}\ day^{-1}$.

Date	Radiation	Conduction	Convection	Evaporation
20F	-23.1	-	- 9.4	-4
21	-42.0	-45.8	- 2.1	-1
22	-36.8	-48.4	- 5.9	-2
23	-25.3	-48.2	- 3.4	-6
24	-60.8	-35.3	+ 9.8	+5
25	0	-29.5	-18.3	-7
26	- 0.4	-26.1	-22.9	-6
27	-40.0	-26.6	- 8.8	+3
28	-	-27.9	-	-
	-238.4	-287.8	-61.0	-18
11M	-52.8	-	-26.8	+7
12	-47.8	-23.7	+ 0.2	+6
13	- 6.3	-25.4	+21.2	-4
14	-47.0	-22.1	-52.0	+6
15	-53.7	-19.4	+ 8.5	+8
16	-33.4	-14.7	- 1.5	+5
17	-18.1	-17.3	+15.4	+1
18	-13.9	-13.9	- 8.5	+1
19	-	-13.2	-	-
	-259.1	-149.7	-43.5	+30
5A	49.7	-	-27.4	-14
6	35.8	-	+ 8.8	-12
7	22.8	-8.6	+ 1.7	- 8
8	6.6	-6.8	+36.0	- 3
9	79.9	-8.3	+17.3	-22
10	48.3	-8.3	0	-15
11	-17.9	-7.1	+ 8.7	+ 3
12	6.2	-7.5	-10.8	- 3
13	-	-8.3	-	-
14	-	-8.0	-	-
	230.5	-62.9	34.7	-74

magnitudes of the net convective and evaporative energy fluxes.

For the 8 days in March, the balance recorded by the instruments was upset by surface flooding of the ice with subsequent freezing. The total heat loss at the upper surface was -272.6 cal. cm.$^{-2}$, compared with a heat flow to the surface from below of -149.7 cal. cm.$^{-2}$. The discrepancy of 122.9 cal. cm.$^{-2}$ may be accounted for by the 2 to 3 cm. of snow ice formed. The density of the lower snow levels was determined to be approximately 0.4 gm. cm.$^{-3}$ by a cylindrical snow extractor which, with little compression, removed 25 cm.$^{-3}$ of snow for weighing. The formation of snow ice of density 0.9 gm. cm.$^{-3}$ in this snow involved the freezing of 0.5 gm. of water per cm.$^{-3}$ of ice and the release of 100 cal. cm.$^{-2}$ for 2.5 cm. of snow ice. This flow of heat accounts for the lack of balance of the measured heat fluxes. It is interesting to note that although convection may be extremely important on individual days, the net effect over a longer period appears to be small compared to the net radiation.

The poor agreement for the April period is serious. The increase in heat content of the snow cover was only about 25 cal. cm.$^{-2}$, so that the effective net heat exchange measured above the cover was approximately 165 cal. cm.$^{-2}$. Referring to the value of -62.9 for the conducted flux, it is seen that almost 230 cal. cm.$^{-2}$ must be accounted for. There is no reason to doubt the magnitude of the net radiation. Figures (6.2.iii) and (6.2.iv) showing the radiation components for 4A and 7A, show reasonable values for the long wave radiation, whose determination required s.w. radiation readings. The conducted heat flux was consistent with continued ice growth. Thus the sources of error are probably in the values obtained for convection and evaporation. Almost certainly, Halstead's equation (5.4.12) for the convective heat flow is not applicable to the ice cover at this stage of the season.

During April, frequent wind calms were observed, which in daytime would lead to signiticant solar heating of the cover. It is possible that buoyant convection, neglected by Halstead is then extremely important. Possibly the net convection is negative rather than positive. Evaporation also is likely to have been more significant. During this period, the snow cover visibly changed texture and increased in packing. This was a result of daytime surface melting. The difficulty of choosing a proper value for the temperature dependent coefficients in Hofmann's evaporation equation (5.5.1) when applied to an atmosphere with large temperature gradients restricts the use of a semi-empirical relation of this type.

There is no particular value in summing the various energy fluxes over a large period of time unless this covers a complete cycle of events, such as the entire history of an annual ice cover, or a whole year for a permanent ice cover. However, summation does give an additional indication of the reliability of the individual flux measurements.

For the period 20F to 12A, the measured energy flux totals are shown below:

Conduction	-961 cal. cm.$^{-2}$
Radiation	-357 "
Convection	-153 "
Evaporation	-182 "

The 20 cm. of ice and average of 50 cm. snow of density 0.35 gm. cm.$^{-3}$ above the ice flux meter, warmed by approximately 8°C, account for a further 150 cal. cm.$^{-2}$. This makes the calculable heat conducted to the upper snow surface equal to 811 cal. cm.$^{-2}$. Radiation and atmospheric heat losses total 692 cal. cm.$^{-2}$. The lack of balance is increased to about 250 cal. cm.$^{-2}$ when surface freezing in March is included. This difference cannot be completely accounted for by probable errors in measurement of radiation and conduction, but is covered by the remarks on the increased importance of buoyant convection and evaporation in April.

For the first month with a positive net radiation in the Central Arctic Basin at about 85°N, both Iakovlev (Ia58) and Laikhtman (La59) have reported values for convective and evaporative heat loss of approximately equal magnitude, which total more than the net incident radiation because of the heat flow from the ice. The quantitative value of these results is limited because of the calculation of evaporation as a residual. Because of continuous darkness for almost five months at the latitude of these observations, an essentially continuous atmospheric temperature inversion would be expected, leading to a positive, rather than net negative convective heat exchange as at Hudson Bay, where all observations were made not more than five weeks from the equinox. In addition to daytime radiation, the greater conduction of heat through the thinner annual ice cover also prevented a permanent inversion from being established.

By contrast, the observations of Orlenko and Smetannikova (OS59) show no regular seasonal tendencies in either magnitude or sign for the energy fluxes of convection and evaporation. The value of this work is extremely dubious, as simultaneous correlation of ice growth and upper surface phenomena is shown, but with ice reported as varying from 120 to 190 cm., a two to three week delay would be expected.

The results of Untersteiner (Un61) have not yet given solar and atmospheric components of the heat budget at Drifting Station A, also in the Central Arctic. As a consequence his discussion draws on Iakovlev's data (Ia58), and is limited to the melting season from May to August.

The processes occurring within the ice cover controlling the flux of conducted heat will be analysed in the following two sections.

6.6 Conducted Surface Heat Flux and the Latent and Specific Heats of Ice.

Correlation of the measured surface heat flux with the theoretically calculated loss due to latent and specific heats is important. It enables a check on the validity of the experimantally determined heat loss and shows the relative importance of freezing and cooling of ice as sources of energy.

Table (6.4.iv) shows that flux measurements at the 20 centimetre level on 30J and 19M are reflected in terms of ice growth on 11F and 6A respectively. Referring to the ice thickness graph (6.1.vii), it is observed that the heat lost between the former dates caused the growth of 21.3 cm. of new ice and the cooling of an average of 97.8 cm. of established ice between the flux meter and the ice-water interface. From table (6.6.i) showing the daily exit of heat from the cover, the total flux of heat lost between 30J and 19M is computed to be 1514.5 cal. cm.$^{-2}$. As far as the simple ice growth equation of Stefan is concerned, this quantity of heat corresponds to an effective latent heat of 71.1 cal. cm.$^{-3}$, or for a density of 0.915 gm. cm.$^{-3}$ to 77.6 cal. gm.$^{-1}$.

This experimental value may now be compared to the theoretically calculated results. The salinity profiles shown in section 6.9 indicate a mean salinity of 5‰ for the Button Bay ice cover. From equation (1.4.1), the latent heat of formation of this ice from sea water of salinity 30‰ is calculated to be 65.8 cal. gm.$^{-1}$. Figure (4.2.ii) indicates that 10.6 cal. gm.$^{-1}$ were lost by cooling of the older established ice, whose average surface temperature was -9.0°C. These two thermal quantities total 76.4 cal.gm.$^{-1}$ being in good agreement with the experimentally determined 77.6 cal. gm.$^{-1}$.

Table (6.6.i)

Heat Flux 20 cm. below Ice Surface

Date	Heat Flux	Date	Heat Flux	Date	Heat Flux
30J	81.5 cal. cm⁻²	24F	35.3 cal.cm⁻²	21M	11.7* cal.cm⁻²
31J	78.3	25	29.5	22	12.1
1F	70.6	26	26.1	23	12.2
2	56.3	27	26.6	24	11.7
3	31.8	28F	27.9	25	12.7
4	28.0	1M	31.2	26	12.9
5	32.5	2	33.0*	27	12.3
6	19.4	3	33.4*	28	10.4
7	9.5	4	33.1*	29	11.4
8	8.3	5	32.0*	30	10.5
9	21.7	6	28.0*	31M	8.0
10	31.9	7	23.0*	1A	7.8
11	33.5	8	21.8	2	10.7
12	33.5	9	27.3	3	9.4
13	33.8	10	27.8	4	8.6
14	31.9	11	24.1	5	9.1
15	27.1	12	23.7	6	9.6
16	37.0	13	25.4	7	8.6
17	42.7	14	22.1	8	6.8
18	44.7	15	19.4	9	8.3
19	46.0	16	14.7	10	8.3
20	45.3	17	17.3	11	7.1
21	45.5	18	13.9	12	7.5
22	48.3	19	12.1	13	8.3
23F	48.2	20M	12.2*	14A	* Estimated.

Assuming that the mean salinity of the cover has been estimated satisfactorily to the nearest part per thousand, a little less than 5% uncertainty is attached to the theoretically calculated quantity. It may thus be assumed that the theory of section 4.2 indicates the relative importance of the two sources of conducted heat with satisfactory accuracy. The period 20F to 12A, discussed for the radiation and atmospheric energy fluxes in the previous section, can be analysed using figure (4.2.ii). The mean ice surface temperature for this period having been $-8^{\circ}C$, the 961 cal. $cm.^{-2}$ at the surface were the sum of 861 and 100 cal. $cm.^{-2}$ from the freezing and cooling processes respectively.

6.7 Ice Surface Temperature, Growth and Thermal Conductivity.

The necessary modifications to enable a practical application of Stefan's simple ice growth equation were completed in section 4.2. At this stage, the heat lost by established ice during the growth of new ice was shown to be calculable by means of equation (4.2.5). The second necessary correction to the equation is due to the time taken for the transmission of thermal energy through the ice cover. In section 6.4, a method enabling the calculation of these times from a limited set of observations was developed. Table (6.4.iv) shows that the surface temperatures on 30J and 19M become effective as a cause of ice growth on 11F and 6A respectively. This fact must be considered in calculating the effective freezing exposure from the table of ice surface temperatures (6.7.i).

The effective latent heat $(L_s + \overline{c.\Delta\theta})$ has been discussed in the previous section, the mean value of this quantity arrived at being 77.0 cal. $gm.^{-1}$.

An expression for the thermal conductivity k, may be obtained by

Table (6.7.i)

Ice Surface Temperature

Date	Temperature		Date	Temperature		Date	Temperature	
	09hrs.	21hrs.		09hrs.	21hrs.		09hrs.	21hrs.
30J	11.5	11.4	24F	11.0	10.8	21M	5.5	
31J	12.3	12.8	25	9.4	9.2	22	5.4	5.3
1F	12.8	12.9	26	8.8	9.1	23	5.4	5.4
2	12.8	11.5	27	8.7	8.9	24	5.3	5.3
3	10.1	9.2	28F	8.9	9.4	25	5.3	5.4
4	8.4	8.6	1M	9.3	8.0	26	5.2	5.2
5	8.6	8.9	2		8.0	27	5.3	4.9
6	8.2	7.0	3		7.9	28	5.1	5.0
7	6.1	5.6	4	Estimated	7.8	29	4.9	4.9
8	5.5	5.4	5		7.8	30	4.8	4.6
9	5.3	6.8	6		7.7	31M	4.6	4.5
10	6.8	7.4	7		7.6	1A	4.5	4.5
11	6.5	8.1	8	7.6	7.7	2A	4.5	4.2
12	7.2	7.5	9	7.8	7.9	3	4.3	3.9
13	7.7	8.1	10	7.8	7.7	4	4.3	4.1
14	7.8	7.9	11	7.7	7.5	5	4.2	4.1
15	7.2	8.1	12	7.6	7.5	6	4.0	3.8
16	8.6	9.3	13	7.4	7.6	7	3.9	3.9
17	9.6	10.0	14	7.1	7.0	8	3.9	3.9
18	10.1	10.5	15	7.1	6.9	9	3.9	3.7
19	10.4	10.7	16	7.0	6.9	10	3.8	3.9
20	10.8	11.2	17	6.4	6.4	11	3.9	3.8
21	11.2	11.4	18	6.3	6.2	12	3.6	3.5
22	11.4	12.0	19	6.0	5.9	13	3.4	3.5
23F	11.3	10.9	20M	5.7		14	3.8	3.7

Temperatures in ^{o}C below the freezing point of sea water ($-1.65^{o}C$).

modifying equation (4.1.3) in the light of the discussion of section 4.2.

$$k = \frac{(h_1^2 - h_0^2) (L_s + \overline{c.\Delta\theta}) \rho}{2 (\theta_0 - \theta_F) . \Delta T} \qquad (6.7.1)$$

where:

$h_0 = 107.7$ cm.

$h_1 = 128$ "

$\rho = 0.915$ gm. cm.$^{-3}$

$L_s + \overline{c.\Delta\theta} = 77.0$ cal. gm.$^{-1}$

$(\theta_0 - \theta_F) . \Delta T = 397.7^\circ$C day $= 3.44 \times 10^7$ $^\circ$C sec.

from which it follows that $k = 4.87 \times 10^{-3}$ cal. cm.$^{-1}$ sec.$^{-1}$ $^\circ$C^{-1}.

Although both methods of establishing the latent heat term allow a considerable margin of error, fortunately the separate uncertainties in the calculated values of L_s and $\overline{c.\Delta\theta}$ tend to cancel when the sum of the two terms is taken. This is because a high overall estimation of the salinity leads to a large value for $\overline{c.\Delta\theta}$ and a low value for L_s, and vice versa for a low estimation of the ice cover's salinity. Consequently the error in the effective latent heat term is probably less than the 5% indicated in section 6.6. The other important error enters on considering the uncertainty in the temperature transmission time, again leading to a possible 5% error in the freezing exposure. The value of the thermal conductivity is thus only certain to within about 10%.

It may be noted that the thermal conductivity of sea ice of 5‰ salinity and a temperature of -5.5°C (the mean ice cover temperature) is predicted to be approximately 4.7×10^{-3} by the theory of chapter 2, summarized graphically in figure (2.5.i). This is well within the limits of the experimental determinations.

6.8 Calculation of Thermal Conductivity by Comparison to a Reference.

Measurement of the thermal conductivity of sea ice by comparison of the temperature gradients in the ice cover and in the ice flux meter reference block, was the least successful operation of the programme.

The necessity for temperature equality between the flux meter and the corresponding level in the sea ice meant that many readings had to be rejected because slowly moving snow drifts led to uneven surface temperature distributions on the cover.

Combination of the uncertainties in the two measurements of temperature difference necessary for comparison, allows a total possible error of at least 15%. Calculation of the mean thermal conductivity of the upper 30 cm. of sea ice gave results varying between 4.1×10^{-3} and 5.4×10^{-3} c.g.s. units. These figures are of little value, but not inconsistent with the theoretical results of chapter 2 and the results for the mean conductivity of the ice cover.

6.9 The Salinity, Density and Crystal Structure of Ice.

On two occasions during the winter, in February and in April, salinity and density profiles were obtained for the upper 90 cm. of the ice cover. Crystal photography of the same ice enabled the later correlation of ice appearance with salinity and density.

The salinity was obtained by hydrometric measurements on the melt of 10 cm. sectioned lengths of 3 inch diameter ice cores. The hydrometer used was direct reading for the salinity of solutions having the distributions of salts found in sea water. Only its zero point was checked by immersion in distilled water prior to the measurements.

Densities were determined by weighing 10 cm. sections in air and in normal heptane. The difference in these weights of course being equal to the weight of normal heptane displaced, so that a determination of the density of the liquid by repeating the experiment with a metal (aluminium) cylinder of known mass and dimensions, allowed calculation of the volume of the ice sample. As mentioned in the specific heat experiments, normal heptane does not dissolve any of the components of sea ice, and because of its low viscosity is very suitable for immersion weighings since few air bubbles are trapped at the ice-heptane interface.

Crystal examination and photography involved viewing thin slides of ice prepared to about 1 mm. thickness, by cutting the standard 10 cm. sections of ice along a common vertical plane. The thin slabs of ice cut on a band saw were finally mounted on glass slides by careful melting and refreezing of a thin boundary layer of ice. A thin specimen is necessary for sharp crystalline boundaries to be seen, since these in general are formed by two crystals overlapping in the direction of observation.

In the composite figure (6.9.i), the salinity, density and crystal structure on 22F are seen. The upper 10 cm. consisted of rapidly growing ice, a view supported by the small crystal size as well as the high salinity. With density increasing after this uppermost layer, probably partially snow ice, the salinity is seen to have decreased and the size of the crystals to have increased, indicating less rapid growth, until a minimum salinity was reached, seen at the 40 cm. level.

It is interesting to note that the density did not reflect the change in salinity. This fact can be explained on the basis of the final statement in section 2.3. The less rapidly growing ice contained fewer air bubbles, but

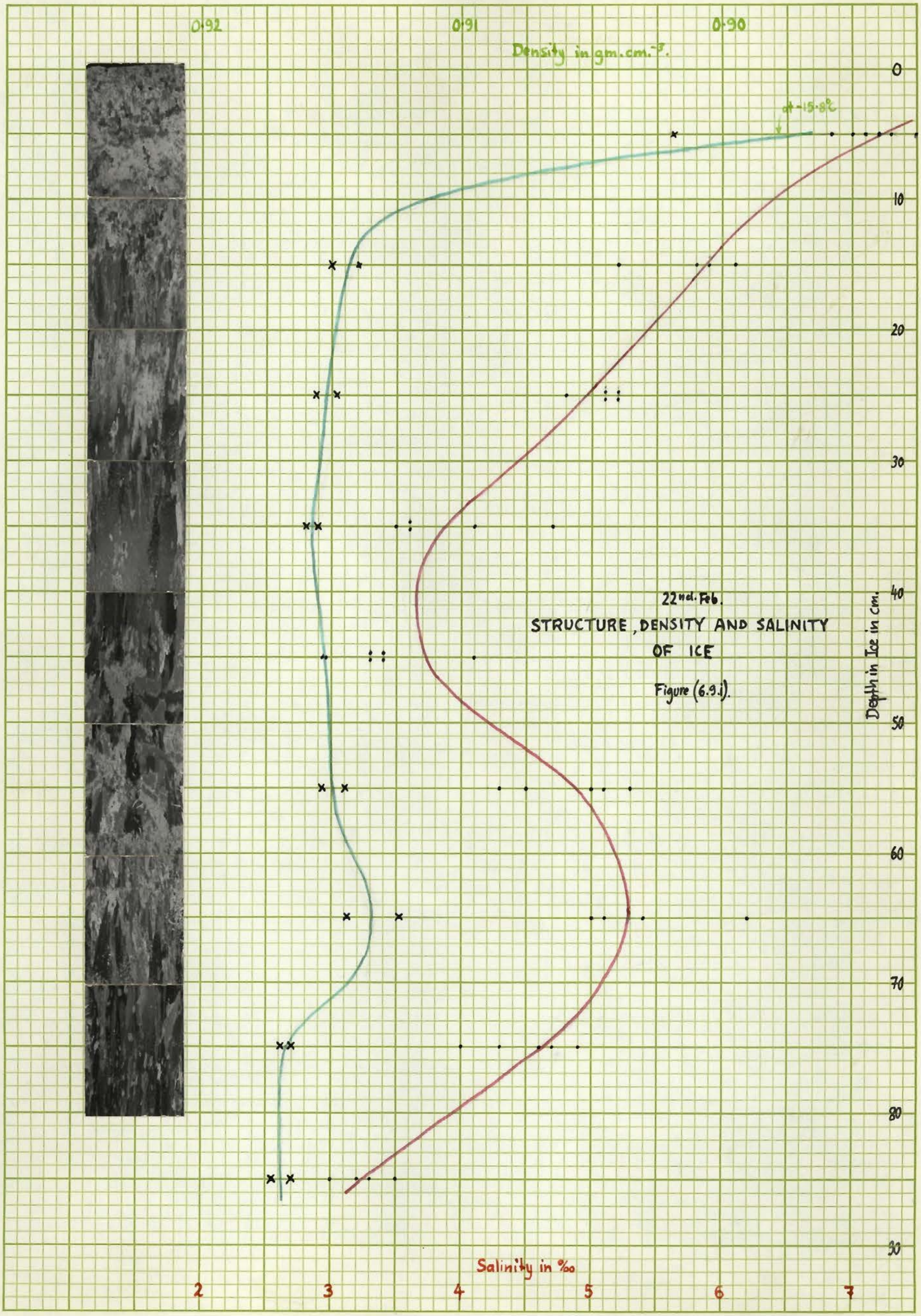

22nd. Feb.
STRUCTURE, DENSITY AND SALINITY OF ICE
Figure (6.9.1).

consequent increase in density was offset by the loss of density due to less brine being trapped, leading to an ice of lower salinity. However, more rapidly growing ice at about 65 cm. indicated as such by both its increased salinity and smaller crystal structure as well as greater air bubble content, does have a slightly lower density. Never the less, the remarkable constancy of the density of sea ice has been displayed.

A later salinity and density profile taken on 3A is shown in figure (6.9.ii). It is seen that considerable brine drainage, a process whose mechanism has been described by Pounder and Little (PL59), occurred in the six weeks interval, the mean salinity of the cover having decreased by about 0.5‰. According to equation (2.3.2), this change would just be detectable in the third figure of the density. The dashed curve in figure (6.9.ii) is the result of using the factor:

$$1 - 4.57\sigma\left(\frac{1}{7.5} - \frac{1}{15.8} \right)$$

obtained from equation (2.3.2) to normalize the densities determined at -7.5°C on 3A to the temperature of -15.8°C at which the ice densities were found on 22F. Comparison of the normalized profiles obtained at the two times now shows a detectable lowering in density due to brine drainage.

6.10 <u>The Decay of the Ice Cover</u>.

Late in May, a final observation of the cover was made from a light helicopter. The bulk of the Button Bay ice still appeared to be mechanically intact, but was covered by up to 70 cm. of water with some islands of wet snow remaining. Of particular interest is the fact that the surface water was perfectly fresh to taste and at a temperature of approximately 0°C,

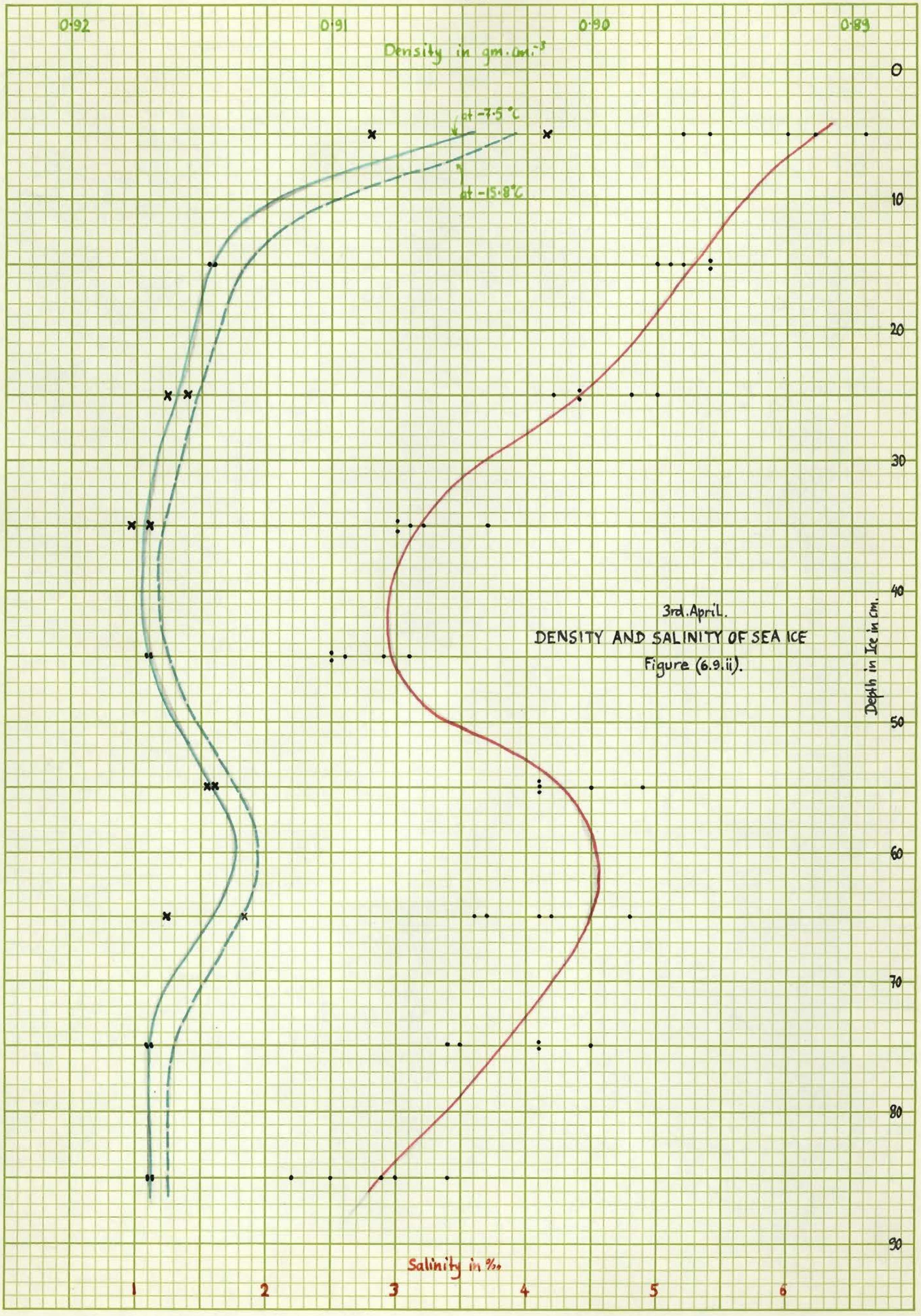
0·92
0·91
0·90
0·89
Density in gm.cm.⁻³
at -7·5 °C
at -15·8°C
0
10
20
30
40
50
60
70
80
90
Depth in Ice in cm.
3rd. April.
DENSITY AND SALINITY OF SEA ICE
Figure (6.9.ii).
Salinity in ‰
1
2
3
4
5
6

showing that even at this relatively advanced stage of decay, the upper ice surface was not in contact with sea water. Referring to section 1.4 it may be appreciated that the final melting point of the ice at this stage was very near to $0^{\circ}C$, and not $-1.6^{\circ}C$, its original freezing point.

Doubtlessly the melting continued from the upper surface until the cover was sufficiently fragile to break up by oceanic movement. At this stage, contact with higher salinity water from the sea would cause disintegration and decay of the ice to proceed rapidly.

The fact that the melting point of the upper layers of the ice cover was above the original temperature of freezing is of some importance to the thermal regime. Supposing only the upper half of the ice were melted without contact with sea water, then for an ice cover reaching a maximum thickness of 135 cm. as at Button Bay, over 100 cal. $cm.^{-2}$ more heat would be required to melt all the ice than was lost by the surface during its formation. The maximum negative energy content of this ice cover, when referred to water at the freezing point, was about 10,000 cal. $cm.^{-2}$ so that the 100 cal. $cm.^{-2}$ required as additional melting heat represents 1% of the total heat exchange.

In calculating the heat content of an ice cover, the surface melt water must be considered as part of the ice. Because this water is at a higher temperature than the sea, the energy content of ice is difficult to estimate when unknown amounts of melt water may drain into the sea.

After the ice has completely melted, the sea is at a higher temperature than at the onset of freezing. Thus, even apart from the effect of the less saline melt water near the surface, a freezing sea has unequal energy states at the beginning of freezing and the completion of melting. An identical energy content and vertical distribution in the sea or its ice cover could be expected but once a year.

REFERENCES

(Ad60) J.R.Addison
Salt Distribution in Sea Ice
Bulletin of the American Physical Society 5, 359, (1960)

(An51) M.L.Anthony
Temperature Distribution in Slabs with a Linear Temperature Rise at One Surface
General Discussion on Heat Transfer, Section 3,
Conduction in Solids and Fluids, London Conference, September 1951.

(An58) D.L.Anderson
A Model for Determining Sea Ice Properties
Arctic Sea Ice, p.148. National Academy of Science - National Research Council Publication 598, (1958)

(An60) D.L.Anderson
The Physical Constants of Sea Ice
Research 13, 310, (1960)

(AM59) W.Ambach und H.Mocker
Messungen der Strahlungsextinktion mittels eines kugelförmigen Empfängers in der oberflächennahen Eisschicht eines Gletschers und im Altschnee.
Arch. Met. Geoph. Bioklim. 10, 84, (1959)

(Ba28) H.T.Barnes
Ice Engineering, p.28
Renouf Publishing Co., Montreal, (1928)

(Bu55) M.I.Budyko
Atlas of Heat Balance
Chief Administration of the Hydrometeorological Service of the Council of Ministers of the U.S.S.R., (1955)

(CJ59) H.S.Carslaw and J.C.Jaegar
Conduction of Heat in Solids, 2nd. Ed.
Clarendon Press, Oxford, (1959)

(Do40) N.E.Dorsey
Properties of Ordinary Water Substance
Reinhold, New York, (1940)

(DG58) M.Diamond and R.W.Gerdel
Radiation Measurements on the Greenland Ice Cap
Corps of Engineers Greenland Ice Cap Research Program
Studies conducted in 1955-56, 1, (1958)

(El40) W.M.Elsasser
Quart. J.Roy.Meteorol. Soc., 66, Suppl. 41, (1940)

(Ge61) R.Geiger
Das Klima der bodennahen Luftschicht
Friedrich Vieweg & Sohn, Braunschweig, (1961)

(GD45) G.Goodall and H.C.Darby
The University Atlas
George Philip and Son, The London Geographical Institute, (1945)

(GD51) J.T.Gier and R.V.Dunkle
Total Hemispherical Radiometers
A.I.E.E. Transactions, 70, (1951)

(Ha54) M.H.Halstead
The Fluxes of Momentum, Heat and Water Vapour in Micrometeorology
Johns Hopkins University Publication in Climatology VII,
No.2, 326, (1954)

(Ho56) G.Hofmann
Verdunstung und Tau als Glieder des Wärmehaushalts
Planta. Archiv für Wissenschaftliche Botanik
Julius Springer, Berlin, 47, 303, (1956)

(Ia55) G.N.Iakovlev
The Thermal Regime of the Ice Cover
Observational Data of the Scientific Research Drifting Station
of 1950-51, Vol. II, Section 7, (1955)

(Ia58) G.N.Iakovlev
Thermal Balance of an Ice Cover of the Central Arctic
Problemi Arktiki, No.5, 33, (1958)

(Ko58) A.G.Kolesnikov
On the Growth of Sea Ice
Arctic Sea Ice, p.157
N.A.S. - N.R.C. Publication 598, (1958)

(KH23) H.H.Kimball and H.E.Hobbs
A New Form of Thermoelectric Recording Pyrheliometer
Journal of the Optical Society of America and Review of Scientific Instruments, 7, 707, (1923

(La52) N.A.Lange
Handbook of Chemistry, 8th. Ed.
Handbook Publishers, Ohio, (1952)

(La59) D.L.Laikhtman
Arkticheskii i Antarkticheskii Nauchno-Issledovatel'skii Institut, Trudy, 226, 42, (1959)

(La60) M.P.Langleben
Distribution of Brine Cells in Sea Ice
Bulletin of the American Physical Society, 5, 359, (1960)

(LM53) D.I.Lawson and J.H.McGuire
The Solution of Transient Heat Flow Problems by Analogous Electrical Networks
The Inst. of Mech. Engineers, Excerpt from Proceedings (A), Vol. 167, 275, (1953)

(Li55) G.Liebmann
Solution of Transient Heat - Transfer Problems
by the Resistance - Network Analogue Method
Transactions of the American Society of Mechanical Engineers
Paper 55-A-61, (1956)

(Li56) G.H.Liljequist
Part 1, Energy Exchange of an Antarctic Snow Field
Short Wave Radiation. Long Wave Radiation and Radiation Balance
(1956)

(Ma91) J.C.Maxwell
Electricity and Magnetism, 3rd. Ed., Vol. I
Dover Publications, New York, (1891)

(Ma33) F.Malmgren
On the Properties of Sea Ice
Norwegian North Polar Expedition with the "Maud", 1918-1925
Scientific Results, Vol. I, No.5, (1933)

(Mi60) A.R.Milne
Shallow Water Under-Ice Acoustics in Barrow Strait
The Journal of the Acoustical Soc. of America, 32, 1007, (1960)

(Na59) Iu.L.Nazintsev
Problemi Arktiki i Antarktiki, No.1, 65, (1959)

(NT54) K.H.Nelson and T.G.Thompson
Deposition of Salts from Sea Water by Frigid Concentration
Journal of Marine Research, Vol. XIII, (1954)

(OS59) L.P.Orlenko and A.V.Smetannikova
Arkticheskii i Antarkticheskii Nauchno-Issledovatel'skii
Institut, Trudy, 226, 48, (1959)

(Po54) D.J.Portman
The Measurement of Radiation
Johns Hopkins University Publication in Climatology VII,
No.2, 289, (1954)

(PL59) E.R.Pounder and E.M.Little
Some Physical Properties of Sea Ice I
Canadian Journal of Physics, 37, 443, (1959)

(Sc60) P.Schwerdtfeger
Observations on Estuary Ice
Canadian Journal of Physics, 38, 1391, (1960)

(Su53) O.G.Sutton
Micrometeorology, A Study of Physical Processes in the
Lowest Layers of the Earth's Atmosphere
McGraw Hill Book Co., (1953)

(St91) J.Stefan
Über die Theorie der Eisbildung insbesondere über die Eisbildung im Polarmeere
Annalen der Physik und Chemie, Neue Folge, Band XLII
Heft 2, 269, (1891)

(TH54) C.W.Thornthwaite and M.H.Halstead
Johns Hopkins University Publication in Climatology VII, (1954)

(Un61) N.Untersteiner
On the Mass and Heat Budget of Arctic Sea Ice
Archiv für Met. Geoph. Bioklim., Band 12, 2.Heft, 151, (1961)